AECL EACL

Licensing Submission

ACR Limited and Severe Core Damage Accidents: Supporting R&D

ACR

108-126810-LS-002
Revision 0

Prepared by
Rédigé par
A.J. White
Director, Reactor Safety

Reviewed by
Examiné par
D. Wren
Manager, ACR R&D

Approved by
Approuvé par
V. Snell
Director, ACR Safety & Licensing

2003 November

CONTROLLED - Licensing

2251 Speakman Drive
Mississauga, Ontario
Canada L5K 1B2

Novembre 2003

CONTRÔLÉ - Permis

2251, rue Speakman
Mississauga (Ontario)
Canada L5K 1B2

AECL EACL

Licensing Submission

ACR Limited and Severe Core Damage Accidents: Supporting R&D

ACR

108-126810-LS-002
Revision 0

2003 November

CONTROLLED - Licensing

2251 Speakman Drive
Mississauga, Ontario
Canada L5K 1B2

Novembre 2003

CONTRÔLÉ - Permis

2251, rue Speakman
Mississauga (Ontario)
Canada L5K 1B2

AECL EACL

Release and Revision History / Liste des documents et des révisions

0939B Rev. 13

Document Details / Détails sur le document

Title / Titre	Total no. of pages / Nbre total de pages
ACR Limited and Severe Core Damage Accidents: Supporting R&D	

CONTROLLED - Licensing / CONTRÔLÉ - Permis

Release and Revision History / Liste des documents et des révisions

Release Document		Revision Révision		Purpose of Release; Details of Rev./Amendement Objet du document; détails des rév. ou des modif.	Prepared by Rédigé par	Reviewed by Examiné par	Approved by Approuvé par
No./N°	Date	No./N°	Date				
1		D1	2003/11/05	Issued for Review and Comment.	A.J. White	V. Snell N. Popov D. Wren	
2		0	2003/11/12	Issued for "Approved for Use."	A.J. White	D.J. Wren	V. Snell

DCS/RMS Input / Données SCD ou SGD

Rel. Proj. Proj. conn.	Project Projet	SI	Section	Serial Série	Sheet Feuille No. N°	Of De	Unit No.(s) Tranche n°
	108	126810	LS	001	1	1	

ACKNOWLEDGEMENTS

The author would like to acknowledge the contributions from D.B. Sanderson, T. Nitheanandan, L.W. Dickson, J.C. Wren, R.S. Swartz, C.K. Chan and M. Mathew. They provided the bulk of the material that is included in the report, as noted with the by-lines on report sections.

TABLE OF CONTENTS

TABLE OF CONTENTS

TABLE OF CONTENTS

TABLES

FIGURES

TABLE OF CONTENTS

SECTION **PAGE**

TABLE OF CONTENTS

SECTION **PAGE**

TABLE OF CONTENTS

SECTION **PAGE**

TABLE OF CONTENTS

SECTION **PAGE**

1. INTRODUCTION

Nuclear reactors are designed, licensed and operated to perform with a high degree of safety and reliability. This is achieved by carefully considering possible accident sequences and ensuring that their consequences are appropriately limited. More probable events are typically accounted for in the design of a reactor's process systems without needing the support of safety systems. For improbable events, safety systems are designed to shutdown the reactor and ensure that the consequences are limited – within regulatory requirements and economically acceptable. Highly improbable events may be predicted to have more severe consequences, but based on probabilistic assessments, targets are met to ensure such events are of sufficiently low frequency to have acceptable public and economic risk.

In designing CANDU®* reactors, consideration is given to accidents involving the failure of a process system (single failure), and failure of a process system with coincident loss of a safety system (dual failure). The more extreme dual failure accidents, sometimes referred to as severe accidents for other reactor designs, can lead to limited damage to the reactor core, and are referred to as:

- Limited Core Damage Accidents: improbable events for which the channel core geometry is maintained.

In the highly unlikely event there are multiple system failures, a limited core damage accident might proceed to a state where the core geometry is lost. Such accidents are referred to as:

- Severe Core Damage Accidents: highly improbable events for which there is the possibility of core disassembly.

CANDU reactors possess a number of inherent and designed features that make them resistant to core damage accidents. Perhaps the most important is the distributed nature of the channel core design, which means there is low temperature moderator surrounding the fuel channels that serves as a secondary heat sink in the unlikely event that primary cooling and emergency cooling are lost (Loss-of-Coolant Accident with Loss of Emergency Core Cooling – LOCA + LOECC). In such an event, the cooling system for the moderator is sufficient to handle the decay heat load from the fuel channels, preserving their integrity and ensuring that the accident does not progress to severe core damage.

AECL's Advanced CANDU Reactor™ (ACR™)† builds on the proven features of CANDU reactors and provides increased resistance to severe core damage accidents. One of the improvements with increased resistance to such accidents is the inclusion of a Reserve Water System. This system consists of a large tank (2500 Mg) at the top of the containment building, with manually-operated lines to the long-term cooling sumps, inlet headers of the reactor coolant system, the secondary side of the steam generators, the calandria vessel and the shield tank, Figure 1-1. As a result, in the highly unlikely event of a severe core damage accident, such as LOCA + LOECC with additional loss of the moderator cooling system, the operator can choose

---

* CANDU® (CANada Deuterium Uranium) is a registered trademark of Atomic Energy of Canada Limited (AECL).

† ACR™ (Advanced CANDU Reactor™) is a trademark of Atomic Energy of Canada Limited (AECL).

to provide gravity-driven make up water to reactor systems such as the moderator. Without moderator cooling or additional water, the heat from the fuel channels will boil off the moderator, eventually leading to core collapse. By providing additional water to the moderator system from the Reserve Water System, the progression of such an accident is significantly delayed.

AECL has led an extensive research program into the behavior of CANDU reactors in core damage accidents. Much of this research is generically applicable to the ACR design. This report briefly outlines core damage accidents and their phenomenology. Then it describes the R&D supporting understanding of core damage accident behavior and progression. This research is divided into 5 main areas:

- Fuel Channel Behavior,
- Fuel and Fission Product Behavior,
- Fission Product Source Term in Containment,
- Hydrogen Behavior and Containment Thermalhydraulics, and
- Core Disassembly.

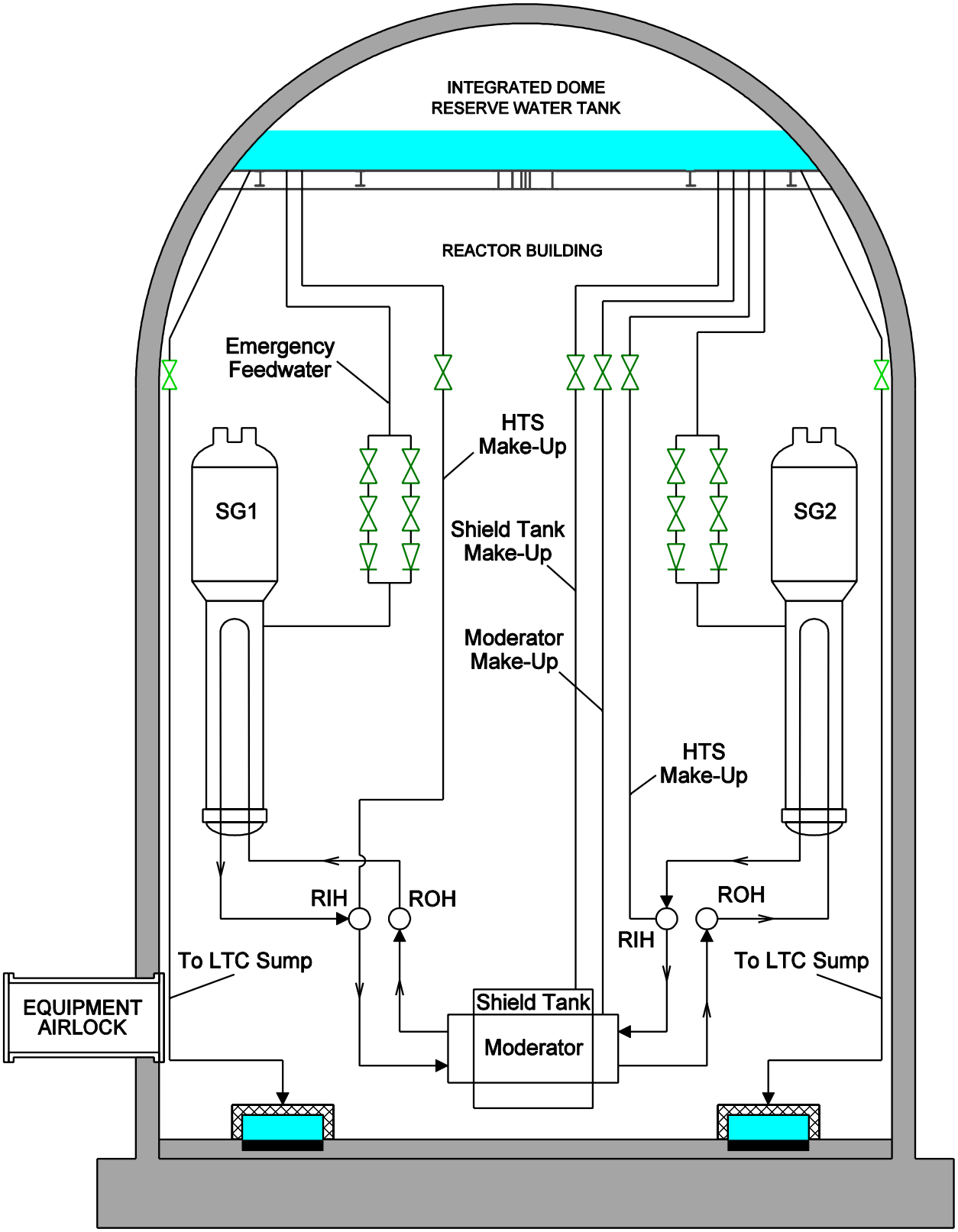

Figure 1-1 ACR Reserve Water System

2. CORE DAMAGE ACCIDENTS AND THEIR PHENOMENOLOGY

2.1 Limited Core Damage Accidents

There are two classes of Limited Core Damage Accidents, those that involve degraded cooling in a single channel at full power, and those that involve degraded cooling of the entire core at decay power.

2.1.1 Degraded Cooling in a Single Channel at Full Power

Degraded cooling at full power can only occur in a single fuel channel. Each fuel channel is independently connected to common Reactor Coolant System components (headers, pumps, etc.) by feeders. There are two potential mechanisms that could result in a severe reduction in coolant flow to an individual fuel channel. A single channel could experience flow blockage (postulated as debris in the header or inlet feeder pipe) or could experience a stagnation break. This is a break in the inlet piping of a fuel channel that is just sufficient to balance the pressure drop across the channel leading to a net loss of coolant flow (or stagnation) of the affected channel. Since the disruption to the RCS is small, the reactor may not scram, and the accident proceeds at power until the affected channel fails, triggering shutdown and ECC injection. The consequences of a single-channel event depend on the extent of the flow reduction. The most likely event (up to 99% flow area blockage) is a limited transient with no fuel channel failure and possible fuel failures. With reductions in flow area greater than 99%, the fuel channel will fail, and if the blockage is almost complete there can be melting, primarily of fuel cladding.

For blockages less than about 99% of the flow area, the worst outcome would be a temperature excursion for the fuel that could lead to fuel failure and release of fission products. Since the fuel channel remains intact, any fission products are contained within the RCS. If the fission product concentrations in the coolant system become high enough the reactor is scrammed.

Blockages greater than 99% of the flow area can lead to failure of the fuel channel. The basic sequence of events and phenomenology for such an accident is as follows:

- In the affected channel, the coolant flow is reduced, but the system remains at full power and pressure.
- With the reduced coolant flow, the coolant stratifies and the uncovered fuel rapidly heats up, transferring heat to the pressure tube.
- As the pressure tube temperature exceeds ~600°C, it will start to deform, expanding radially (ballooning) under the influence of the system pressure.
- The pressure tube creep rate is highly dependent on temperature. As a result, non-uniformity in the temperature distributions due to coolant stratification is likely to lead to strain localization and failure of the pressure tube at the top, Figure 2-1.
- If the blockage is greater than 99.7% of the flow area, the fuel overheating could be sufficient to lead to limited melting of Zircaloy-4 fuel components prior to the failure of the pressure tube.
- For a complete (100%) flow blockage, the coolant will void more uniformly and the fuel will rapidly heat up, melting fuel cladding. Molten material relocating onto the bottom of the

pressure tube due to gravity will cause strain localization and failure at the site of contact with the pressure tube, Figure 2-1.

- Rapid pressurization of the fuel channel annulus, and impinging hot effluent from the pressure tube break will cause the calandria tube to fail.
- Steam and fuel fragments are ejected through channel break into the calandria, Figure 2-2.
- A high-pressure steam bubble forms and causes a pressure transient in the moderator; the moderator is subsequently depressurized through rupture discs on relief ducts.
- Jet material from the fuel channel rupture impinges on neighboring channels opposite the break. The jet also causes movement (pipe whip) of the affected channel, but this does not lead to propagation of channel failures.
- Small amounts of hot fuel material and molten cladding interact with the moderator
- Failure of the fuel channel causes the reactor to trip and coupled with failure of the moderator rupture discs, provides a new flow path for the coolant to cool the remaining material in the affected channel. Depressurization of the Reactor Coolant System will lead to injection of ECC, and eventually Long Term Cooling (LTC) to maintain cooling for the core.
- Adequate fuel cooling is maintained in all other channels. The only radiological release occurs from fuel in the affected channel.

2.1.2 Degraded Cooling at Decay Power

Degraded cooling at decay power occurs with a "dual failure" of impairment to RCS flows and to ECC (Here ECC refers to the combination of Emergency Core Coolant injection and the Long Term Cooling (LTC) systems). The reactor is scrammed with the LOCA, and the fuel heats up under decay power. Extreme scenarios for this family of accidents are large LOCAs with loss of ECC that typically involve core voiding, fuel overheating, fuel and fuel channel deformations at moderate and low RCS pressures, hydrogen generation and release of fission products from the fuel. Deformation of the fuel channel creates heat transfer paths from the fuel to the alternate heat sink (i.e., the moderator), thereby limiting the consequences.

The consequences of a Large LOCA + LOECC depend on the break size and degree of ECC impairment. Dual trains of ECC injection and LTC in the ACR address single component failure events and make complete loss of ECC unlikely. For the purposes of discussing the phenomenology of the accident sequence, complete loss of ECC is assumed, with no mitigating additional coolant from the Reserve Water System.

The basic sequence of events and phenomenology is as follows:

- With the break, the reactor trips and the Reactor Coolant System depressurizes.
- Under decay power, fuel transfers heat to the stratified coolant, eventually voiding the channel.
- As the fuel heats up, chemical heat from the oxidation of Zr fuel components with steam adds to the decay heat; the fuel bundles slump, decreasing subchannel flows, and eventually disassemble.
- In extreme cases, bundles will further fragment and there could be limited Zr melting – molten material tends to remain in inter-element voids due to surface tension.

- Release of fission gases from the fuel pressurizes the cladding causing localized ballooning (due to small free volume). Cladding may fail due to overstrain, oxygen embrittlement, or Be-braze crack penetration.
- As the pressure tube temperature exceeds ~600°C, it will start to deform. In the absence of sufficient internal pressure to cause ballooning, the pressure tube will sag into contact with the calandria tube, Figure 2-3.
- Stored energy in the pressure tube, and heat from the fuel, is conducted to the moderator. The modes of heat transfer are radiation, and conduction through areas in contact with the calandria tube.
- The maximum fuel temperature is limited by radiative and conductive heat transfer to the moderator. The fuel can be severely damaged, but there is limited melting. Core channel geometry is maintained because the moderator keeps the fuel channels cooled.
- Fission products released following failure of the fuel cladding and degradation of the UO_2, are transported toward the break in the RCS. Some fission products will be retained in the RCS due to mechanisms such as condensation on cooler surfaces outside of the core, impaction in complex piping geometries and scrubbing in water remaining in cooler out-of-core piping.
- The effluent from the break in the Reactor Coolant System entering containment will include steam, water, hydrogen and fission products.
- The break discharge pressurizes containment, mitigated by Local Air Coolers (LACs).
- Water aerosols condense and settle, trapping most fission products. Radiolytic reactions can lead to formation of volatile iodine species (particularly in the longer term).
- Standing flames could result from hydrogen released at the break resulting in thermal impacts on equipment in the range of such flames.
- The hydrogen concentration within containment is controlled by dispersion (LAC fans) to limit local concentrations and by passive autocatalytic recombiners, preventing energetic hydrogen reactions.

2.2 Severe Core Damage Accidents

All severe core damage accidents proceed at low RCS pressures. These accidents only occur if there is a loss of primary heat sink, with multiple failures of emergency heat sinks (e.g. LOCA + LOECC + loss of moderator cooling + loss of reserve water system make-up). The phenomena of early phases are similar to those of a limited core damage accident with degraded cooling at decay power. Without cooling, however, the moderator boils off and fuel upper channels heat up and collapse onto lower channels. As the moderator level decreases, the channels collapse further and a suspended debris bed is formed. Core collapse proceeds gradually, and eventually the entire core collapses into a terminal debris bed in the bottom of the calandria – a state which can be maintained provided that there is cooling water in the shield tank which surrounds the calandria vessel.

The basic sequence and phenomenology of a severe core damage accident is as follows:

- The initial sequence proceeds as described for a limited core damage accident with degraded cooling at low power. The system depressurizes, the fuel heats up transferring heat to the pressure tubes, and the pressure tubes sag into contact with the calandria tubes.
- With a failure of the moderator cooling system (and no addition of water from the Reserve Water System), the moderator slowly boils off, steam being released through the relief ducts at the top of the calandria vessel.
- As the level of the moderator decreases, the upper fuel channels will become uncovered and heat up. These fuel channels will sag onto lower channels, and eventually break into long segments, forming a course suspended debris bed, Figure 2-4.
- As the channels overheat, steam in the calandria vessel gains access to hot zirconium components, and oxidation contributes chemical heat.
- As lower channels become uncovered, they fail, and the debris bed migrates downward and compacts.
- Eventually the weight load causes complete core collapse to the bottom of calandria vessel.
- The initial collapse quenches hot debris, but eventually the decay heat boils off the remaining water in the calandria vessel.
- The dry debris bed heats in a non-oxidizing environment and compacts. Corium in contact with the lower calandria vessel shell and the upper surface of the debris bed are solid, whereas the interior of the debris bed may contain molten material, Figure 2-5. The surface to volume ratio of the debris bed is large providing for good heat transfer
- The cooling provided by the shield tank keeps the calandria vessel intact. Assuming that the shield tank cooling system is unavailable, boiling will reduce the level of the shield tank. This can be made up from the Reserve Water System if this function is available.
- Fission products are released during early fuel transients, and during core degradation and melting, but are retained within containment, primarily in the aqueous phase.
- Hydrogen is released from extensive oxidation reactions, and is controlled by dispersions (LAC fans) and by passive recombiners in containment.
- Local Air Coolers prevent overpressurization of containment by and by removing heat and steam from the containment atmospheres.
- The time required to boil the shield tank volume down to the level of the debris bed is considerable owing to the large volumes of water that must be vaporized. If the Reserve Water System is available, this time is extended.
- The flooding level in the containment building, from all sources of water, including the portion of the Reserve Water System dedicated to flooding the LTC sumps, is such that the bottom of the shield tank will be cooled at all times. Should the debris bed fail the bottom of the calandria vessel, it will then be retained in the bottom of the shield tank.

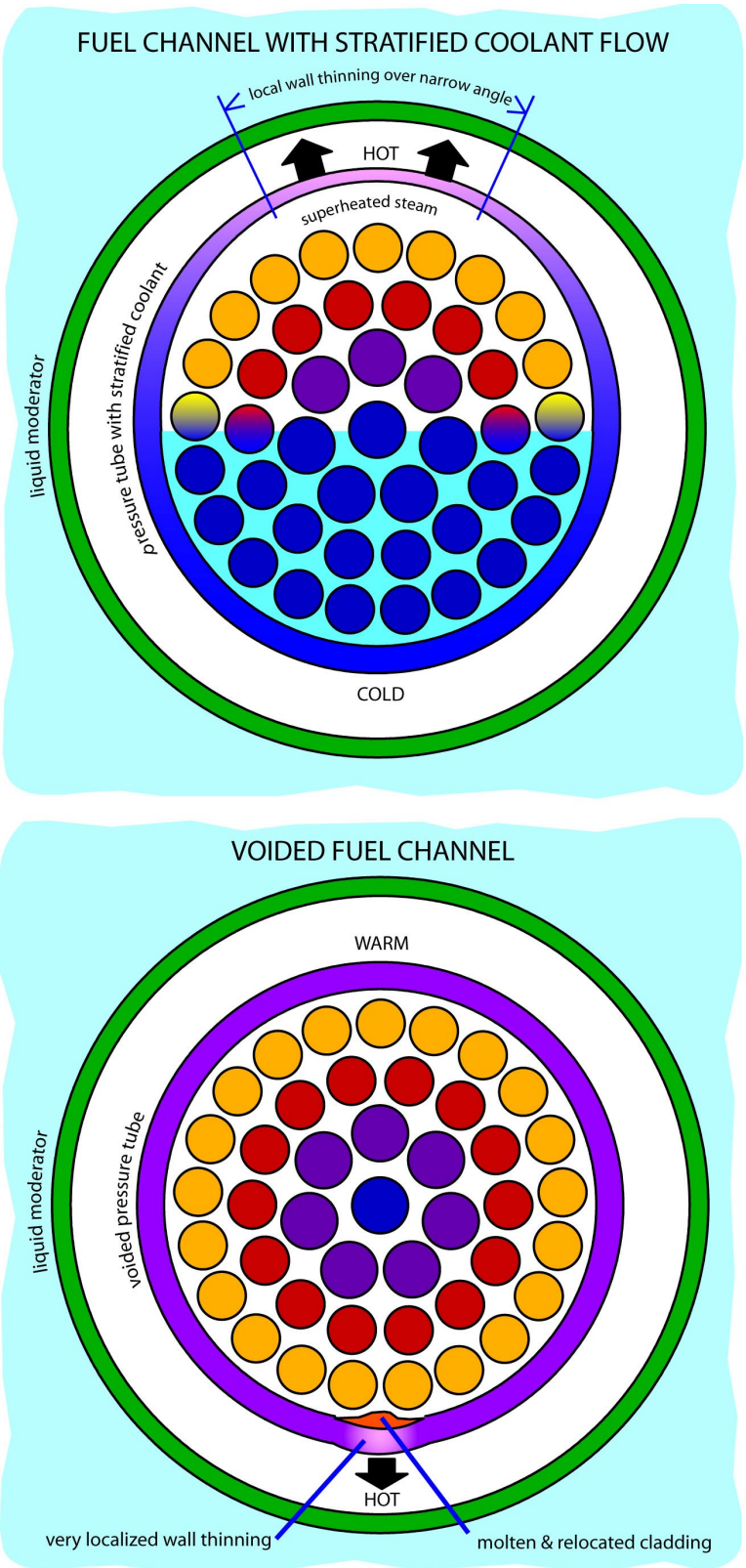

Figure 2-1 Failure Mechanisms for a Fuel Channel with Degraded Cooling at Full Power

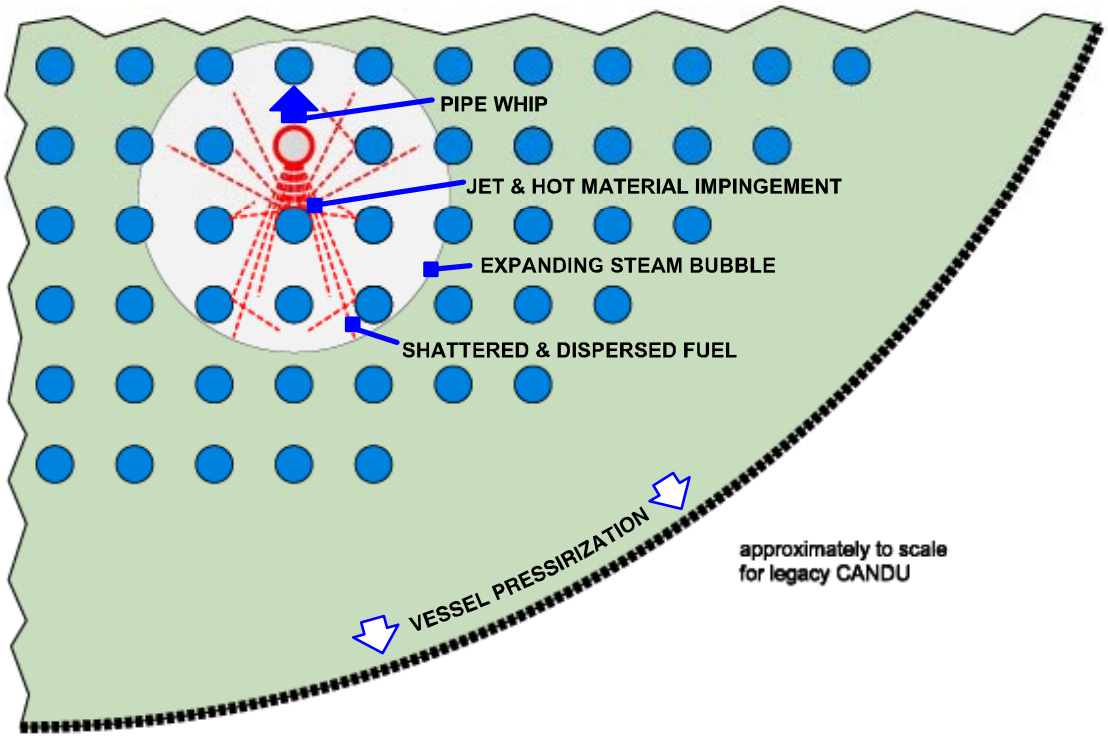

Figure 2-2 Consequences of Fuel Channel Failure under Degraded Cooling at Full Power

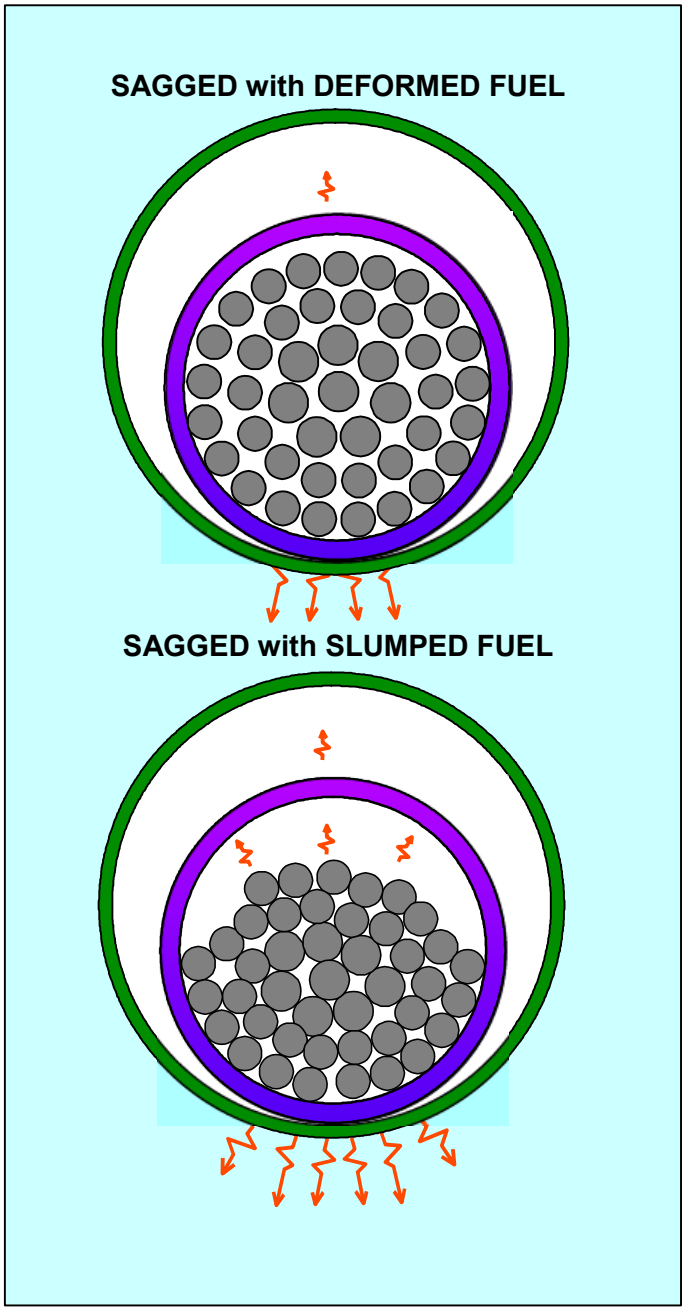

Figure 2-3 Pressure Tube Sagging into Contact with Calandria Tube

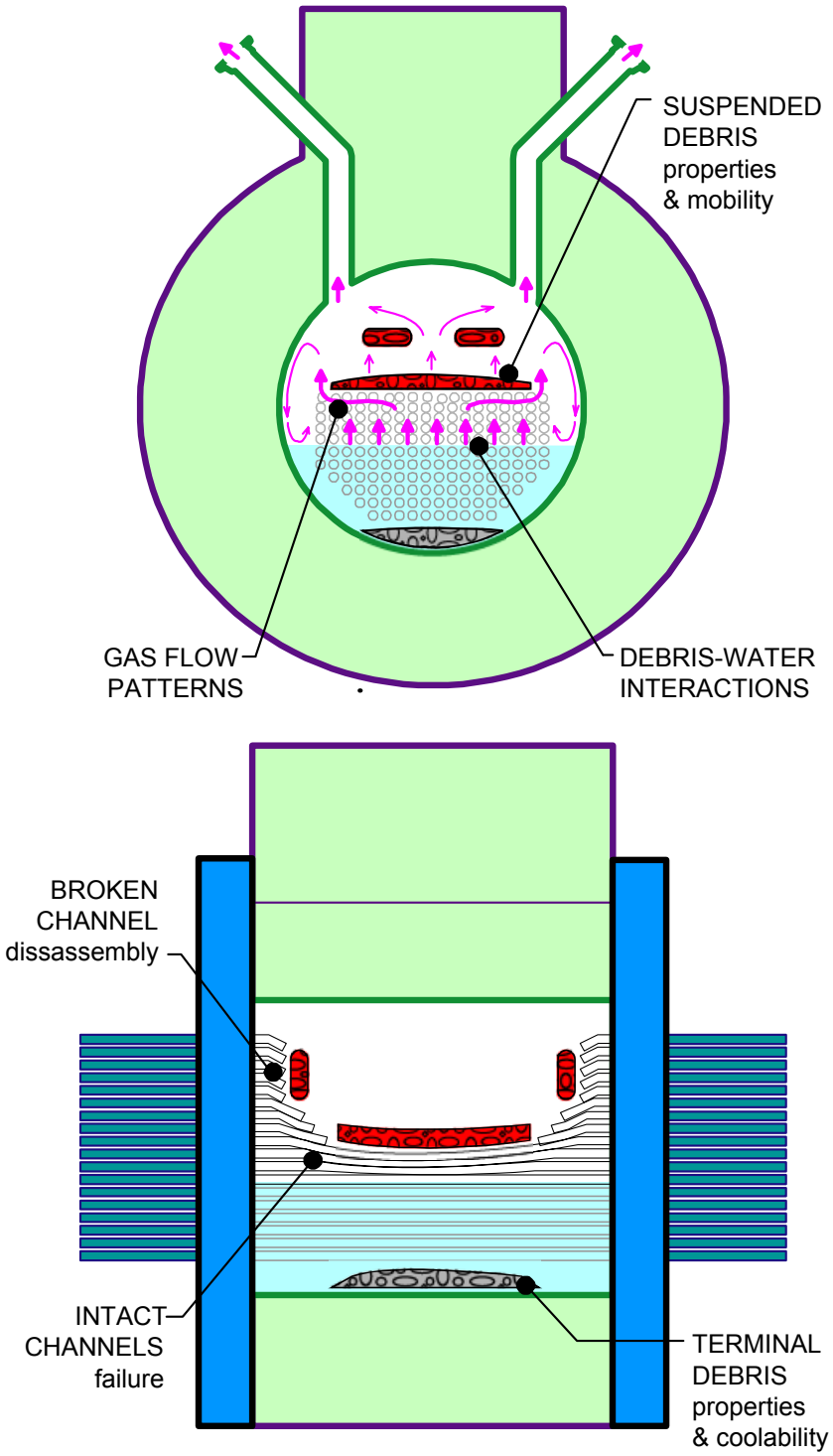

Figure 2-4 Formation of a Suspended Debris Bed in a Severe Core Damage Accident

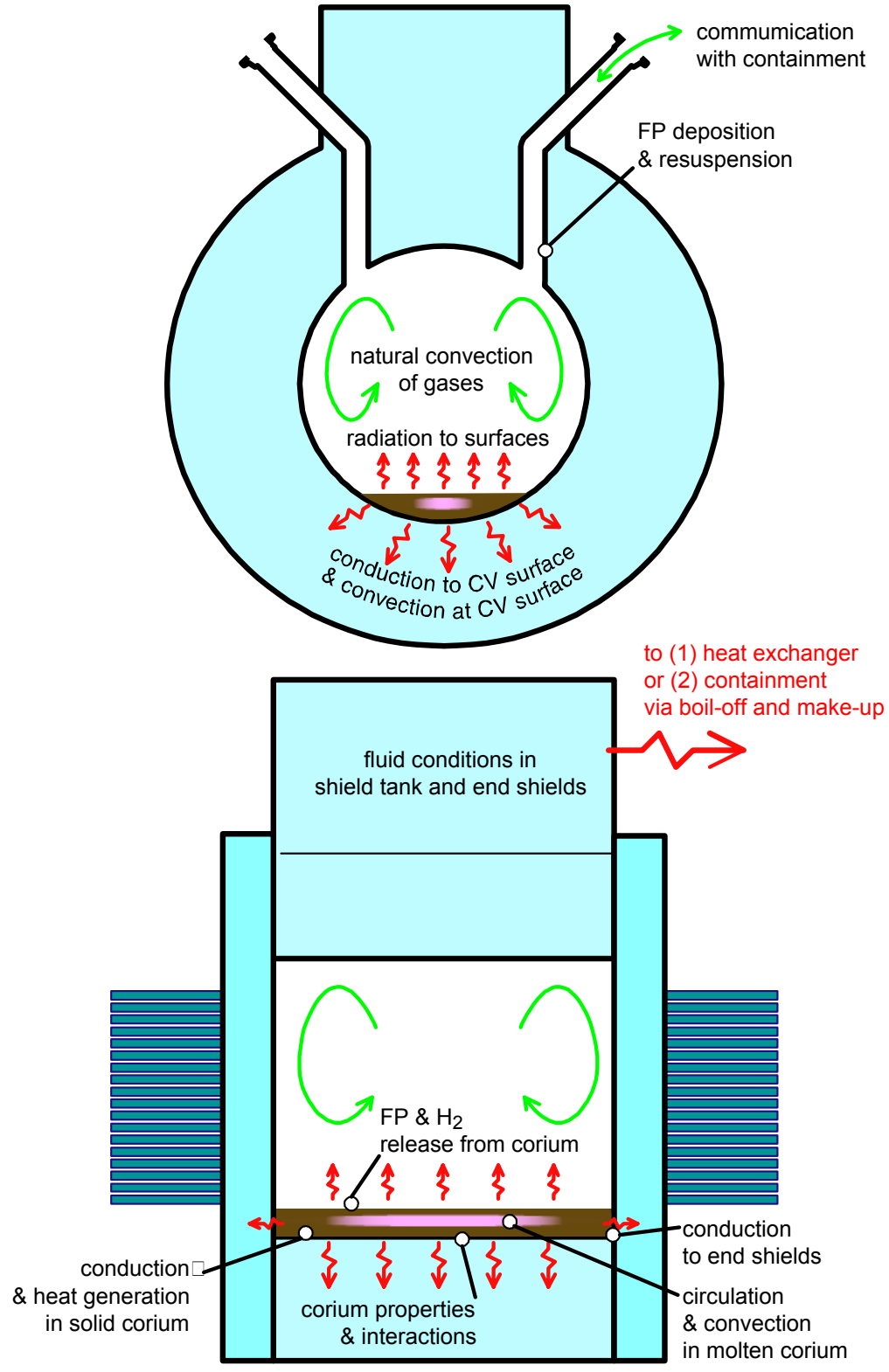

Figure 2-5 Behavior of a Terminal Debris Bed in a Severe Core Damage Accident

3. FUEL CHANNEL BEHAVIOR

(D.B. Sanderson and T. Nitheanandan)

3.1 Limited Core Damage Accidents with Degraded Cooling at Decay Power

In this section, our current understanding of the behavior of a CANDU fuel channel under core damage accident conditions is summarized. The knowledge base comes from over 30 years of R&D on the current CANDU fuel channel design [1,2], which forms the basis for our understanding of the new ACR fuel channel design.

3.1.1 Fuel Channel Integrity

During an event with degraded heat removal, the pressure-tube temperature increases due to convective heat transfer from the hot coolant and radiation from the overheated fuel bundles. As the pressure-tube temperature increases, its yield stress decreases and it will begin to deform plastically under applied loads. Depending on the temperature and pressure transients experienced by the pressure tube, it may sag towards the bottom of the calandria tube or radially expand (balloon).

In assessing the consequences of a postulated accident sequence, one of the determining factors is the integrity of the fuel channels. If the fuel channels remain intact, the moderator cooling will maintain core geometry. The assessment of the integrity of fuel channel components is made systematically:

1. Determine the temperature and pressure transient experienced by the pressure tube to ascertain whether or not conditions are such that it will deform,
2. Based on the temperature distribution in the pressure tube, determine the potential for localized deformation and rupture, and
3. Determine the ability of the calandria tube to withstand the pressure and temperature transients that result from pressure tube deformation and/or rupture.

3.1.2 Pressure Tube Sag

The creep rate of Zr-2.5Nb becomes significant at temperatures higher than 625°C [3,4]. As a result, when pressure-tube temperatures escalate beyond 625°C, the pressure tube tends to sag downwards due to the load exerted by the weight of the fuel (and the weight of the pressure tube itself) and contacts the calandria tube in a strip along the bottom [5] (Figure 2-3). The area over which the pressure tube and the calandria tube are in contact is governed by the amount of circumferential strain.

Large-scale sag experiments [5,6] investigated the sag characteristics when a pressurized and overheated pressure tube is loaded with material simulating the mass of the fuel. These experiments included small-scale sag experiments and large-scale (half-length of a pressure tube) experiments to study creep/sag with and without internal pressure. The experiments used reactor typical fuel channel components and simulated decay power through the use of electrically heated fuel element simulators. Testing was conducted over a wide range of conditions where pressure-tube heatup rate, annulus spacer position, internal pressure and moderator-water subcooling were varied. The dryout behavior of the calandria tube and the circumferential strain

behavior following pressure-tube sag were also studied in these tests. The main conclusions reached in these tests were:

- At temperatures above 700°C, the pressure tubes significantly deflected downwards with internal fuel loading.
- The rate of increase of temperature on the upper half of the pressure tube was unaffected by the contact between the pressure tube and calandria tube along the bottom.
- The pressure tube remained round within 2% of the diameter during sag.
- The area of sag contact depended strongly on contact load and the moderator subcooling.
- The heat transfer coefficient between the pressure tube and the calandria tube varied around the circumference, mainly because of the variation in the gap between the two tubes. A high contact-heat transfer coefficient was found at the bottom of the tubes where the separation was controlled by the roughness of the tubes. The heat transfer progressively decreased towards the top as the thickness of the gas filled gap increased.
- Higher pressure-tube heatup rates increased the initial contact temperature, the time in dryout, and the dryout area on the calandria tube for a given moderator subcooling.
- When line contact occurred during sagging contact, the rewetting front moved more quickly in the axial direction than in the circumferential direction.
- The film boiling that occurred on the calandria tube during tests quenched in all cases when the power was still on, even though the subcooling decreased during the test.
- Lower subcooling increased the time in dryout.
- In the experiments with the large film boiling patches, the calandria tube, not the pressure tube, deformed to increase the area of contact.
- The presence of a garter spring increased the time to contact between the pressure tube and the calandria tube, decreased the pressure-tube sag and resulted in a smaller dryout patch. Local deformation occurs in the pressure tube at the point of garter spring support.

Overall, the above tests and subsequent analysis have demonstrated the effectiveness of the moderator as a heat sink to remove decay and stored heat from a fuel channel during a postulated low-pressure LOCA + LOECC scenario.

3.1.3 Pressure Tube Integrity During Coolant Boil-Off

Overheated Zr-2.5Nb pressure tubes tend to strain circumferentially if the fuel channel remains pressurized. The rate of deformation is dependent on temperature, time at temperature, and stress [3]. The stress is a function of the internal pressure, radius of the tube and the wall thickness. For temperatures in excess of its yield point, the pressure tube deforms outwards under the influence of high internal pressure and, if the conditions are sustained, will come into contact with the surrounding calandria tube. If the pressure tube is exposed to relatively uniform heating conditions, the tube will tend to strain in a uniform fashion. If, however, the hydraulic conditions within the fuel channel result in a temperature gradient around the circumference of the pressure tube, the deformation will be localized.

At high temperatures, Zr-2.5Nb is ductile and can accommodate considerable strain before rupture [7,8]. Therefore, pressure-tube failure can only occur as a result of severe thinning or

necking at a given location. Because a ballooning pressure tube contacts the calandria tube and then is restrained and cooled, failure could only occur before contact if the strain was highly localized. Such conditions could arise from either stratified coolant conditions in which the top of the pressure tube is exposed to steam while the bottom is kept relatively cool by the presence of liquid, or by contact with fuel elements, bearing pads, or molten metal relocating to the bottom of the pressure tube. Channel integrity issues due to fuel element, bearing pad, and molten metal contact are discussed further below.

The temperature gradients formed around a pressure tube are a function of the local coolant conditions, fuel temperatures and localized heat fluxes. If the voiding rate is high, as in a large LOCA, the steam, coolant and fuel temperatures are expected to be relatively uniform and result in low circumferential temperature gradients in the pressure tube. If the voiding rate is low, the circumferential temperature gradient may be large with the top of the pressure tube heating up faster than the bottom of the tube. The pressure tube may deform locally and rupture prior to contact with the calandria tube, depending on the coolant pressure, the rate of heat up and the localization of the temperature gradient. Thus, the integrity of the pressure tube depends on the coolant boil-off rate, pressure tube heat-up rate and the fuel channel internal pressure.

An experimental program was conducted at AECL where the development of circumferential temperature gradients in a pressure tube containing stratified two-phase coolant was studied [9-11], Figure 3-1. The experiments simulated different phases of feeder draining expected during a LOCA. Three distinct scenarios were studied: coolant boil-off, steady steaming, and steam cooling. A total of 17 experiments were performed to determine the potential circumferential variations under different conditions of power, pressure and coolant flow. Pressures ranging from 1 to 5.6 MPa and fuel-element simulator (FES) bundle powers of 40 to 200 kW (20 to 111 kW/m), with variations in water level and steam flow, were investigated. The pressure-tube internal pressure, pressure-tube heat-up rate (bundle power), liquid level in the pressure tube and the steam or water inflow were controlled in these experiments. One end of the pressure tube was vented and the other end was closed to give a constant pressure. The test section consisting of a pressure tube and calandria tube was immersed in a tank of water. The channel was filled with water heated to saturation temperature at the start of each test. The power to the FES bundle was increased to the required level and the heat from the FESs began to boil off the stratified liquid at the bottom of the pressure tube.

These tests have shown that circumferential temperature gradients developing on a pressure tube as the coolant boils off are unlikely to challenge the integrity of the pressure tube for the conditions expected of a LOCA in current generation CANDU reactors. The data also indicates that with an internal pressure of ~4 MPa, a top-to-bottom temperature difference of ~590°C is required to rupture the pressure tube. In comparison, at 5.6 MPa, a top-to-bottom temperature difference of 435°C is likely to cause a rupture in a fuel channel, demonstrating the expected trend that as the internal pressure increases the top-to-bottom temperature difference required to fail a pressure tube decreases. The data from the experiments was used in validation of the thermalhydraulics code CATHENA [12].

3.1.4 Pressure-Tube Ballooning and Moderator Subcooling Requirements

For degraded channel cooling events where the internal pressure is sufficiently high, the pressure tube can uniformly balloon into contact with the calandria tube.

Accidents that result in overheated fuel temperatures and deformation of the pressure tube and subsequent ballooning contact with the calandria tube rely on the combined performance of the pressure tube and calandria tube to maintain channel integrity [13, 14]. For such events, channel integrity depends on the mode of heat transfer on the outside of the calandria tube following pressure tube contact – film boiling results in higher calandria-tube temperatures than does nucleate boiling. Information on the behavior of the fuel channel under such conditions has been obtained through reactor-typical experiments and analysis. It was observed during these experiments that the mode of heat transfer from the calandria tube to the moderator depends mainly on the moderator subcooling, the pressure-tube temperature at the time of contact, the incident heat flux to the pressure tube and channel pressure at the time of contact.

The initial contact between the hot pressure tube and the cold calandria tube results in a spike in the heat flux to the moderator. The magnitude of the spike depends on the pressure-tube temperature at contact and the contact conductance between the pressure and calandria tubes. The magnitude of the spike and the critical heat flux (CHF) on the outer surface of the calandria tube determine the boiling regime on the outer surface of the calandria tube (film or nucleate boiling). If the calandria tube remains in nucleate boiling, the calandria tube remains cool (<130°C), and has sufficient strength to arrest further deformation of the pressure tube. Heat can then be removed from the fuel, by conduction and radiation to the pressure tube and calandria tube, and then by convection to the moderator. If the calandria tube goes into extensive film boiling (CHF exceeded), calandria-tube temperatures increase (>400°C) and further fuel channel deformation is possible. Steps are therefore taken to ensure that the calandria tube remains in nucleate boiling following contact with an overheated pressure tube.

For this type of event, the pressure tube acts as a passive fuse, deforming only when it overheats sufficiently to create a low-resistance heat transfer path to the moderator. The low resistance is due to the short physical distance from the fuel to the pressure tube, the relatively thin walls of the pressure tube and calandria tube, and the enhanced heat transfer through the two contacting tubes. A number of studies have been conducted to determine the contact conductance between pressure tubes and calandria tubes, and the role of pressure tube deformation and roughness.

A series of experiments, called the contact boiling tests, examined the moderator subcooling requirements for various conditions. In these tests, a section of pressure tube was heated using electric heaters inside a calandria tube, which was submerged in a tank of water, Figure 3-2. Deformation behavior was inferred from the internal pressure, pressure-tube temperature transient, and the time and temperature at which the pressure tube contacted the calandria tube. A photograph of a ballooned pressure tube from a typical contact boiling experiment is shown in Figure 3-2b.

The boiling regimes observed in the contact boiling experiments were used to determine the subcooling requirements for the power reactors [7]. Minimum moderator subcooling requirements are set to ensure that fuel channel integrity is not threatened as a result of an overheated pressure tube contacting its calandria tube.

3.1.5 Impact of Localized Hot Spots on Pressure Tube Integrity

Experimental and analytical studies have demonstrated that under certain conditions the integrity of a pressure tube may be compromised when localized hot spots are allowed to develop on a

pressure tube. Local hot spots on the pressure tube may develop from: (a) bearing-pad (BP) contact (b) fuel element (FE) contact or (c) molten-material contact.

When a fuel element, bearing pad, or molten metal comes into contact with the pressure tube at high temperatures, the majority of the pressure tube's circumference will be heated by convection and thermal radiation. At the contact locations, however, conduction heat transfer combines with convection and thermal radiation heat transfer modes and localized hot spots develop. Whether the pressure tube will fail locally depends on the magnitude of the hot spots, as well as the global temperature and pressure transients the pressure tube experiences. After the pressure tube sags or balloons into contact, heat transfer to the calandria tube is enhanced and the impact of local heating is diminished.

In the following sections the available data on the three possible methods of contact heat transfer during LOCA is summarized.

3.1.5.1 Pressure-Tube Integrity and Bearing-Pad Contact

A series of small and large-scale experiments have been conducted to assess the thermal-mechanical response of the pressure tube to hot spots created by conduction from overheated fuel elements through their bearing pads [15,16]. Small Zircaloy appendages attached to the fuel elements, called bearing pads, support the fuel bundles inside the pressure tube. Heat transfer through the bearing pad to pressure tube contact could potentially cause a local hotspot, which would in turn influence local deformation patterns.

Twelve full-scale experiments [15] were conducted in which electrically heated fuel element cladding, with attached bearing pad, were held in contact with a section of pressure tube, Figure 3-3. The mass of the bundles was represented by use of tungsten cans as shown in Figure 3-3a. Tests were conducted in steam and simulated steam (75% Ar and 25% O_2 gas) atmospheres.

The experimental program has shown that the hot spots created by bearing-pad contact were relatively small, that temperature gradients were similarly small (less than 40ºC), and that adjacent bearing pads tended to limit and smooth out the bearing pad induced hot spots around the pressure-tube circumference. Following the appearance of a bearing-pad induced hot spot; the pressure-tube section was observed to bulge locally (aneurysm) beneath the bearing pads, limiting the contact area by increasing the gap between the two surfaces. The rate of heat transfer from the bearing pads to the pressure tube was reduced as contact deteriorated and thus did not threaten pressure-tube integrity.

The above findings were further studied by post-test analysis using the CATHENA fuel channel code [16] that showed the contact conductance between the bearing pad and the pressure tube decreasing during the ballooning phase for each test. The localized bulging of the pressure tube beneath the bearing pad reduced the rate of heat transfer and thus became self-limiting.

3.1.5.2 Pressure-Tube Integrity and Fuel-Element Contact

The potential exists for an overheated fuel element to deform and come into contact with its pressure tube by a number of mechanisms:

- Localized bulging of the pressure tube beneath supporting bearing pads (as noted above) which would allow the pressure tube to contact the fuel element between the pads,
- Fuel element sagging due element weight and reduced structural strength at elevated temperatures, and
- Fuel element bowing due to differential thermal expansion between fuel elements in a fuel bundle.

When an overheated fuel element contacts its pressure tube, it creates a localized hot spot. This hot spot could lead to localized plastic strain similar to the situation for bearing pad contact.

Two experimental programs have been performed to assess the thermal-mechanical response of the pressure tube to contact from an overheated fuel element. The first program was a series of small-scale, single effect tests to investigate heat transfer coefficients under well-controlled conditions. The second was a series of eight integrated experiments where overheated fuel element simulators were forced into contact with a pressure tube during ballooning, Figure 3-3. These tests used pressure tubes and electrically heated fuel element simulators, similar to those used in the bearing-pad / pressure-tube interaction program. The fuel-element to pressure tube contact loads in the tests represented roughly one half the weight of a fuel bundle. This is substantially higher than the contact loads expected during a postulated LOCA + LOECC event where an overheated fuel element deforms into contact with its pressure tube and are thus considered conservative.

The small-scale and integrated experimental programs have shown that fuel-element to pressure-tube contact heat transfer (and hence formation of a pressure-tube hot spot) is strongly dependant on the contact load between the two surfaces and the temperature of the fuel element prior to initial contact. The larger-scale experiments have also shown that if the temperature gradients at the hot spots created by fuel element contact are greater than 80ºC, pressure-tube integrity may be threatened by excess localize strain when system pressures are above 3 MPa.

3.1.5.3 Pressure-Tube Integrity and Molten Metal Contact

For severely degraded channel cooling, and for events where the zirconium/steam reaction can add significant energy to a channel, the channel conditions could lead to the formation of small amounts of molten material.

Two series of experiments have been conducted to assess the thermal-mechanical response of a CANDU fuel channel to molten material contacting the inside surface of its pressure tube. The first series of experiments focused on the impact of small quantities of molten Zircaloy-4 (from overheated fuel elements and their associated end caps) relocating onto the pressure tube during a large break LOCA+LOECC. The second series studied the impact of molten material contact on fuel channel failure times during postulated single channel severe flow blockage events. This second series of tests will be further discussed in Section 3.2.

For the seventeen tests completed as part of the first series, melt masses of 23 to 110 g were dropped onto pressure tubes pressurized from 1 to 8 MPa with moderator subcoolings of 10 to 40ºC [17,18]. The test apparatus consisted of a single graphite heater rod concentrically placed in a 1.7-m long section of pressure tube inside a section of calandria tube, Figure 3-4. The fuel channel section was immersed in a tank of subcooled light water. A Zircaloy-4 ingot was placed inside machined slots within the graphite heaters that simulated decay power. In the tests, a

pressure tube pressurized with argon and heated internally with the graphite heater balloons into contact with its calandria tube. The power to the graphite heater was increased following ballooning contact to melt the Zircaloy-4 ingot and the molten material flowed onto the bottom of the ballooned fuel channel assembly.

These tests demonstrated that for the relatively small masses (up to 110 g) and channel pressures up to 8 MPa, fuel channel integrity was maintained provided the calandria tube was in stable nucleate boiling prior to molten material contact. For the tests done at 8 MPa, however, there was noticeable deformation of the pressure-tube/calandria-tube combination beneath the melt even though channel integrity was maintained. The findings from the two tests at high system pressures (more indicative of a single channel flow blockage event) led to the extension of this program with a revised objective of determining the amount of molten material required to fail a fuel channel at full system pressure. This R&D program (discussed in Section 3.2) provides a technical basis for the timing of fuel channel failure for a postulated single channel severe flow blockage event.

3.1.6 Impact of Garter Springs on Fuel Channel Integrity

The spacer design for current generation CANDU reactor is a snug-fit Inconel garter spring with a coil diameter of ~6 mm. The purpose of this spacer is to maintain a physical gap between the hot pressure tube and cool calandria tube during normal operating conditions. During LOCA+LOECC conditions, the pressure tube must deform around (ballooning scenario) or between (sagging scenario) garter springs in order to contact its calandria tube and make effective use of the moderator as a heat sink. The presence of garter springs has been shown to not interfere with pressure-tube ballooning [13] or have a significant effect on pressure-tube/calandria-tube contact times for a low-pressure sagging scenario [6]. In both instances, it has also been shown that the presence of the garter springs has no significant impact on the radial heat transfer from the pressure tube to the water-cooled calandria tube.

R&D has also been performed to assess the potential for an alloying interaction between the Inconel garter spring and the Zr-2.5Nb pressure tube during a high-temperature LOCA+LOECC transient where pressure-tube temperatures may exceed 1000ºC. This program consisted of a series of experiments where the influence of oxide thickness, temperatures and atmosphere on the interaction kinetics was studied. The major finding of this work was that Inconel and Zr-2.5Nb will interact to form a low-melting temperature alloy at temperatures as low as 960°C in an inert atmosphere. Nevertheless, in an oxidizing atmosphere, such as that found in the CANDU annulus system, the protective ZrO_2 surface layer on the pressure tube is maintained. This oxide layer raises the threshold temperature for the alloying interaction from 960ºC to ~1350°C.

Should it happen, the Inconel / Zr-2.5Nb reaction occurs by diffusion of Ni/Cr/Fe into Zr-2.5Nb which leads to the formation of a low-melting alloy. The severity of the alloying interaction depends on the amount of Inconel that interacts with the Zr-2.5Nb and ranges from through-wall penetration to minor microstructural changes of the pressure-tube material. In either case, the interaction was limited to the pressure tube and integrity of the surrounding calandria tube was not affected.

3.1.7 Thermal-Chemical Behavior of the Fuel Channel in the Late Phases of a LOCA+LOECC

During the later stages of a LOCA+LOECC event, steam is the only coolant available within the channel. If the Zircaloy-4 cladding temperatures exceed ~1000ºC, decay power is supplemented by the exothermic zirconium/steam reaction and hydrogen in produced. The rate of the reaction is low at 1000°C, but is much faster at higher temperatures providing a positive feedback mechanism for channel overheating. Heat removal from the channel under such conditions is axially by steam flow and radially to the moderator. The balance between the heat generation and removal rates dictates the peak fuel temperatures, fission product releases and hydrogen production rates.

At relatively high values of steam flow (>100 g/s), the convective cooling provided by the steam is sufficient to prevent most of the fuel cladding and pressure tubes from attaining temperatures much above 1000°C. For nearly stagnant conditions (<1 g/s), the heat transfer by convection is negligible and fuel temperatures can be sufficiently high for the zirconium / steam to take place. At low steam flow rates, however, the zirconium/steam reaction is limited by the available steam. Under such conditions, radial heat transfer to the moderator effectively limits fuel temperatures and hydrogen production is limited by the unavailability of steam for the zirconium/steam reaction. For intermediate steam flow rates, a trade-off exists between the availability of steam for zirconium oxidation and its contribution to convective cooling. Under a narrow range of flow conditions, the exothermic zirconium/steam reaction can account for about half of the heat generated within the fuel channel, and can cause very high temperature transients.

Separate effect and integrated experiments have been performed to understand the thermal-chemical behavior of a CANDU fuel channel under such conditions. The separate effect tests provided information on zirconium oxidation kinetics under well-controlled conditions [19-21] and the integrated experiments assessed the impact of the energy released from this exothermic process on channel thermal behavior [22-25].

The integrated experiments used reactor-typical geometries with either electrically heated fuel element simulators [22,23] or actual UO_2 fuel bundles heated externally with a hydrogen/steam torch system [24,25]. Both series of tests provided information on the thermal, mechanical and chemical behavior of the fuel bundle under LOCA+LOECC conditions that was later used in code development and validation. The CHAN series of experiments (those that utilized the electrically heated elements) [22,23] had better control of boundary conditions and thus formed the basis for the development and validation of computer models in this area.

In the CHAN series, the test section consisted of a 28-element bundle of fuel element simulators surrounded by a reactor-grade pressure tube mounted inside a water-cooled Zircaloy-2 calandria tube. During the experiment, superheated steam at 700ºC entered the test section from the steam superheater, Figure 3-5. The 28 electrically heated fuel element simulators then heated the steam until zirconium surfaces in the test section were at sufficient temperatures to sustain the exothermic zirconium-steam reaction. The reaction produced hydrogen and energy, which further raised surface temperatures to over 1700ºC. The steam and hydrogen gas mixture left the test section and flowed into the condenser where the steam was condensed and hydrogen production monitored. The data from these integrated experiments provided valuable

information of the integrated response of a fuel channel under simulated LOCA+LOECC conditions, which was used to validate CATHENA under such conditions [26]. The experiments and subsequent analysis also demonstrated the effectiveness of the moderator for removing cooling the fuel under such conditions.

3.2 Fuel Channel Behavior in a Single-Channel Event with Degraded Cooling at Full Power

As noted in Section 2.1.1, there are accident scenarios where the potential exists to have near stagnant flows in a fuel channel when the reactor is at full power and full system pressure. The pressure tube is expected to fail early in such a transient (as noted in Section 2.1.1) due to non-uniform straining. Pressurization of the fuel channel annulus, and impinging hot effluent from the pressure tube will cause the calandria tube to fail, ejecting steam and fuel fragments into the moderator. Failure of the fuel channel will trip the reactor, helping to limit the consequences of the event. Failure of the fuel channel also creates a coolant flow path through the calandria (and failed rupture discs) providing coolant for the fuel and limiting the consequences of the event.

The regulatory body within Canada (Canadian Nuclear Safety Commission) has requested the nuclear industry to assess the consequences of a single-channel event, should the pressure tube not fail due to non-uniform strain. Under such a scenario, the pressure tube would balloon into contact with its water-cooled calandria tube, transfers its stored energy to the calandria and cool down. The fuel, on the other hand, would continue to heat up and would eventually melt its cladding, end caps and end plates. Some of this molten Zr-4 would alloy with the UO_2 and the resultant molten material would relocate onto the lower surface of the ballooned pressure tube, Figure 3-6. This molten material would create an intense localized hot spot on the ballooned pressure tube / calandria tube combination, resulting in localized strain and failure. The molten material and other fuel debris would then be ejected from the channel into the moderator where it would generate a high-pressure steam bubble. The magnitude of the pressure pulse from the fuel channel rupture and subsequent interaction between the molten material and water would be dependant on the channel pressure and coolant temperature, amount of molten material available at the time of channel failure and the rate of heat transfer from the melt to the water. Together these parameters will determine the potential for an energetic steam explosion.

The R&D described in this section provides the technical basis to support the expectation that the pressure tube fails early in the transient. Also included is supplemental R&D to provide information on the expected behavior of the fuel channel, should the pressure tube not fail during ballooning.

3.2.1 Pressure Tube Ballooning and Failure Mechanisms

Sections 3.1.3 and 3.1.4 described the ballooning behavior of pressure tubes at pressures below 6 MPa, typical of the early stages of a large break LOCA for a standard CANDU power plant design. R&D has provided the basic understanding and models for predicting the ballooning behavior of Zr-2.5Nb pressure tubes, including the prediction of failure times for given stress and temperature transients. There has also been a significant amount of research on the deformation and failure of CANDU pressure tubes at pressures above 8 MPa.

There has been a total of twenty pressure-tube ballooning experiments performed where the system pressure was above 8 MPa. These were a combination of small-scale tests (where 0.5-m long sections of tubes without calandria tubes were directly heated by direct current or induction power supplies) and integrated tests (where the pressure tube was located inside a calandria tube and indirectly heated by an internal heater, Figure 3-2). The results of these experiments and the low-pressure tests have been used to validate the pressure-tube deformation model in CATHENA and to develop failure maps.

The tests have shown that circumferential temperature gradients as low as 55ºC are sufficient to cause a pressure-tube rupture during ballooning at 10 MPa. This supports the position that it is highly improbable that 6-m long pressure tubes would not fail during the early stages of a single channel event as circumferential temperature gradients higher than this are expected to develop during the initial coolant boiloff stage of the event.

In addition to failures induced by non-uniform circumferential temperature gradients during coolant boiloff, it has been determined that small quantities of molten Zircaloy-4 are enough to create localized failure of a voided pressure tube prior to ballooning contact with its calandria tube. If conditions within the fuel channel were such that any significant amount of molten material (from fuel cladding, end caps, and end plates) was generated and this material were to relocate onto the pressure tube, an intense localize hot spot would develop and lead to even earlier failure of the pressure tube. This has been demonstrated experimentally using the apparatus shown in Figure 3-4 where roughly 70 g of molten Zircaloy-4 was dropped onto a non-ballooned pressure tube at pressures ranging from 5 to 10 MPa.

Should the pressure tube not fail prior to ballooning contact during a single channel event, the fuel would continue to heat up and larger quantities of molten material would be generated. This would accumulate on the bottom of the pressure tube which is cooled by contact with the calandria tube. Eventually sufficient local heating will cause the pressure and calandria tubes to fail. The amount of molten material required to fail the fuel channel under such conditions has been speculated to be on the order of tens of kilograms. Recent experiments at AECL, however, have shown that as little as 150 g of molten zirconium is sufficient to fail a ballooned fuel channel when system pressures are above 8 MPa.

In addition to the above R&D to determine channel failure times and assess the amount of molten material available at the time of channel failure, the CANDU industry has embarked on a program to assess the consequences of ejecting a substantial amount of molten material (~25 kg) from a CANDU fuel channel into water. These tests, performed under the Molten Fuel Moderator Interaction (MFMI) program are discussed in the following section.

3.2.2 Molten Fuel Moderator Interaction Experiments

As noted in Section 3.2.1, the fuel channel is expected to fail before any substantial amount of molten material is generated during an event with degraded cooling to a single channel. As part of the defence in depth approach, however, current safety assessments for CANDU power plants conservatively consider a scenario that involves the generation of up to 25 kg of molten material inside the channel before channel failure. This molten material would then be ejected (with a driving pressure of ~10 MPa) into the moderator where it interacts with water and generates a steam pressure pulse. The magnitude of this pressure pulse depends on the interaction mode

between the melt and the water. Current predictions are that the melt will be finely fragmented upon ejection and that it will transfer its energy to the moderator as it is dispersed, creating a modest pressure pulse in the calandria vessel. An alternative process would have the melt interacting with the water in a classical "steam explosion" mode where large quantities of the melt fragment after ejection, creating a very large pressure pulse (or steam explosion) in the calandria vessel. As the potential for subsequent damage in the calandria is related to the magnitude of this pressure pulse, significant debate on the operative mode for a realistic event has occurred.

AECL is undertaking an experimental program (on behalf of the CANDU Owners Group) to confirm that the predicted interaction mode is operative to show that a highly energetic "steam explosion", and associated high-pressure pulse, is highly unlikely. The experimental apparatus for the Molten Fuel Moderator Interaction (MFMI) tests has been assembled, Figure 3-7 and is currently undergoing commissioning. The experiments will heat up a mixture of UO_2, Zr, and ZrO_2, representative of the molten material expected in a fuel channel, inside an insulated 1-m length of pressure tube. Once the molten material has reached the desired temperature, ~2400°C, the pressure inside the tube will be raised to about 10 MPa, and the pressure tube will fail at a pre-machined flaw, releasing the molten material into the surrounding tank of water. The experiments will use two different amounts of molten material (5 and 25 kg), and will investigate the effects of the material interacting with tubes representing neighbouring fuel channels.

3.3 Summary

For both low- and high-pressure accident scenarios, there is a large body of knowledge available to provide the basis for the ACR fuel channel from more than 3 decades of studying current-generation CANDU fuel channel behavior under accident conditions. This knowledge base includes the thermal-mechanical behavior of pressure tubes and calandria tubes, factors affecting pressure tube integrity such as temperature gradients, and the thermal-chemical behavior of a fuel channel. Only minor extensions are required to address phenomena that are sensitive to the dimensional changes in the ACR channel (e.g. pressure tube deformation in a larger diameter calandria tube).

3.4 References

1. L.A. Simpson, P.M. Mathew, A.P. Muzumdar, D.B. Sanderson, V.G. Snell, "Severe Accident Phenomena and Research for CANDU Reactors," Proceedings of the 10th Pacific Basin Nuclear Conference, Kobe, Japan, October 1996
2. M.H. Bayoumi, W.C. Muir, "Methodology for Fuel Channel Integrity in Large Break Loss of Coolant Accident," Proceedings of the CNS Annual Conference, Toronto, ON, June 1997
3. R.S.W. Shewfelt, L.W. Lyall, D.P. Godin, "A High-Temperature Creep Model for Zr-2.5 wt% Nb Pressure Tubes," Journal of Nuclear Materials, Vol. 125, pp. 228-235, (Also available as AECL 8156), 1984
4. R.S.W. Shewfelt, L.W. Lyall, "A High-Temperature Longitudinal Strain Rate Equation for Zr 2.5% Nb Pressure Tubes," Journal of Nuclear Materials, Vol. 132, pp. 41-46, 1985

5. G.E. Gillespie, R.G. Moyer, G.I. Hadaller, G.I., "An Experimental Investigation of the Creep Sag of Pressure Tubes Under LOCA Conditions," Proceedings of the 5th Annual CNS Conference, Saskatoon, SK 1984

6. Q.M. Lei, M.H. Bayoumi, "Assessment of Effects of Pressure Tube to Calandria Tube Sagging Contact on Safety Analysis Results," Presented at 22nd Annual Conference of the Canadian Nuclear Society, Toronto, June 10-13, 2001.

7. G.E. Gillespie, R.G. Moyer, G. Hadaller, J.G. Hildebrandt, "An Experimental Investigation into the Development of Pressure Tube/Calandria Tube Contact and Associated Heat Transfer under LOCA Conditions," Proceedings of the 6th Annual CNS Conference, Ottawa, ON, pp. 2.24-2.30, June 1985

8. R.S.W. Shewfelt, D.P. Godin, "Ballooning of Thin-Walled Tubes with Circumferential Temperature Variations," Res Mechanica, Vol. 18, pp. 21-23, Available as AECL 8317, 1986

9. Q.M. Lei, D.B. Sanderson, M.L. Swanson, G.A. Walters, H.E. Rosinger, "Experimental and Theoretical Investigation of Pressure Tube Circumferential Temperature Gradients During Coolant Boil-Off," Proceedings of the 13th Annual CNS Conference, Saint John, NB, June 1992

10. P.S. Yuen, K.A. Haugen, D.G. Litke, R.G. Moyer, H.E. Rosinger, "The Experimental Measurement of Circumferential Temperature Distributions Developed on Pressure Tubes Under Stratified Two-Phase Flow Conditions: Tests 1 to 5," Proceedings of the 10th Annual CNS Conference, Ottawa, ON, pp. 9.18-9.25, June 1989

11. B.G. Taylor, D.G. Litke, D.B. Sanderson, "Temperature Gradients on Pressure Tubes Due to Steam During Stratified Two-Phase Flow Experiments," Proceedings of the 12th Annual CNS Conference, Saskatoon, SK, June 1991

12. Q.M. Lei, T.M. Goodman, D.B. Sanderson, "Modelling Thermalhydraulic/ Thermal-Mechanical Behaivour of a Fuel Channel with Stratified Two-Phase Flow Using CATHENA," Proceedings of the Fifth International Conference on Simulation Methods in Nuclear Engineering, Montreal, PQ, September 1996

13. G.E. Gillespie, R.G. Moyer, P.D. Thompson, "Moderator Boiling on the External Surface of a Calandria Tube in a CANDU Reactor during a Loss-of-Coolant Accident," Proceedings of the International Meeting on Thermal Nuclear Reactor Safety, Chicago, IL, Available as AECL-7664, August 1982

14. D.B. Sanderson, R.G. Moyer, R. Dutton, "Effectiveness of the Moderator as a Heat Sink During a Loss-of-Coolant Accident in a CANDU-PHW Reactor," Proceedings of the International Centre for Heat and Mass Transfer Conference, Cesme, Turkey, May 1995.

15. R.G. Moyer, D.B. Sanderson, R.W. Tiede, H.E. Rosinger, "Bearing-Pad/Pressure-Tube Rupture Experiments," Presented at the 13th Annual CNS Conference, Saint John, NB, June 1992

16. T. Nitheanandan, Q.M. Lei, R.G. Moyer, "The Analysis of Bearing-Pad to Pressure-Tube Contact Heat Transfer Experiments," Proceedings of the 17th Annual CNS Conference, Fredericton, NB, June 1996

17. M.J. Brown, D.G. Litke, Q.M. Lei, D.B. Sanderson, "Molten Zircaloy-4/ Ballooned Pressure Tube Interaction Experiments," Proceedings of the 12th Annual CNS Conference, Saskatoon, SK, June 1991

18. D.B. Sanderson, K.W. Demoline, K.E. Locke, A.P. Muzumdar, "Experiments to Determine the Thermal-Mechanical Response When Molten Zircaloy-4 Flows onto a Ballooned Pressure Tube," Proceedings of the 10th Annual CNS Conference, Ottawa, ON, pp. 9.26-9.30, June 1989

19. V.F. Urbanic, T.R. Heidrick, "High-Temperature Oxidation of Zircaloy-2 and Zircaloy-4 in Steam," Journal of Nuclear Materials, Vol. 75, pp. 251-261, 1978

20. V.F. Urbanic, "Oxidation of Zirconium Alloys in Steam at 1000 to 1850°C," In Zirconium in the Nuclear Industry, ASTM STP 633, Lowe, A.L., Sr., and Parry, G.W., (eds.), American Society for Testing and Materials, pp. 168-181, 1977

21. V.F. Urbanic, W.W. Smeltzer, "Oxidation Properties of a Zirconium-2.5% Niobium Alloy in the Temperature Range 650 to 1000°C," Journal of the Electrochemical Society, Vol. 119, pp. 1527-1531, 1972

22. P.J. Mills, D.B. Sanderson, K.A. Haugen, G.G. Haacke, "Twenty-Eight-Element Fuel-Channel Thermal-Chemical Experiments," Proceedings of the 17th Annual CNS Conference, Fredericton, NB, June 1996

23. D.B. Sanderson, K.A. Haugen, R.G. Moyer, H.E. Rosinger, "Out-of-Pile Fuel Channel Experiments for Severe Accident Conditions," Proceedings of the American Nuclear Society International Topical Meeting on Safety of Thermal Reactors, Portland, OR, pp. 92-100, July 1991

24. S.L. Wadsworth, G.I. Hadaller, R.M. Sawala, E. Kohn, "Experimental Investigation of CANDU Fuel Deformation during Severely Degraded Cooling", Proceedings of the International ANS/ENS Topical Meeting on Thermal Reactor Safety, San Diego, CA, February 1986

25. G.I. Hadaller, R. Sawala, E. Kohn, G.H. Archinoff, S.L. Wadsworth, "Experiments Investigating the Thermal-Mechanical Behavior of CANDU Fuel under Severely Degraded Cooling," Proceedings of the 5th International Meeting on Thermal Nuclear Reactor Safety, Karlsruhe, Germany, September 1984.

26. Q.M. Lei, D.B. Sanderson, H.E. Rosinger, "High-Temperature Validation of CATHENA Against a 28-Element Thermal-Chemical Experiment," Proceedings of the 15th Annual CNS Conference, Montreal, PQ, June 1994

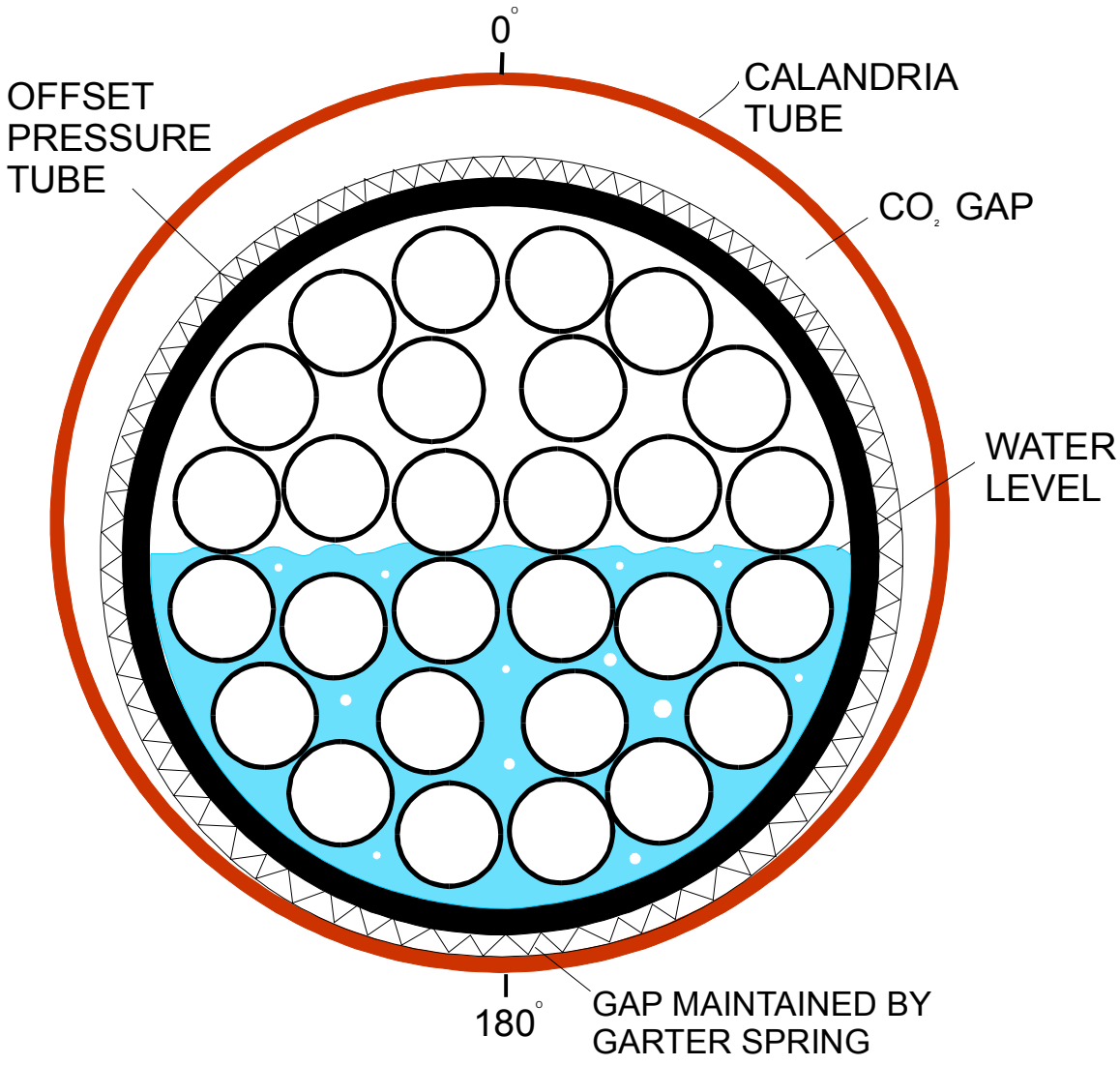

Figure 3-1 A Cross-section View of a Fuel Channel During Coolant Boiloff

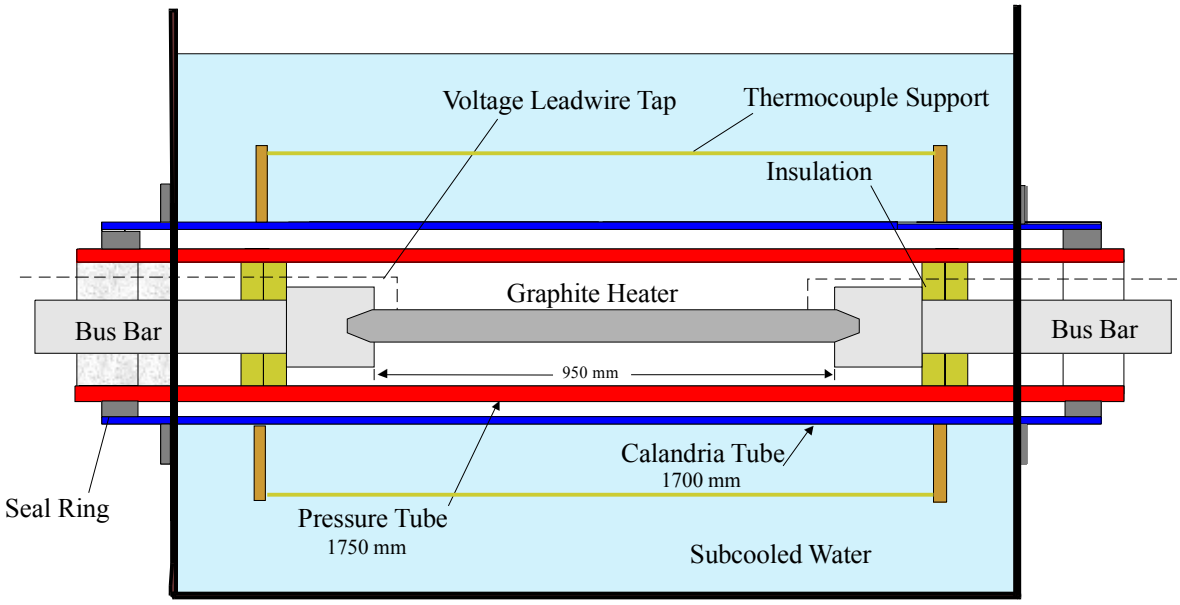

(a)

(b)

Figure 3-2 A Schematic Showing Apparatus used for the Contact Boiling/Moderator Subcooling Tests (a) and Post-test Photograph of one End of a Ballooned Pressure Tube (b)

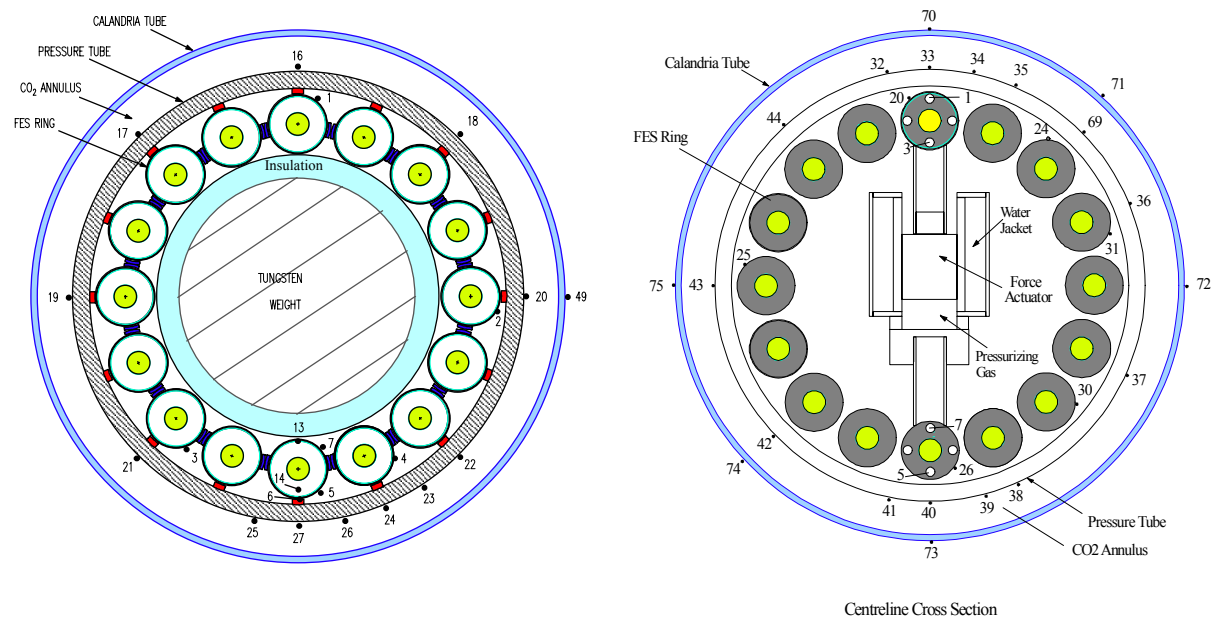

Figure 3-3 Cross-Section of Test Assemble Used to Determine Thermal-Mechanical Response of a Ballooning Pressure Tube to (a) Bearing-Pad and (b) Fuel Element Contact

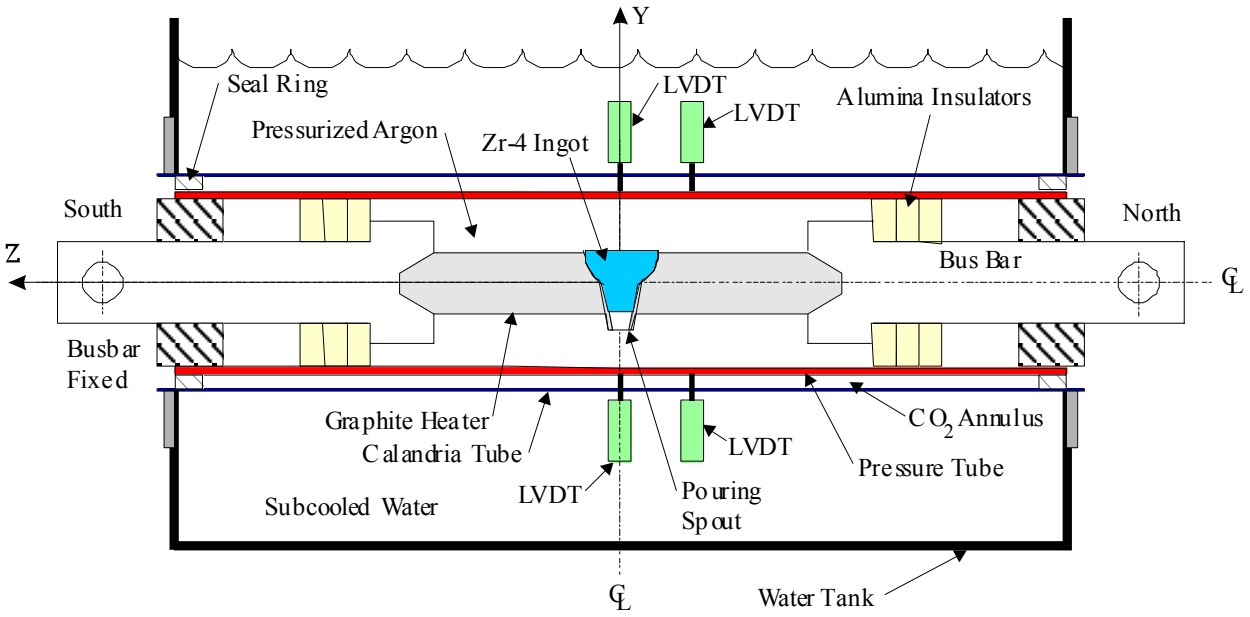

Figure 3-4 Schematic of Test Assemble Used to Determine Thermal-Mechanical Response of a Pressure Tube to Molten Material Contact

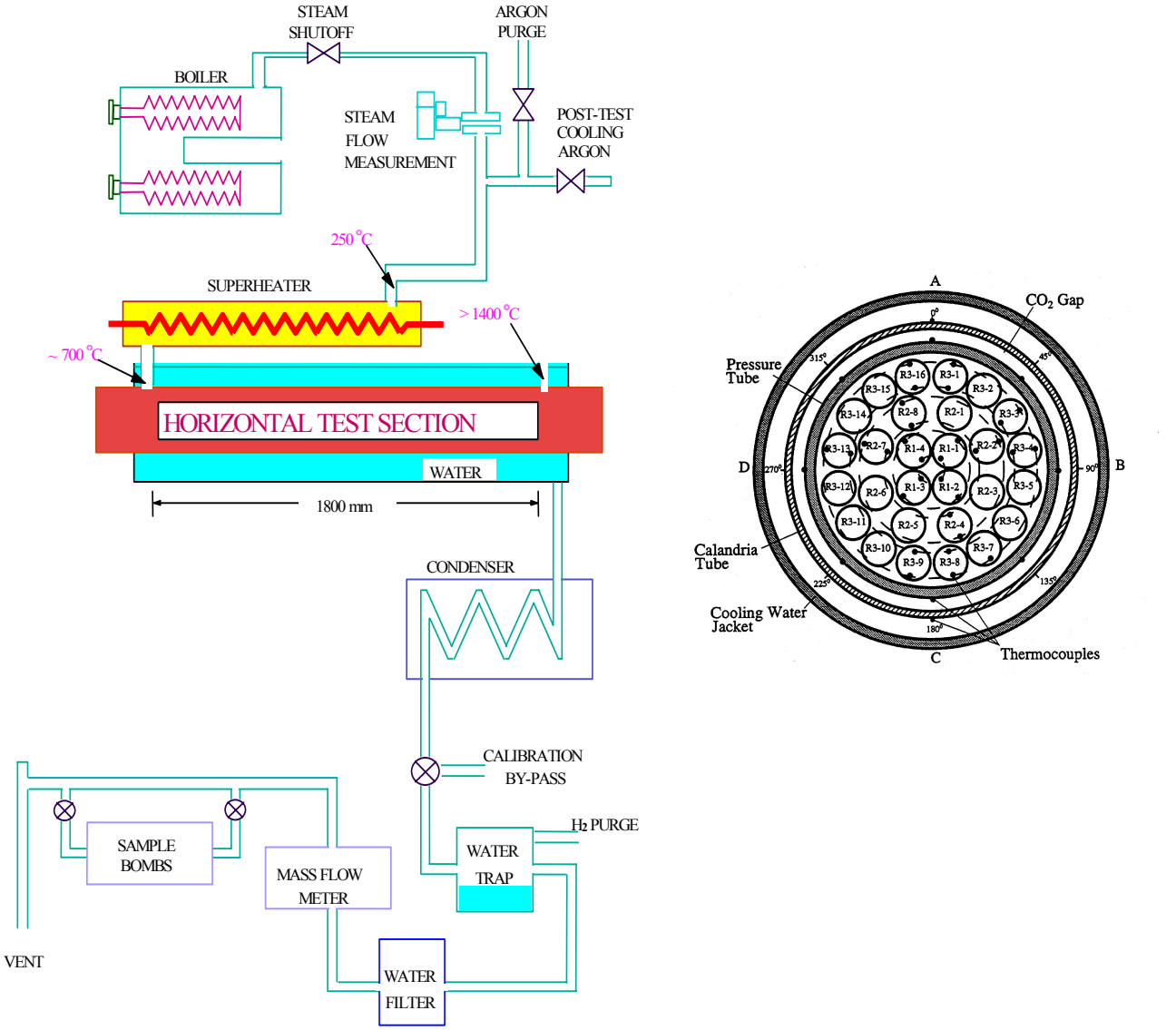

(a) (b)

Figure 3-5 Layout of the CHAN Thermal-Chemical Experimental Facility (a) and Cross-section of the Fuel Channel Showing Electrically Heated Fuel Elements and Instrumentation

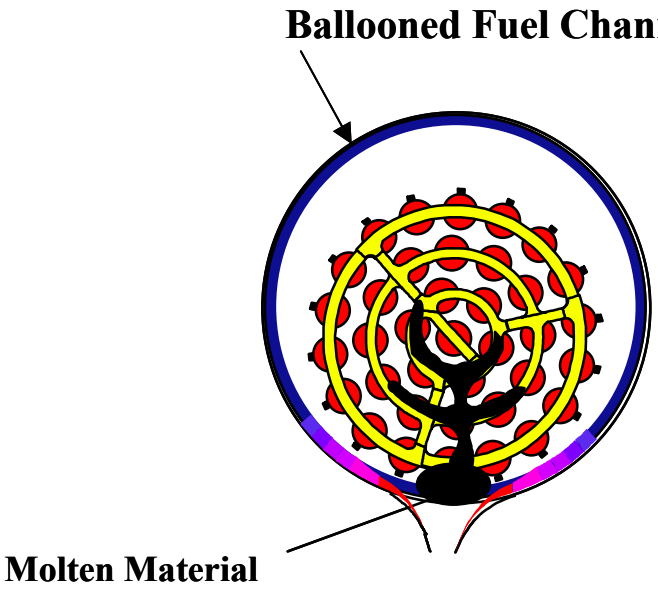

Figure 3-6 Schematic Showing Fuel Channel Failure Mechanism due to Relocation of Molten Material onto a Ballooned Pressure Tube

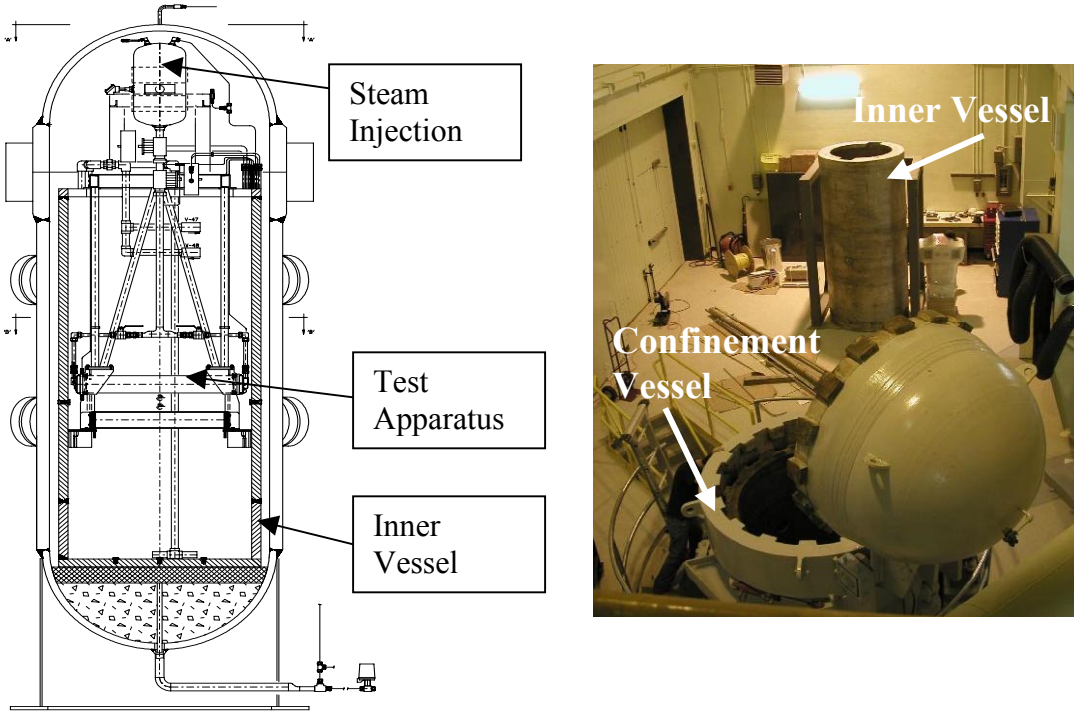

Figure 3-7 Schematic (a) and Photograph (b) of the Molten Fuel Moderator Interaction Test Facility

4. FUEL AND FISSION PRODUCT BEHAVIOR
(L.W. Dickson)

4.1 Fuel Behavior

CANDU fuel response to an accident with degraded cooling at decay power (LOCA + LOECC) is characterized by a rapid decrease to decay power levels and a rapid fuel-cladding heatup due to radial redistribution of the stored energy in the fuel. System depressurization causes the internal fission-gas pressure to stress and expand the fuel cladding [1]. Fuel cladding expansion causes a rapid increase in the void volume and a corresponding rapid drop in pressure inside the element, due to the small initial void volume. Cladding failure and oxygen embrittlement may also occur at this stage. As a core damage accident event progresses, additional phenomena occur including cladding melting and relocation, UO_2/Zircaloy interaction and dissolution, and urania oxidation and volatilization.

The behavior of CANDU fuel under accident conditions has been extensively studied to develop a complete understanding of the mechanisms involved. The research strategy has been to conduct separate-effects tests, develop models of the behavior, integrate the models into computer codes to predict the accident response, and to perform integrated all-effects tests for computer code validation. This section provides an overview the Canadian experimental database underlying our understanding of ACR fuel behavior under core damage accident conditions.

4.1.1 Laboratory Separate-Effects Tests

This section summarizes the laboratory separate-effects experiments performed on cladding strain and failure, cladding oxidation and embrittlement, cladding melting and relocation, UO_2/Zircaloy interaction and dissolution, and urania oxidation and volatilization.

4.1.1.1 Cladding Strain and Failure Tests

Laboratory tests were conducted to study the ballooning and failure properties of Zircaloy fuel cladding [3-6]. Over 700 tests were performed to study the effects of material properties (as received, heat-treated and Zr-Be brazed[1]), internal pressure, maximum temperature, heating rate and test atmosphere (vacuum and steam). In temperature ramp tests (heating rate from 5 to 100°C/s), the effect of steam oxidation becomes significant when the temperature exceeds 1000°C. The oxidation increases the strength of the cladding but reduces its ductility. Two different high-temperature cladding failure mechanisms were identified: (1) failure due to local over-strain, which includes “fracture” by growth of voids by power-law creep and “rupture” due to dynamic recovery or recrystallization, and (2) failure due to beryllium-assisted intergranular cracking. A mechanistic microstructural model for CANDU cladding strain and failure under transient conditions was developed [6].

[1] The Zr-Be brazing is used to attach appendages (bearing pads, element spacers and heat-transfer enhancing buttons) to the cladding.

4.1.1.2 Fuel Cladding Oxidation and Embrittlement Tests

The Zircaloy-4 fuel cladding will be oxidized in many reactor accident scenarios, impairing its ability to remain intact under the loads induce by the injection of emergency core cooling (ECC). Urbanic and Heidrick conducted experiments and developed a model for cladding oxidation at high temperatures in steam [7]. Sawatzky proposed the following quench failure criterion for CANDU fuel cladding: the cladding may fail if less than half the cladding thickness has an oxygen concentration less than 0.7 wt% [8]. Tests were performed to verify this criterion [9]. Capsules of fuel cladding were oxidized in steam at temperatures between 1000 and 1500°C and quenched with water (Figure 4-1). The results, whether or not the capsules remained intact, were compared with the predictions of various failure criteria. The Sawatzky criterion was shown to be suitable for CANDU fuel cladding subjected to the loads induced by ECC injection.

4.1.1.3 Cladding Melting and Relocation Tests

High-temperature bundle-sag tests were performed to obtain an understanding of the interactive phenomena involved in the generation and relocation of molten material in a fuel bundle [10,11]. Unirradiated fuel bundles located inside an insulating shroud were heated to high temperatures using an oxy-hydrogen torch. Two 37-element bundles were heated to 1700°C and a 19-element bundle (made by removing the outer ring of elements from a 37-element bundle) was heated to 1900°C. The zirconium-steam reaction increased the temperatures observed in the tests. Molten materials formed and relocated to inter-pellet gaps, fuel pellet cracks and regions of inter-element contact. Relocation resulted in a reduction of the surface area of the melt compared to the initial bundle geometry. This reduction in surface area was credited with reducing the rate of Zircaloy oxidation [12]. Two mechanisms resulting in a reduction in the area of Zircaloy-4 cladding exposed to the steam were confirmed in smaller scale tests: the formation of a zirconium oxide crucible around the fuel pins, and the relocation of molten cladding within the crucible [13]. The reduction in the surface area exposed to steam limits the temperature escalation under accident conditions.

4.1.1.4 UO_2/Zircaloy Interaction and Dissolution Tests

Experiments were performed on the dissolution of UO_2 in molten Zircaloy-4 in the temperature range from 2000 to 2500°C [14-17]. The samples were prepared by installing a charge of Zircaloy-4 in a hole drilled into a UO_2 fuel pellet. Tests were also performed using Zircaloy-4 charges containing 25 atom% oxygen. The samples were heated as rapidly as possible from 1550°C to the target temperature (initial heating rates of 11°C/s, declining to ~7°C/s as the target temperature was approached) in a high-purity argon atmosphere. To account for UO_2 dissolution occurring during heating, the "isothermal" heating period was timed from the moment that the alloy charge melted. The test results indicate that the melt saturates rapidly with respect to uranium content (Figure 4-2). Studies of the dissolution of ZrO_2 in molten Zircaloy-4 were also performed and melting points of Zircaloy-4 / oxygen alloys were measured in this test program.

4.1.1.5 Urania Oxidation and Volatilization Tests

Tests were performed to study the oxidation and volatilization of UO_2 in air, steam and inert gaseous environments at temperatures ranging from 1500 to 2100°C [18,19]. Three series of tests were performed on volatilization of unirradiated UO_2 and two series of tests were

performed using irradiated UO_2 samples. Higher oxygen partial pressures produced higher rates of UO_2 volatilization for a given temperature. The volatilization rate showed an Arrhenius-type dependence on temperature, with the activation energy increasing with decreasing oxygen partial pressure. No significant differences were observed between the volatilization rates for irradiated and non-irradiated samples; the slightly lower steam-atmosphere volatilization rate of irradiated UO_2 compared to unirradiated UO_2 was likely due to a slight addition of hydrogen to the steam in the irradiated-fuel tests. Volatilization rates were also measured in steam between 1200 and 1700°C in a larger-diameter apparatus at lower gas velocity. The volatilization rates in the large-diameter apparatus were lower, but they showed approximately the same activation energy as the rates in the smaller-diameter apparatus. The data from these tests are being used to develop and validate models for oxidation and volatilization of UO_2 [20,21].

4.1.2 Integrated In-Reactor Tests

Integrated in-reactor tests of CANDU fuel behavior under loss-of-coolant accident (LOCA) and limited core damage accident conditions were performed to provide data for reactor safety code validation.

4.1.2.1 CANDU Fuel LOCA Tests

Six CANDU-type fuel elements, containing UO_2 fuel and clad in Zircaloy, were subjected to transient conditions simulating a hypothetical large-break LOCA in a CANDU reactor [1,22,23]. The maximum transient cladding temperatures were about 1000°C. Two single-element experiments were conducted in the X-2 loop of the NRX research reactor at the AECL Chalk River Laboratories. The other four elements were tested together in a single transient in the Power Burst Facility at the Idaho National Engineering Laboratory. The fuel elements were instrumented both internally and externally to measure fuel and cladding temperatures, and internal element pressures. Coolant temperature and pressure were also monitored during the tests. These in-reactor tests showed that CANDU fuel elements can tolerate moderate cladding-strain levels without failure under typical LOCA conditions [1]. A small diametral cladding strain is effective in rapidly reducing the internal gas pressure, because of the relatively low void volumes in CANDU fuel elements. The cladding strain was non-uniform along the element. The cladding was shown to be stronger in the heat-affected zones than the as-received regions. No significant effect of irradiation on the cladding or fuel pellets, or of fission products on the cladding was observed. The transient fission-gas release during these tests was a small fraction (<0.1%) of the available inventory. Several parameters from the tests were used for comparison with computer code calculations, including fuel cladding strain, internal element gas pressure, the mechanisms and timing of fuel element failure, fuel centreline temperature, cladding microstructure, and the thickness of zirconia and oxygen-stabilized α-Zircaloy layers on the cladding.

4.1.2.2 Blowdown Test Facility Experiments

The Blowdown Test Facility (BTF) experiments were performed in the NRU reactor at the Chalk River Laboratories under the sponsorship of the CANDU Owners Group (COG) [24,25]. Four BTF in-reactor experiments were performed to improve the understanding of CANDU fuel and

fission-product behavior under accident conditions, and to provide data for use in reactor safety code validation.

The insulated BTF test assemblies were oriented vertically in a Zircaloy re-entrant flow tube, which fitted inside a thick-walled stainless-steel pressure tube (test section) located in the reactor core (Figure 4-3) [25-27]. The BTF test section and the NRU reactor core had separate heat transport systems. Test assemblies in the BTF were cooled with pressurized water or saturated steam. An accident sequence was initiated by isolating the in-reactor test section from the rest of the coolant loop, and voiding the coolant through an instrumented blowdown line and a wire-mesh filter into a sealed tank. Steam, inert gas and cold water were used for post-blowdown cooling in the BTF. The blowdown line was instrumented to measure coolant thermal hydraulic parameters and fission-product gamma emissions.

The BTF test conditions are summarized in Table 4-1.

In the BTF-107, a three-element cluster of CANDU-sized fuel elements (Figure 4-4) was subjected to severely degraded cooling conditions resulting in a high-temperature (≥2400°C) transient (Figure 4-5) [28-30]. A partial flow blockage developed during the test due to relocation of a molten U-Zr-O alloy and the high-temperature transient was terminated with a cold-water quench. Figure 4-6 shows a cross-section of the bottom end of the fuel assembly following the test.

The other three experiments in the BTF program, BTF-104, BTF-105A and BTF-105B, were conducted with single CANDU-sized fuel elements at maximum temperatures of 1500-1900°C in a steam-rich environment. The tests were performed to evaluate the behavior of a CANDU fuel element and the resultant fission-product release and transport in a LOCA/LOECC scenario.

- The BTF-104 experiment provided data on fuel behavior, and volatile fission-product release and transport (Kr, Xe, I, Cs, Te and Ba) from a previously irradiated fuel element at a volume-averaged fuel temperature of about 1500°C [31-33]. Figures and 4-7 and 4-8 show typical cross-sections from the BTF-104 test section following the test.
- The BTF-105A experiment used an internally instrumented fresh fuel element [34-38]. The BTF-105A test provided data for validation of transient fuel performance codes and tested instrumentation for the BTF-105B experiment.
- The BTF-105B experiment investigated fission-product release and transport from a previously irradiated fuel element at an average fuel temperature of 1800°C [39,40]. Due to improved measurements of fuel-cladding temperature, flow and neutron flux, and better control of steam condensation in the test section, the thermal hydraulic boundary conditions for the BTF-105B test were better quantified than for previous BTF tests.

The BTF-107, BTF-104 and BTF-105A test data have been used for validation of the ELOCA-IST transient fuel behavior code. The BTF program met its overall objectives of improving our understanding of CANDU fuel and fission-product behavior under accident conditions, and providing integral test data for use in reactor-safety code validation.

4.2 Fission-Product Behavior

Analyses of fission-product release from fuel and transport in the reactor coolant system are performed to determine the quantities and speciation of fission products released into

containment under accident conditions [2,41-43]. These analyses are part of the source term analysis methodology. The results are used in the assessment of radiation doses to the general public, station staff and plant equipment.

The experiments conducted to improve our understanding of fission product release and transport behavior under accident conditions include laboratory separate effects tests (e.g., fission product thermochemistry experiments, and end-fitting aerosol retention experiments) hot-cell fission product release experiments conducted using irradiated fuel samples, and in-reactor fission product release experiments.

4.2.1 Laboratory Fission-Product Behavior Tests

Laboratory tests conducted to improve our understanding of fission-product release and transport include studies of fission product thermochemistry, and fission product vapour and aerosol retention in heat transport system components.

4.2.1.1 Knudsen Cell – Mass Spectroscopy

It is important to know the chemical composition and thermodynamic properties of the fission product species released from fuel at high temperature under postulated accident conditions. Such information can be obtained using Knudsen cell-mass spectroscopy. A Knudsen cell is a small container, made of a corrosion resistant metal, with a small hole in its cap. The sample to be investigated is heated in the Knudsen cell to the desired temperature and the gases effusing out of the cell are analyzed using a mass spectrometer. Information about the nature and properties of the effusing species is obtained from an analysis of the mass spectra. A schematic diagram of our Knudsen cell-mass spectroscopy facility is shown in Figure 4-9. This facility has been used to study the high-temperature behavior of CANDU fuel and fission product important for safety studies.

Rare-earth elements form a significant fraction of the fission product produced during nuclear fission. High-temperature Knudsen cell-mass spectroscopy experiments were carried out with lanthanum doped-uranium dioxide solid solutions to understand the volatilization of rare earths present in irradiated nuclear fuel [44]. Lanthanum can be considered representative of the majority of rare-earth elements. These experiments showed that the vapour pressure of lanthanum oxide over $(La,U)O_2$ solid solutions follows Henry's law, i.e., its value is directly proportional to its concentration in the solid phase. Also, the vapour pressure of lanthanum oxide over the solid solutions, after correction for its concentration in the solid phase, is similar to that of UO_2.

Iodine is an important fission product and its volatility is affected by the oxidation state of fuel and the fission product present in the fuel [45,46]. Molybdenum is a major fission product and can exist in several oxidation states. The relationships between I volatility and Mo oxidation state in fuel was investigated using Knudsen cell-mass spectroscopy. This study showed that I volatility is similar in $UO_2/MoO_x/CsI$ systems with Mo in oxidation states 0, +2 and +4 but is much higher with molybdenum in oxidation state +6 [47,48]. The results suggest that I volatility in fuel increases significantly if the oxidation of Mo goes beyond +4 stage. Similarly high I volatility was observed over U_3O_8/CsI mixtures [46].

Strontium is also a significant fission product but very little direct experimental information is available about its release from fuel as the main radioactive isotope of strontium (^{90}Sr) is a β-emitter and not a γ-emitter, and in majority of the fission product release and transport tests γ-spectrometry is used to monitor the fission product release. High-temperature Knudsen cell-mass spectroscopy experiments were performed with "solid solutions" of SrO in UO_2 to determine the effect of UO_2 on SrO volatility. These experiments showed that the vapour pressures of Sr species over "solid solutions" SrO in stoichiometric UO_2 were similar to those over pure SrO [49]. There was no measurable decrease in the SrO volatility because of its "dissolution" in stoichiometric UO_2.

The Knudsen cell-mass spectroscopy facility was also used to study the vaporization of Pd from multi-component alloys of the fission product precious metals. The results of the experiments were used to develop a thermodynamic model for the phase equilibrium in the Mo-Tc-Ru-Rh-Pd quinary system. This model is used to predict the vaporization of the fission product precious-metal alloys found in irradiated nuclear fuel [50].

The information obtained in the Knudsen cell-mass spectroscopy studies described above will be used in the development and validation of the CANDU and ACR safety analysis codes SOURCE-IST and SOPHAEROS-IST.

4.2.1.2 End-Fitting Aerosol Retention Tests

Fission-product transport and retention in the heat transport system between the fuel and the break location may have a significant effect on the timing and characteristics of the fission product released into containment. There is an extensive international database on fission product vapour and aerosol transport in piping systems, but there is little data specific to CANDU conditions and geometries. Experiments were performed on CsI retention in a full-scale CANDU 6 end fitting under turbulent dry-steam flow conditions representative of a LOCA/LOECC scenario (Figure 4-10) [51-55]. The end fitting is a component of the CANDU heat transport system where a significant amount of fission product vapour and aerosol deposition may occur because of the rapidly declining temperatures and the tortuous flow path. Tests were conducted at steam flows between 2 and 20 g/s, CsI concentrations of 42 and 170 mg/m^3, and system pressures of 100 and 150 kPa. Tests were conducted with and without a CANDU fuel bundle at the entrance to the end fitting. Some tests included a resuspension phase following the deposition phase to investigate revaporization and resuspension of CsI deposits in a pure steam flow. The results of the experimental program provide a basis for crediting the retention of 25-50% of the CsI vapours and aerosols entering the end fitting under LOCA/LOECC conditions, depending on the steam flow and aerosol concentration. Data from these end-fitting CsI retention experiments will be used for the validation of the SOPHAEROS fission-product transport code.

4.2.2 Hot-Cell Fission-Product Release and Transport Tests

Over 300 tests using clad and unclad fuel samples have been performed to date in the Canadian hot-cell fission-product release and transport test program. These tests cover a range of conditions, including:

- Maximum temperatures from 400 to 2100°C,

- Fuel sample heating rates from 0.2 to 50°C /s, and
- Gaseous environments of hydrogen, Ar/H_2 mixtures, steam/H_2 mixtures, steam and air.

Fission-product release and transport data were collected using on-line γ-spectrometers focused on the fuel sample itself and on a downstream coil of tubing, as well as using post-test γ-scanning of the apparatus. Many tests were conducted as soon as possible following the irradiation of the fuel or the fuel samples were re-irradiated in a low power position in the NRU research reactor prior to a test to permit the detection of radioisotopes with half-lives of the order of days to years by γ-spectroscopy. Aerosol collectors were installed for some tests. Solid-state oxygen sensors located upstream and downstream of the sample were used to measure the extent of fuel sample oxidation during the test [56]. The results of the HCE4 (Hot-Cell Experiment 4) experiment are discussed in some detail, and the results of other Canadian hot-cell fission-product release tests are summarized in the following subsections.

4.2.2.1 HCE4 Experiment

The HCE4 (Hot-Cell Experiment 4) experiment was performed to study fission-product releases from CANDU fuel at ~1600°C and their deposition on heat transport system piping materials [57]. A general schematic of the experimental apparatus is shown in Figure 4-11. The furnace was mounted on a travelling track, and achieved heating rates of up to 8°C s^{-1} by moving the pre-heated furnace over the fuel sample. While the furnace was moved, the fuel sample (located inside an alumina furnace tube) was held stationary in the field of view of a γ-spectrometer by means of a magnetic pushrod assembly. The hot zone of the furnace could be moved over the fuel sample with no loss of carrier gas or system pressure. Three sets of tests were conducted to assess the effects of gaseous environment, fuel element length, and heating rate on fission-product release. The fuel samples were from the Darlington reactor (burnup of ~9 GW·d/Mg U, maximum linear power of 42 kW/m) and an irradiation in the NRU reactor (burnup of 6 GW·d/Mg U, maximum linear power of 64 kW/m). The test conditions and key results are summarized in Table 4-2. A sample plot of fission product release as a function of time during the J03 test is shown in Figure 4-12.

The first set of tests in the HCE4 experiment (tests J01-J04) was performed to assess the effect of environment (inert, steam and air) on fission-product release from clad samples of CANDU fuel at ~1600°C. The releases of the volatile fission products (Kr, Xe, Cs and I) from the clad fuel samples were low (<10%) in the Ar/2%H_2 environment, and high (75-100%) in the steam and air environments. The ^{129m}Te release in the inert atmosphere test was negligible. The ^{129m}Te releases in the oxidizing atmospheres varied significantly (30-80%) and did not appear to depend on the nature of the oxidant (steam or air). Some Ru release (~15%) was observed beginning about 3600 s after the onset of rapid Cs release in the air environment. No Ru release was observed in the inert or steam atmosphere tests. No statistically significant releases of Ba, Eu, La, Nb, Nd, Pr, Y and Zr were observed in these tests.

The second set of tests in the HCE4 experiment (tests J03, J04, J07 and J08) was performed to assess the effect of fuel element length on fission-product release from clad samples of CANDU fuel at ~1600°C in a 76 mol% steam and 0.5 mol% H_2 (balance Ar) environment. For most fission products released under the test conditions (Xe, Kr, Cs and I), no significant differences were found between the releases from clad fuel samples of different lengths (20 and 100 mm). The fractional ^{129}Te release seems to have been higher from one of the shorter fuel samples, but

the uncertainty in this result is large due to poor counting statistics. The difference in the ^{129m}Te releases may arise from its affinity for unoxidized Zircaloy and local differences in the extent of clad oxidation. These results indicate that it may not be necessary to account specifically for any effect of fuel element length on releases of volatile fission products from the fuel in CANDU safety analysis. The possible exceptions to this conclusion are those species that are known to have a specific chemical interaction with the cladding that may be affected by steam ingress into the fuel element, e.g., Te and Sb.

The third set of tests in the HCE4 experiment (tests J05, J06, J09 and J10) was performed to assess the effect of heating rate on fission-product release from full-pellet-cross-section fuel fragment samples in an inert (Ar/2%H_2) environment. Good results were obtained on releases of volatile fission products (Cs, I) in these tests, but the noble gas (Kr, Xe) release data are not as reliable because of experimental difficulties. There appeared to be little effect of heating rates between 0.2 and 6°C/s on fission product release from fuel samples heated to ~1600°C in an inert (Ar/2%H_2) atmosphere. Heating rate effects are thought to be more significant for fission products located on grain boundaries and the fuel used in the HCE4 experiment had a relatively small grain-boundary inventory.

Consistent with previous observations, oxidizing gaseous environments increased the releases of most fission products under the HCE4 experiment conditions. No significant effect of fuel element length was observed for most fission products released. There was no significant effect of heating rate on fission-product releases from full-cross-section fuel fragment samples for the particular fuel and the range of heating rates studied.

4.2.2.2 MCE1 Experiment

The kinetics of fission-product releases from unclad UO_2 fuel samples were measured in inert and oxidizing conditions during the MCE1 hot-cell post-irradiation annealing experiment [58,59]. The fuel samples used in the MCE1 experiment were taken from a CANDU fuel rod that had been irradiated to a burnup of 10.7 GW·d/Mg U at a linear power of 43 kW/m. Eight individual tests were performed using irradiated UO_2 samples heated in an Ar/2%H_2 mixture to a maximum temperature between 1700 and 2100°C, followed by annealing for 1500 s, then cooling. In some of the tests, the UO_2 was exposed to air for 900 s during the annealing period. Changing from inert to oxidizing conditions increased the release rates of I, Cs, Ru and Nb. Under oxidizing conditions, Ru was released more rapidly than I or Cs. High rates of UO_2 volatilization occurred in the oxidizing environment tests, and resulted in greater than 50% release of the low-volatility fission products Zr, La and Ce. Above about 1900°C, significant releases of Ba were observed under both oxidizing and inert conditions. Complete volatilization of the UO_2 fuel sample was observed in the tests conducted in air at temperatures of 2000 and 2100°C.

4.2.2.3 UCE12 Experiment

In the UCE12 (Universal Cell Experiment 12) experiment, tests were conducted on unclad fragments of irradiated UO_2 fuel, and on segments of irradiated fuel rods with press-fitted Zircaloy end caps ("mini-elements") [60]. These tests provide useful information on the role of the Zircaloy cladding in mitigating fission-product releases from CANDU fuel. The tests were done in inert, steam and air atmospheres at temperatures between 1100 and 1600°C. About

10-25% of the Cs was released from unclad UO_2 fuel samples in inert atmosphere during heating to 1550°C. The addition of steam caused a more rapid release. The intragranular bubbles in steam-oxidized samples serve as reservoirs for some of the Cs inventory; this inventory may be released on oxidation of the uranium oxide to U_3O_8 in air. In oxidizing atmosphere mini-element tests, the delay in oxidative release relative to the tests conducted with unclad fuel samples corresponded to the time required for full oxidation of the cladding. The Cs release rates from oxidized mini-elements were lower than the release rates from unclad oxidized fuel samples, likely due to decreased gas transport in the gap between the oxidized cladding and the fuel pellet. There was a significant difference in the integral Cs release in companion tests performed in air with mini-elements having one end cap (T20, 100% Cs release) and two end caps (T16, 45% Cs release). Reduction of the fuel by UO_2-Zircaloy interaction reduced the Cs release rate in the inert-atmosphere mini-element tests.

4.2.2.4 HCE2 Experiment

The kinetics of fission-product releases from high-burnup CANDU (20-24 GW·d/Mg U) and LWR (57 GW·d/Mg U) fuel were measured in the HCE2 hot-cell annealing experiment under simulated severe accident conditions [61-64]. The Zircaloy-clad fuel samples were heated in an inert environment and then exposed to flowing steam or air at atmospheric pressure at temperatures between 1350 and 1750°C. A simultaneous measurement of the fuel oxidation rate was made during these tests. Both the CANDU and LWR fuels showed the same qualitative release behavior. The Kr release kinetics could be divided into four different stages. During heating under inert conditions, a burst-release of Kr was detected starting between 1200 and 1400°C. The initiation temperature and the quantity of gas released in this stage were found to depend on the irradiation history of the fuel sample. The second stage only occurred in fuel heated to temperatures greater than 1400°C and could also be characterized as a burst-type release, although the peak rate and total quantity released in this stage increased with annealing temperature. A third peak of gas release occurred upon changing to an oxidizing environment. This peak was produced by a temperature escalation in the fuel resulting from the exothermic oxidation of the Zircaloy cladding. A final large gas release occurred after most of the Zircaloy cladding was oxidized (presumably due to oxidation of the UO_2). The kinetics of Cs release were similar to Kr, except for lower Cs releases in the first stage, and a delay of several hundred to several thousand seconds relative to Kr, most notably during the first and fourth release stages. Differences between the fission-product releases from the CANDU and LWR fuel samples were attributed to the different irradiation histories, and the different Zr/UO_2 ratios in the fuel specimens.

4.2.2.5 HCE3 Experiment

Fission-product release from Zircaloy-clad segments of CANDU fuel was measured in the six tests of the HCE3 experiment in argon, steam and air environments at peak temperatures between 1500 and 1900°C [65]. On-line γ-spectrometry showed significant fractional releases for Xe, Kr, I, Cs, Te and Ru. Post-test deposition measurements also detected releases of Sn, Sb, Ag, Ba, Zr and Nb. In all tests, the release behaviors of Cs, I and noble gases were very similar to each other. The release rates of Kr, Xe, I and Cs were very low before complete cladding oxidation; their peak release rates in steam after complete clad oxidation were not very temperature-dependent. Very little Cs was released before complete oxidation of the cladding,

probably because this fuel had a small Cs gap inventory; the gap inventory of noble gases was <1% after irradiation. These results suggest that the releases observed in inert atmosphere below 1400°C or before complete cladding oxidation in other experiments were releases of gap inventory. The release rates during UO_2 oxidation in steam showed very little temperature dependence. Release of Te began at about the same time as oxidative release of Cs. The two high-temperature steam tests (H01, 1900°C and H03, 1800°C) showed a release of ~4% of Ru. An air test conducted at a temperature of 1900°C (H02) showed the greatest release of Ru (~90%) for a clad sample with two end-caps. Ruthenium release began well after oxidative release of volatile fission products (delay of >2000 s).

4.2.2.6 MCE2 Experiment

The MCE2 T19 test was conducted using an unclad fuel sample in a steam environment at a temperature of 2000°C [66]. The roughly cylindrical fuel sample (~2.2 mm in diameter and 5 mm in length) was obtained from a CANDU-sized fuel rod irradiated in one of the light water loops in the NRU reactor at a final linear power of ~32 kW/m to a discharge burnup of 19 GW·d/Mg U. The fuel sample was heated in an "inert" environment ($Ar/2\%H_2$) and then exposed to the steam environment at the target temperature for ~420 s. The observed releases were ~25% for ^{144}Ce, 98% for ^{137}Cs, ~0% for ^{154}Eu, 46% for ^{95}Nb, 81% for ^{106}Ru, and ~0% for ^{95}Zr.

4.2.2.7 Grain-Boundary Inventory Measurements

The ^{85}Kr grain-boundary inventory (GBI) was measured for several CANDU power reactor fuel rods, with burnups between 4 and 22 GW·d/Mg U and peak linear power ratings between 26 and 58 kW/m [67-70]. The GBI experiments were focused on measuring the grain-boundary inventory (GBI), to provide data to help validate fuel performance codes. Knowledge of the GBI is also important for reactor safety analysis because the fission product present on the grain boundaries are more easily released under accident conditions. Samples were cut from central, mid-radial and peripheral locations in the fuel pellets. Both the GBI and the total inventory showed significant radial variation for some fuel rods. The peripheral GBI percentages (<5% for all rods) did not show any correlation with maximum linear power. The central GBI percentages were effectively the same as peripheral and mid-radial GBI percentages up to a peak linear power of about 38 kW/m, at which point the central GBI percentages began to increase to about 40-50%. Mid-radial GBI values for some high-power rods were also comparable to the central GBI, indicating expansion of a "high-GBI" region out from the centre of the fuel rod with increasing linear power. For the highest-power highest-burnup fuel rod, the GBI varied from 3.5% at the periphery to 90% in the centre. Most of the inventory generated in the central region of this rod, however, had been vented to the fuel-to-clad gap during the power reactor irradiation. Volume-average GBI values were in the range 1 to 9%.

4.2.2.8 Direct-Electric-Heating Tests

Direct-electric-heating (DEH) tests were performed as part of the TG1 (Temperature Gradient 1) experiment to obtain fission-product release data under conditions relevant to some reactor accident scenarios, including rapid temperature transients and large centre-to-surface fuel temperature gradients [71,72]. The DEH technique uses ohmic heating of the UO_2, produced by

passing an electric current axially through a section of a sintered UO_2 fuel pellet inside its original Zircaloy cladding. The ohmic heating of the UO_2, combined with surface heat removal by the surrounding helium coolant flow, produced a radial temperature profile approximating the profile for fission- or decay-heated fuel. The 11 tests conducted in the TG1 experiment simulated various transient heating rates and high-temperature annealing conditions [72]. Post-test ceramographic examinations showed columnar grain growth and evidence of UO_2 melting. Releases of Kr, and release and redistribution of Cs were observed. The cumulative amount of Kr released was higher at higher dwell powers. Cesium was released from the centre of the fuel sample where temperatures were the highest. The measured Kr releases were in good agreement with the total of Cs migration and release.

4.2.3 In-Reactor Fission-Product Behavior Tests

Three in-reactor fission-product behavior test programs have been conducted at AECL: the sweep-gas and defect experiments performed in the X-2 loop in the NRX research reactor, and the blowdown test facility experiments performed in the NRU research reactor.

4.2.3.1 Sweep-Gas Tests

The Sweep-Gas tests are a series of in-reactor experiments performed on full-sized CANDU fuel elements in the NRX research reactor to measure the fission-gas releases from UO_2 fuel under typical reactor operating conditions (steady-state and typical reactor power ramps) [73-82]. Two of the experiments examined the steady-state releases of fission gases. Other experiments studied the effects of severe thermal transients simulated by loop blowdown. In these latter experiments, the fuel was allowed to dry out so that cladding temperatures reached a maximum of about 1000ºC. During all of these experiments, the fuel experienced shutdown and startup transients as a normal part of the operation of the reactor. Sweep gas data was measured for many of these normal operating transients.

Most of the fuel elements used in the sweep gas tests had peripheral slots in the UO_2 pellets. One of the fuel elements used in these tests had holes drilled along the fuel pellet centreline. The interior of the fuel elements was continuously purged with a slow flow of purified He/2%H_2 gas, which carried the released fission gases past a γ-spectrometer. The experiments were performed over a range of fuel element linear power ratings from 17 to 62 kW/m, with a focus on powers above 45 kW/m where most fission-gas release occurs. Isotopes of Kr, Xe, Rb, Cs and Ba were detected during the sweep-gas tests. Iodine isotopes were not detected directly because iodine undergoes chemical reactions with the fuel cladding and sweep-gas tubing. The gap inventory of iodine was inferred from the release rates of the radioactive Xe isotopes produced by radioactive decay of iodine following reactor shutdowns. The Rb, Cs and Ba isotopes detected were likely produced by radioactive decay of noble gases.

Fission-gas releases observed during steady-state operation in the sweep-gas tests were rather low. The releases during startups and shutdowns were more significant. The releases observed during dryout transients were higher, but it should be noted that the transient fission-gas releases in both dryout and LOCA transients with fuel central temperatures up to 2300ºC were less than 1.5% of inventory. Post-test metallographic examinations indicated that fuel cracking is an important transient fission-gas release mechanism.

4.2.3.2 Defected Fuel Tests

In-reactor experiments were conducted to investigate the performance of defected fuel elements containing deliberate or known fabrication flaws [83-88]. These experiments were primarily conducted in the X-2 pressurized light-water loop in the NRX research reactor. Several elements were defected prior to irradiation with artificially drilled holes or machined slits in the fuel cladding. In other experiments, the defects in the elements were characteristic of failures found in power plant fuel elements. The initial defects in the naturally defected elements were smaller than the defects in the artificially defected ones. The fission-product release behavior was monitored using γ-spectroscopy while the irradiations were conducted at fuel element linear powers between 14 and 67 kW/m up to a maximum burnup of 278 MWh/kgU.

The release-to-birth ratio (R/B) of the fission products released from the fuel is the key parameter used in the assessment of defected fuel performance. During steady-state operation, the R/B ratio increases with the power and burnup of the fuel element, as well as with the size of the defect. For defected fuel elements operating as linear power ratings greater than 20 kW/m, the dependence of R/B on the decay constant (inverse of radioisotope half life) with a dependence between $\lambda^{-1/2}$ and $\lambda^{-3/2}$. This behavior is consistent with theoretical models based on simple diffusion in the fuel matrix ($\lambda^{-1/2}$), and diffusion plus first-order kinetics in the fuel-to-cladding gap ($\lambda^{-3/2}$). Transport of iodine in the gap is more restricted than that of the noble gases. Fuel oxidation has a significant effect on the rate of fission-product releases from the fuel matrix of defected fuel elements. Detailed models of defected fuel behavior and fission-product release have been developed [86,88].

4.2.3.3 Blowdown Test Facility Experiments

The Blowdown Test Facility (BTF) experimental program was described in Section 4.1.2.2. Four in-reactor experiments were performed in the BTF program to improve our understanding of CANDU fuel and fission-product behavior under accident conditions, and to provide data for use in reactor safety code validation. The integral fission-product releases in the BTF experiments are listed in Table 4-3 for comparison purposes. The BTF-107 test had the highest fractional releases of volatile fission products (Kr, Xe, I, Cs and Te) of any BTF test. The fractional releases in the BTF-107 test did not show any apparent dependence on fission-product half-life. The BTF-107 test was conducted under the most severe conditions, i.e., the highest maximum fuel temperatures, and the largest amount of fuel liquefaction due to UO_2/Zircaloy interaction and dissolution.

The BTF-104 test showed similar releases of long-lived volatile fission products (Kr and Cs) to those observed in BTF-107, but there was a marked dependence of fractional fission-product release on half-life in the BTF-104 test. This was likely due to the high linear power during the BTF-104 pressurized-water irradiation (leading to high grain-boundary and gap inventories of long-lived fission products), and the shorter time at high temperature after fuel failure compared to the BTF-105B test (~1500 vs. 2400 s). The high grain-boundary and gap inventories of long-lived fission products would be released shortly after fuel cladding failure. The short-lived fission products were mainly located inside the fuel grains at the beginning of the transient and would require additional time at high temperature or fuel oxidation by steam ingress into the fuel element following element failure to be released from the fuel grains during the transient.

The BTF-105A test had the lowest fractional fission-product releases. This was mainly due to the low fuel burnup, the relatively low fuel element linear power during the pressurized-water and saturated-steam irradiations (50 vs. 60 kW/m), and the simultaneous occurrence of element failure and a rapid quench leading to a very short time at high temperatures after element failure leaving little time for fuel oxidation or fission-product diffusion.

The volatile fission-product releases (Kr, Xe, I and Cs) in the BTF-105B test were between 10 and 40%. Somewhat lower ^{134}Cs and ^{137}Cs fractional releases were observed in the BTF-105B test compared to BTF-104 and BTF-107, likely due to the cooling effect of the cladding thermocouple clamps (Figure 4-13). The cooler local fuel temperatures near the cladding thermocouple clamps would lead to lower diffusional releases of Cs from the fuel and greater retention at the pellet periphery of Cs released from the hotter region near the fuel centreline. In the BTF-105B test, the best-estimate fractional releases of some of the short-lived isotopes of the volatile fission products were higher than in the BTF-104 test, and overall the releases showed less dependence on fission-product half-life than was observed in BTF-104. This was likely due to the longer time at high temperature after fuel failure in the BTF-105B test, giving more opportunity for fuel oxidation and diffusional release of fission products from the fuel grains.

Stainless Steel (Type 347), Carbon Steel (Type A105), Zr-2.5%Nb and Inconel-600 coupons were placed just downstream of the fuel element during the BTF-104 experiment. The main objective for including these coupons was to characterize the fission-product deposition/retention of these materials at temperatures between 500 and 700°C in a steam-hydrogen atmosphere. The coupons were examined by gamma-spectrometry and scanning electron microscopy (SEM). The retention of iodine and cesium varied between the materials. The retention was greatest on the stainless steel coupons, followed by carbon steel and Inconel. The Zr-2.5%Nb coupons had the least retention. There was one order of magnitude less iodine deposited on the Zr-2.5%Nb coupons than on the stainless steel coupons. The tellurium retention was similar on the coupons of all four materials. The overall fission-product deposition data from this test (~90% retention in the piping system between the fuel and the tank for the "volatile" fission products (Cs, I, Te)) indicate the potential for crediting fission-product retention in the primary circuit piping in reducing the releases into containment under similar conditions [89].

The fission-product release, deposition and aerosol measurements from the BTF-104 and BTF-105B tests are being used to validate the SOURCE and SOPHAEROS codes. The BTF program met its overall objectives of improving our understanding of CANDU fuel and fission-product behavior under accident conditions, and providing integral test data for use in reactor-safety code validation.

4.3 Summary

There is an extensive database on the behavior of fuel and fission products in current-generation CANDU reactors under accident conditions. This knowledge is directly applicable to ACR, and only requires minor extensions to account for dimensional changes (thicker cladding) and the use of Dysprosium as a burnable poison in the central fuel element of the ACR bundle.

4.4 References

1. E. Kohn, P.J. Fehrenbach and J.H.K. Lau, "CANDU Fuel Behavior under LOCA Conditions," AECL Report AECL-9788, 1989 April.
2. A.J. White and C. Blahnik, "Phenomenology for Limited and Severe Core Damage Accidents in an ACR," AECL Report 108-126810-LS-001, 2003 September.
3. D.G. Hardy, "High Temperature Expansion and Rupture Behavior of Zircaloy Tubing," National Topical Meeting on Water Reactor Safety, Salt Lake City, Utah, U.S.A., 1973.
4. S. Sagat, H.E. Sills, J.A. Walsworth, D.E. Foote and D.F. Shields, "Deformation and Failure of Zircaloy Fuel Sheaths Under LOCA Conditions," AECL Report AECL-7754, 1982 October.
5. E. Kohn and S. Sagat, "Beryllium Assisted Cracking of Zircaloy," Presented at 6th Canadian Fracture Conference, Harrison Hot Springs, B.C., Canada, 1982 June 17-18.
6. S. Sagat, H.E. Sills and J.A. Walsworth, "Deformation and Failure of Zircaloy Fuel Sheaths Under LOCA Conditions," Zirconium in the Nuclear Industry: Sixth International Symposium, ASTM STP 824, American Society for Testing and Materials, 1984, pp. 709-733, also released as AECL Report AECL-8415.
7. V.F. Urbanic and T.R. Heidrick, "High-Temperature Oxidation of Zircaloy-2 and Zircaloy-4 in Steam," J. Nucl. Mater. 75 (1978) 251-261.
8. A. Sawatzky, "A Proposed Criterion for the Oxygen Embrittlement of Zircaloy-4 Fuel Cladding," Zirconium in the Nuclear Industry (Fourth Conference), ASTM STP 681, American Society for Testing and Materials, 1979.
9. A.J. White, A. Sawatzky, S. Jones and G.A. Ledoux, "A Failure Criterion For CANDU Fuel Cladding Subjected To Thermal-Quench Loads," Proc. Thermal Reactor Safety Meeting, Portland, Oregon, 1991 July, pp. 555-562.
10. E. Kohn, G.I. Hadaller, R.M. Swala, G.H. Archinoff and S.L. Wadsworth, "CANDU Fuel Deformation During Degraded Cooling (Experimental Results)," Proc. Can. Nucl. Soc. 6th Annual Conf., ISSN 0227-1907, Ottawa, Canada, 1985 June 3-4, pp. 16.39 – 16.45.
11. R. Choubey, D.J. Wren, A.E. Unger, K.J. George and P.J. Fehrenbach, "Metallographic Examination of a CANDU Fuel Bundle Heated Under Severe Accident Conditions," Proc. Can. Nucl. Soc. 7th Annual Conf., ISSN 0227-1907, Toronto, Canada, 1986 June 9-10, pp. 30-38.
12. O. Akalin, C. Blahnik, B. Phan and F. Rance, "Fuel Temperature Escalation in Severe Accidents," Proc. Can. Nucl. Soc. 6th Annual Conf., ISSN 0227-1907, Ottawa, Canada, 1985 June 3-4, pp. 16.26 – 16.32.
13. P.M. Mathew and D.G. Evans, "Relocation of Molten Zircaloy in a CANDU Subchannel Geometry," Proc. 4th International Conference on CANDU Fuel, Pembroke, Canada, 1995 October 1-4, ISBN # 0-919784-53-4, Vol. 1, pp. 3B-11 to 3B-20.
14. P.J. Hayward and I.M. George, "Dissolution of UO_2 in Molten Zircaloy-4, Part 1: Solubility from 2000 to 2200°C," J. Nucl. Mater. 208 (1994) 35-42.

15. P.J. Hayward and I.M. George, "Dissolution of UO_2 in Molten Zircaloy-4, Part 2: Phase Evolution During Dissolution and Cooling," J. Nucl. Mater. 208 (1994) 43-52.

16. P.J. Hayward and I.M. George, "Dissolution of UO_2 in Molten Zircaloy-4, Part 3: Solubility from 2000 to 2500°C," J. Nucl. Mater. 232 (1996) 1-12.

17. P.J. Hayward and I.M. George, "Dissolution of UO_2 in Molten Zircaloy-4, Part 4: Phase Evolution During Dissolution and Cooling of 2000 to 2500°C Specimens," J. Nucl. Mater. 232 (1996) 13-22.

18. D.S. Cox, F.C. Iglesias, C.E.L. Hunt, N.A. Keller, R.D. Barrand, J.R. Mitchell and R.F. O'Connor, "Oxidation of UO_2 in Air and Steam with Relevance to Fission Product Releases," Proc. Am. Chem. Soc. Symp. On Chemical Phenomena Associated with Radioactivity Releases during Severe Nuclear Plant Accidents, Anaheim, California, 1986 September 9-12, U.S. Nuclear Regulatory Commission Report NUREG/CP-0078.

19. D.S. Cox, F.C. Iglesias, C.E.L. Hunt, R.F. O'Connor and R.D. Barrand, "High-Temperature Oxidation Behavior of UO_2 in Steam and Air," Proc. Internat. Symp. on High Temperature Oxidation and Sulphidation Processes, Hamilton, Ontario, Canada, 1990 August 26-30, Pergamon Press, New York, ISBN 0-18-040415-4.

20. D.S. Cox, C.E.L. Hunt, Z. Liu, F.C. Iglesias, N.A. Keller, R.D. Barrand and R.F. O'Connor, "A Model for the Release of Low-Volatility Fission Products in Oxidizing Conditions", Proc. 12^{th} Annual Conf. Can. Nucl. Soc., Saskatoon, Saskatchewan, Canada, 1991 June 9-12, also released as AECL Report AECL-10440.

21. B.J. Lewis, B.J. Corse, W.T. Thompson, M.H. Kaye, F.C. Iglesias, P.H. Elder, R.S. Dickson and Z. Liu, "Vaporization of Low-Volatile Fission Products Under Severe CANDU Reactor Accident Conditions," Canadian Nuclear Society: Fifth International Conference on CANDU Fuel, 1997 September 21-25, Toronto, Ontario, Canada, pp. 145-159.

22. P.J. Fehrenbach, I.J. Hastings, J.A. Walsworth, R.C. Spencer, J.J. Lipsett, C.E.L. Hunt and R.D. Delaney, "Zircaloy-Sheathed UO_2 Fuel Performance During In-Reactor LOCA Transients," AECL Report AECL-8569, 1984 October.

23. J.A. Walsworth, P.J. Fehrenbach, J.H.K. Lau and E. Kohn, "Calculated and Measured Behavior of Zircaloy Fuel Sheaths During In-Reactor LOCA Tests," AECL Report AECL-9268, 1986 October.

24. P.J. Fehrenbach and J.C. Wood, "Description of the Blowdown Test Facility: COG Program on In-Reactor Fission Product Release, Transport, and Deposition Under Severe Accident Conditions," AECL Report, AECL-9343, 1987 June.

25. J.A. Walsworth, R.J. Zanatta, L.W. Dickson, N.A. Keller, R.D. MacDonald, P.J. Fehrenbach and S.L. Wadsworth, "The Canadian In-Reactor Blowdown Test Facility (BTF) Program in Support of Reactor Safety," Proc. International Symposium on Research Reactor Safety, Operations and Modifications, Chalk River, Ontario, Canada, IAEA Report, IAEA-SM-310/102, 1989 October.

26. J.A. Walsworth, R.J. Zanatta, A.R. Yamazaki, D.D. Semeniuk, W. Wong, L.W. Dickson, C.E. Ferris and D.H. Burton, "The NRU Blowdown Test Facility

Commissioning Program," presented at the 10th Annual Canadian Nuclear Society Conf., Ottawa, 1989 June.

27. L.W. Dickson, R.D. MacDonald, A.R. Yamazaki, D.D. Semeniuk, R.J. Zanatta, and J.A. Walsworth, "Nuclear Commissioning of the NRU Blowdown Test Facility," presented at the 2nd International Conf. CANDU Fuel, Pembroke, 1989 October.

28. R.D. MacDonald, J.W. DeVaal, D.S. Cox, L.W. Dickson, M.G. Jonckheere, C.E. Ferris, N.A. Keller and S.L. Wadsworth, "An In-Reactor Loss-Of-Coolant Test with Flow Blockage and Rewet," Proc. Thermal Reactor Safety Meeting, Portland, Oregon, 1991 July, also released as AECL Report AECL-10464, 1991 October.

29. J.W. DeVaal, N.K. Popov, R.D. MacDonald, L.W. Dickson, R.J. Dutton, D.S. Cox and M.G. Jonckheere, "Post-Test Simulations of BTF-107: An In-Reactor Loss-Of-Coolant Test with Flow Blockage and Rewet," Proc. Third International Conference on CANDU Fuel, Pembroke, Ontario, Canada, 1992 October, also released as AECL Report AECL-10758, 1993 March.

30. N.K. Popov, B.N. Hanna, J.W. DeVaal, C. Wong, L.W. Dickson, R.J. Dutton and M.G. Jonckheere, "Post-Test Analysis of the BTF-107 Severe-Fuel-Damage Experiment Using the CATHENA Thermalhydraulics Code," Proc. International Conference on New Trends in Nuclear System Thermalhydraulics, Pisa, Italy, 1994 May.

31. L.W. Dickson, P.H. Elder, J.W. DeVaal, J.D. Irish and A.R. Yamazaki, "Preliminary Results of the BTF-104 Experiment: An In-Reactor Test of Fuel Behavior and Fission-Product Release and Transport Under LOCA/LOECC Conditions," Proc. 16th Annual Conference Canadian Nuclear Society, Saskatoon, Saskatchewan, Canada, 1995 June.

32. L.W. Dickson, J.W. DeVaal, J.D. Irish, P.H. Elder, M.G. Jonckheere and A.R. Yamazaki, "The BTF-104 Experiment: An In-Reactor Test of Fuel Behavior, and Fission-Product Release and Transport Under LOCA/LOECC Conditions," Proc. Fourth International Conference on CANDU Fuel, Pembroke, Ontario, Canada, 1995 October.

33. N.K. Popov, L.C. Walters, T.V. Tran, J.W. DeVaal, L.W. Dickson and J.D. Irish, "Post-Test Analysis of the BTF-104 Severe-Fuel-Damage Experiment Using the CATHENA Thermalhydraulics Code," proceedings of the ASME-JSME Fourth International Conference on Nuclear Engineering (ICONE-4), New Orleans, Louisiana, 1996 March 10-14, Volume 3, pp. 205-213.

34. J.W. DeVaal, J.D. Irish, L.W. Dickson, S.T. Craig, M.G. Jonckheere and L.R. Bourque, "Preliminary Results of the BTF-105A Test: An In-Reactor Instrument Development and Fuel Behavior Test," Proceedings of the Fifth International Conference on CANDU Fuel, Toronto, 1997 September 21-25.

35. P.J. Valliant, J.D. Irish and S.T. Craig, "Post-Irradiation Examination Results from the BTF-105A LOCA/LOECC Test," Proceedings of the Sixth International Conference on CANDU Fuel, Niagara Falls, Canada, 1999 September 26-29.

36. L.C. Walters, J.W. DeVaal and N.K. Popov, "Development of a Model for Calculating Sheath Thermocouple Finning Losses for Application in the In-Reactor Severe Fuel

Damage Tests," Canadian Nuclear Society Simulation Symposium, Niagara-on-the-Lake, Ontario, Canada, 1997 September 7-9.

37. N.K. Popov, J.W. DeVaal, L.C. Walters and J.D. Irish, "Post-Test Analysis of the BTF-105A Severe-Fuel-Damage Test Using the CATHENA Thermalhydraulics Code," Proc. Sixth International Conference on Nuclear Engineering (ICONE-6), San Diego, California, 1998 May 10-15.

38. P.B. Middleton, R.C.K. Rock and S.L. Wadsworth, "FACTAR 2.0 Code Validation," Proceedings of the Fifth International Conference on CANDU Fuel, Toronto, 1997 September 21-25.

39. J.D. Irish, S.T. Craig, L.R. Bourque, M.G. Jonckheere, G. Kyle, P.J. Valliant, L.W. Dickson and R.T. Peplinskie, "Preliminary Results of the BTF-105B Experiment: An In-Reactor Test of Fuel Behavior and Fission-Product Release and Transport Under LOCA/LOECC Conditions," Proceedings of the 19th Annual Conference of the Canadian Nuclear Society, Toronto, 1998 October 18-21.

40. J.D. Irish, S.T. Craig and P.J. Valliant, "Preliminary Fission-Product and Post-Irradiation Examination Results from the BTF-105B LOCA/LOECC Test," Proceedings of the Sixth International Conference on CANDU Fuel, Niagara Falls, Canada, 1999 September 26-29.

41. A.L. Wright, B. Adroguer, A. Alonso, B.R. Bowsher, U. Brockmeier, D.S. Cox, R.R. Hobbins, K-D. Hocke, F. Iglesias, A.V. Jones, D.E. Leaver, J.A. Martinez, D.A. Powers and I. Shepherd, "Primary System Fission Product Release and Transport – A State-of-the-Art Report to the Committee on the Safety of Nuclear Installations," U.S. Nuclear Regulatory Commission Report NUREG/CR-6193, also released as Organization for Economic Cooperation and Development Report NEA/CSNI/R(94)2 and Oak Ridge National Laboratory Report ORNL/TM-12681, 1994 June.

42. F.C. Iglesias, B.J. Lewis, P.J. Reid and P. Elder, "Fission Product Release Mechanisms During Reactor Accident Conditions," J. Nucl. Mater. 270 (1999) 21-38.

43. L.W. Dickson and R.S. Dickson, "Fission-Product Transport and Retention in the PHTS Under Accident Conditions," Proc. 20th Annual Conf. Can. Nucl. Soc., Paper C2-2, Montreal, 1999 May 30 - June 2.

44. S. Sunder, R. McEachern and J.C. LeBlanc, "High temperature, Knudsen Cell-Mass Spectroscopic Studies on Lanthanum Oxide/Uranium Dioxide Solid Solutions," J. Nucl. Mater. 294 (2001) 59-63.

45. J. McFarlane, J.C. LeBlanc and D.G. Owen, "High-Temperature Chemistry of Molybdenum, Cesium, Iodine and $UO_{2+x,}$" AECL Report AECL-11708, 1996 November.

46. J. McFarlane and J.C. LeBlanc, "High-Temperature Knudsen Cell Studies of Cesium Iodide in Hyperstoichiometric Uranium Dioxide," J. Nucl. Mater. 256 (1998) 145-154.

47. S. Sunder and R.F. O'Connor, "Knudsen Cell-Mass Spectroscopic Studies on the Relationship between Molybdenum Oxidation and Iodine Volatility in CANDU Fuel," In CANDU Fuel for the Future, Proceedings of the Seventh International Conference on CANDU Fuel, Publ. Can. Nucl. Soc. Toronto, Canada, Vol. 1, pp. 355-364 (2001).

48. S. Sunder, "The Relationship between Molybdenum Oxidation State and Iodine Volatility in Nuclear Fuel," Nucl. Technol. In press for November Issue (2003).

49. S. Sunder, and R.F. O'Connor, "Knudsen Cell-Mass Spectroscopic Studies of Sr Vapour Pressures Over Strontium Oxide/Uranium Dioxide Mixtures and Solid Solutions," presented at the 8th International Conference on CANDU Fuel, Honey Harbour, ON (2003).

50. M.H. Kaye, W.T. Thompson, B.J. Lewis, S. Sunder and R. O'Connor, "A Thermodynamic Model for Noble Metal Alloy Inclusions in Nuclear Fuel Rods and Application to the Study of Loss-of-Coolant-Accidents," Proceedings of the Seventh International Conference on CANDU Fuel, Publ. Can. Nucl. Soc. Toronto, Canada, Vol. 2, pp. 3A-33-3A-47 (2001).

51. J. McFarlane, R.K. Rondeau and S.R. Mulpuru, "Facility to Study Aerosol Retention in Full-Scale Reactor System Components," Proc. OECD/CSNI Workshop on Nuclear Aerosols in Reactor Safety, Cologne, Germany, 1998 June 15-18, CSNI, 2000.

52. J. McFarlane and R.K. Rondeau, "Retention of CsI Aerosol in a Full-Scale End Fitting. Data Report 1 (Tests EF4 to EF10)," AECL Report RC-2236, 1999.

53. J. McFarlane and R.K. Rondeau, "Retention of CsI Aerosol in a Full-Scale End Fitting Data Report 2 (Tests EF11 and EF12)," AECL Report RC-2433, 2000.

54. J. McFarlane and R.K. Rondeau, "Retention of CsI Aerosol in a Full-Scale End Fitting Data Report 3 (Tests EF13 through EF16)," AECL Report RC-2607, 2000.

55. J. McFarlane, A.J. Elliot and R.K. Rondeau, "Retention of CsI Aerosol in a Full-Scale End Fitting: Data Report 4 (Tests EF17 and EF18)," AECL Report RC-2781, 2002.

56. D.S. Cox, R.F. O'Connor and W.W. Smeltzer, "Measurement of Oxidation/Reduction Kinetics to 2100°C Using Non-Contact Solid-State Electrolytes," Solid State Ionics 53-56 (1992) 238-254.

57. L.W. Dickson and R.S. Dickson, "Fission-Product Releases from CANDU Fuel at 1650°C: The HCE4 Experiment," Proc. 7th International Conference on CANDU Fuel, Kingston, Canada, 2001 September 23-27, Canadian Nucl. Soc., Toronto, ISBN 0-919784-71-2, Vol. 2, pp. 3B-21 to 3B-30.

58. D.S. Cox, C.E.L. Hunt, Z. Liu, N.A. Keller, R.D. Barrand, R.F. O'Connor and F.C. Iglesias, "Fission-Product Releases from UO_2 in Air and Inert Conditions at 1700-2350 K: Analysis of the MCE-1 Experiment," Proc. Amer. Nucl. Soc. Internat. Topical Meeting on Safety of Thermal Reactors, Portland, Oregon, 1991 July 21-25.

59. D.S. Cox, C.E.L. Hunt, Z. Liu, F.C. Iglesias, N.A. Keller, R.D. Barrand and R.F. O'Connor, "A Model for the Release of Low-Volatility Fission Products in Oxidizing Conditions," AECL Report AECL-10440, 1991 July.

60. R.S. Dickson, Z. Liu, D.S. Cox, N.A. Keller, R.F. O'Connor and R.D. Barrand, "Cesium Release from CANDU Fuel in Argon, Steam and Air: The UCE12 Experiment," Proc. Can. Nucl. Soc. 34th Annual Conf., Montréal, Québec, 1994 June 5-8, Vol. 1, Session 3C.

61. D.S. Cox, Z. Liu, P.H. Elder, C.E.L. Hunt and V.I. Arimescu, "Fission-Product Release Kinetics from CANDU and LWR Fuel During High-Temperature Steam Oxidation Experiments," Proc. IAEA Technical Committee Meeting on Fission Gas Release and Fuel Rod Chemistry Related To Extended Burnup, Pembroke, Ontario, Canada, 1992 April 28 – May 1, IAEA-TECDOC-697, 1993 April, pp. 153-164.

62. D.S. Cox, Z. Liu, R.S. Dickson and P.H. Elder, "Fission-Product Releases During Post-Irradiation Annealing of High-Burnup CANDU Fuel," Proc. 3rd International Conference on CANDU Fuel, 1992 October 4-8, ISBN 0-919784-25-9, pp. 4-61 to 4-73.

63. B. Szpunar, B.J. Lewis, V.I. Arimescu, R.S. Dickson, L.W. Dickson and M.I. Baskes, "Multi-Component Gas Transport in CANDU Fuel Rods During Severe Accidents," Proc. 7th International Conf. on CANDU Fuel, Kingston, Canada, 2001 September 23-27, Can. Nucl. Soc., Toronto, ISBN 0-919784-70-4, Vol. 1, pp. 329-352.

64. B. Szpunar, B.J. Lewis, V.I. Arimescu, R.S. Dickson and L.W. Dickson, "Multi-Component Gas Transport in the Fuel-to-Clad Gap of CANDU Fuel Rods During Severe Accidents," J. Nucl. Mater. 294 (2001) 315-329.

65. R.D. Barrand, R.S. Dickson, Z. Liu and D.D. Semeniuk, "Release of Fission Products from CANDU Fuel in Air, Steam and Argon Atmospheres at 1500-1900°C: The HCE3 Experiment," Proc. 6th Int. Conf. CANDU Fuel, Niagara Falls, Canada, 1, 271-280, Canadian Nucl. Soc., Toronto, ISBN 0-919784-64-X (1999).

66. B.J. Lewis, B.J. Corse, W.T. Thompson, M.H. Kaye, F.C. Iglesias, P. Elder, R. Dickson and Z. Liu, "Low Volatile Fission-Product Release and Fuel Volatilization During Severe Reactor Accident Conditions," J. Nucl. Mater. 252 (1998) 235-256.

67. C.E.L. Hunt, F.C. Iglesias, D.S. Cox, N.A. Keller, R.D. Barrand, R.F. O'Connor, J.R. Mitchell, G.W. Wood and R. Mikuch, "Fission Product Grain-Boundary Inventory," Proc. Can. Nucl. Soc. 10th Annual Conference, Ottawa, Ont., also released as AECL Report, AECL-10036, 1989 June.

68. P.H. Elder, D.S. Cox, L.W. Dickson and R.V. Murphy, "New Post-Irradiation Examination Techniques at Chalk River Laboratories: Gamma Tomography and Grain-Boundary-Inventory Measurements on Irradiated Fuel," IAEA Technical Committee Meeting on Recent Developments on Post-Irradiation Examination Techniques for Water Reactor Fuel, Cadarache, France, 1994 October 17-21, IAEA Report IAEA-TECDOC-822, 1995 September, pp. 133-144.

69. P.H. Elder, D.S. Cox, Z. Liu, R.S. Dickson and Z. Bilanovic, "Measurement of Krypton Grain-Boundary Inventories in CANDU Fuel," Proceedings of the Fourth International Conference on CANDU Fuel, Pembroke, Ontario, Canada, 1995 October 1-4.

70. R.S. Dickson, R.F. O'Connor and D.D. Semeniuk, "Grain-Boundary Inventories of Krypton in CANDU Fuel," Proc. Seminar on Fission Gas Behavior in Water Reactor Fuels, Cadarache, France, 2000 September 26-29, OECD/NEA Nuclear Science Report, ISBN 92-64-19715-X, pp. 337-346, also released as AECL Report AECL-CONF-00145.

71. Z. Liu, R.S. Dickson, L.W. Dickson, Z. Bilanovic and D.S. Cox, "Fission-Product Release During Transient Heating of Irradiated CANDU Fuel," Trans. Am. Nucl. Soc., 79 (1998) 123, presented at 1998 ANS Winter Meeting, Washington, D.C., 1998 November 15-19.

72. Z. Liu, R.S. Dickson, L.W. Dickson, Z. Bilanovic and D.S. Cox, "Fission-Product Release During Transient Heating of Irradiated CANDU Fuel," Nucl. Technol., 131 (2000) 22-35.

73. I.J. Hastings, C.E.L. Hunt, J.J. Lipsett and R.G. Gray, "Transient Fission Product Release during Dryout in Operating UO_2 Fuel," AECL Report AECL-7832, 1982.

74. J.J. Lipsett, C.E.L Hunt, and I.J. Hastings, "Transient Fission Product Release within Operating UO_2 Fuel Elements during Power Cycles", AECL Report AECL-8069, 1983.

75. I.J. Hastings, C.E.L. Hunt, J.J. Lipsett and R.D. MacDonald, "Behavior of Short-Lived Fission Products within Operating UO_2 Fuel Elements," Res mechanica 6 (1983) 167.

76. C.E.L Hunt, J.J. Lipsett and I.J. Hastings, "Release of Short-Lived Fission Products from Operating Fuel under Oxidizing Conditions", AECL Report AECL-8564, 1984.

77. I.J. Hastings, C.E.L. Hunt, R.D. Delaney, "Short-Lived Fission Product Release from the Surface and Center of Operating UO_2 Fuel," AECL Report AECL-8353, 1984.

78. I.J. Hastings, C.E.L. Hunt and J.J. Lipsett, "Release of Short-Lived Fission Products from UO_2 Fuel: Effects of Operating Conditions," J. Nucl. Mater. 130 (1985) 403, also released as AECL-8498.

79. J.J. Lipsett, I.J. Hastings, C.E.L Hunt, P.J. Fehrenbach, R.D. Delany, L.L. Larson and R.C. Spencer, "Short-Lived Fission Product Release within a UO_2 Fuel Element during In-Reactor LOCA Transients," Advances in Ceramics 17 (1985) 173.

80. I.J. Hastings, C.E.L Hunt, J.J. Lipsett and R.D. MacDonald, "Tests to Determine the Release of Short-Lived Fission Product from UO_2 Fuel Operating at Linear Powers of 45 and 60 kW/m: Methods and Results," AECL Report AECL-7920, 1985.

81. P.J. Fehrenbach, I.J. Hastings, J.J. Lipsett, C.E.L. Hunt, D.H. Rose and R.D. Davidson, "High-Temperature Transient Fission-Gas Release from UO_2 Fuel: Microstructural Observations," Presented at ANS/ENS Topical Meeting on Thermal Reactor Safety, San Diego, California, 1986 February, AECL Report AECL-9709, 1988 September.

82. C.E.L. Hunt, B.J. Lewis and L.W. Dickson, "Transient Fission-Product Release During Reactor Shutdown and Startup," AECL Report AECL-11842, 1997 December.

83. R.D. MacDonald, and J.J. Lipsett, "The Behavior of Defected Zircaloy-Clad UO_2 Fuel Elements with Graphite Coatings Between Fuel and Sheath Irradiated at Linear Powers of 48 kW/m in Pressurized Water," AECL Report AECL-6787, 1980 May.

84. R.D. MacDonald, J.J. Lipsett, E.E. Perez and, P.K. Kos, "Purposely Defected UO_2 – Zircaloy Fuel Elements Irradiated in Pressurized Light Water at Linear Powers of 55 kW/m," AECL Report AECL-7751, 1983 May.

85. R.L. da Silva, "Irradiation of a CANDU UO_2 Fuel Element with Twenty-Three Machined Slits Cut Through the Zircaloy Sheath," AECL Report AECL-8260, 1984 September.

86. B.J. Lewis, “Fundamental Aspects of Defective Nuclear Fuel Behavior and Fission Product Release,” J. Nucl. Mater. 160 (1988) 201-217.

87. R.D. MacDonald, M.R. Floyd, B.J. Lewis, A.M. Manzer and P.T. Truant, “Detecting, Locating and Identifying Failed Fuel in Canadian Power Reactors,” AECL Report AECL-9714, 1990 February.

88. B.J. Lewis, R.D. MacDonald, N.V. Ivanoff and F.C. Iglesias, “Fuel Performance and Fission Product Release Studies for Defected Fuel Elements,” Nucl. Technol. 103 (1993) 220-245.

89. R.S. Dickson and L.W. Dickson, “Post-Test Analysis of the BTF-104 Severe Fuel Damage Experiment Using the VICTORIA Fission Product Transport Code,” presented at Third OECD Specialist Meeting on Nuclear Aerosols in Reactor Safety, Cologne, Germany, 1998 June 15-18, NEA/CSNI/R(98)4, 2000 February.

Table 4-1 Summary of BTF Test Conditions

Parameter	BTF-107 Test	BTF-104 Test	BTF-105A Test	BTF-105B Test
Test type	LOCA	LOCA/LOECC	LOCA/LOECC	LOCA/LOECC
Fuel elements	1 pre-irradiated, 2 fresh	1 pre-irradiated	1 fresh	1 pre-irradiated
Pre-transient cooling	Pressurized water	Saturated steam	Saturated steam	Saturated steam
Maximum fuel temperature (°C)	≥ 2500 (peak)	~ 1800 (volume-average)	~ 1800 (volume-average)	~ 1800 (volume-average)
Transient duration (s)	~ 70	~ 2100	~ 2900	~ 4200
Time at high temperature after fuel failure (s)	~ 20	~ 1500	< 60	~ 2400

Table 4-2 Integral Fission-Product Releases (%) [1] from Fuel Samples Heated to ~1600°C (HCE4 Experiment)

Test	J01	J02	J03	J04	J05	J06	J07[2]	J08[2]	J09	J10
Fuel Length /mm	20	20	20	100	5	5	107	20	5	5
Clad	Yes	Yes	Yes	Yes	No	No	Yes	Yes	No	No
Environment	Ar/H_2	Air	H_2O/H_2	H_2O/H_2	Ar/H_2	Ar/H_2	H_2O/H_2	H_2O/H_2	Ar/H_2	Ar/H_2
Heating Rate /°C·s^{-1}	-	-	-	-	0.2	1-2 / 5	-	-	1-2	~6
Max. Temp. / °C	1620	1645	1640	1650	1630	1630	1630	1635	1630	1610
Time at Temp. /s	5733	6712	6360	6462	4840	5780	3737	4052	4240	1960
^{140}Ba	1 ± 3	0 ± 4	0 ± 3	0 ± 4	1 ± 2	0 ± 4	–	–	0 ± 5	2 ± 2
^{134}Cs	2 ± 5	75 ± 1	84 ± 1	82 ± 2	24 ± 2	19 ± 2	59 ± 1	100 –9	24 ± 2	16 ± 2
^{137}Cs	0 ± 6	74 ± 2	86 ± 1	84 ± 2	24 ± 3	18 ± 3	68 ± 1	70 ± 2	18 ± 4	13 ± 4
^{156}Eu	6 ± 4	5 ± 5	4 ± 6	7 ± 5	10 ± 6	3 ± 9	–	–	10 ± 13	0 ± 6
^{131}I	11 ± 4	100 –10	79 ± 3	100 –10	16 ± 3	13 ± 5	–	–	6 ± 9	7 ± 4
^{85}Kr	8 ± 1	100 –11	74 ± 10	73 ± 8	4 ± 1	13 ± 2	58 ± 8	57 ± 7	15 ± 2	10 ± 2
^{140}La	1 ± 4	1 ± 4	2 ± 4	0 ± 3	1 ± 2	3 ± 3	–	–	0 ± 6	0 ± 4
^{95}Nb	0 ± 6	0 ± 5	4 ± 5	0 ± 4	2 ± 3	0 ± 3	0 ± 2	0 ± 2	1 ± 2	0 ± 2
^{147}Nd	9 ± 8	0 ± 11	15 ± 8	12 ± 11	3 ± 9	0 ± 17	–	–	ND [5]	8 ± 10
^{144}Pr	0 ± 5	0 ± 5	2 ± 5	1 ± 5	0 ± 5	0 ± 5	0 ± 3	0 ± 2	0 ± 5	0 ± 4
^{106}Ru [3]	0 ± 4	13 ± 3	1 ± 3	0 ± 3	0 ± 3	0 ± 3	2 ± 2	0 ± 2	0 ± 4	4 ± 2
^{103}Ru	0 ± 4	19 ± 3	0 ± 4	0 ± 3	0 ± 3	2 ± 3	0 ± 16	1 ± 12	0 ± 3	0 ± 2
^{129m}Te [4]	2 ± 17[4]	37 ± 14[4]	86 ± 12[4]	34 ± 12[4]	7 ± 8[4]	26 ± 11[4]	–	–	18 ± 15[4]	0 ± 7[4]
^{131m}Xe	5 ± 1	100 –7	84 ± 7	90 ± 6	5 ± 1	11 ± 1	–	–	22 ± 2	15 ± 2
^{91}Y	4 ± 5	0 ± 10	17 ± 4[d]	0 ± 5	4 ± 3	0 ± 12	–	–	1 ± 16	6 ± 4
^{95}Zr	0 ± 6	0 ± 5	7 ± 5	0 ± 3	2 ± 3	0 ± 3	0 ± 1	0 ± 1	2 ± 2	0 ± 2

[1] Statistical uncertainty values are ± 1σ. Non-physical negative release percentages that were not statistically significant were reassigned a value of zero. Release percentages of 100% were assigned negative uncertainties only.

[2] From an element irradiated in a light-water loop (BTF test section) in the NRU research reactor; other samples were from an element irradiated in a Darlington power reactor.[3] Detected as ^{106}Rh.

[4] Non-physical ^{129m}Te release percentages (>100%) were obtained in some tests due to ^{144}Pr interference with the 696 keV peak, and a large uncertainty in the relative fission and gamma yields of ^{144}Pr and ^{129m}Te. The ^{129m}Te releases quoted in this table were scaled to the ^{137}Cs releases in test J03.

[5] The ^{147}Nd gamma-ray at 531 keV was not detected in this test.

Table 4-3 Integral Fission-Product Releases in the BTF Experiments

Isotope	Integral Release* In BTF-107 (%)	Integral Release* In BTF-104 (%)	Integral Release* In BTF-105A*** (%)	Integral Release* In BTF-105B (%)
Noble Gases				
^{85m}Kr	37 ± 3	10 ± 4	2 ± 1	25 ± 6
^{85}Kr	-	47 ± 6	-	24 ± 7
^{87}Kr	-	8 ± 2	-	10 ± 3
^{88}Kr	37 ± 2	7 ± 2	3 ± 2	11 ± 3
^{133m}Xe	-	20 ± 2	-	23 ± 8
^{133}Xe	15 ± 7 **	23 ± 6	0.3 ± 0.3	27 ± 19
^{135}Xe	30 ± 4	14 ± 2	3 ± 2	30 ± 8
Iodine				
^{131}I	56 ± 2	33 ± 5	$0.2\ ^{+2.0}_{-0.1}$	21 ± 7
^{133}I	68 ± 34	20 ± 5	$0.2\ ^{+2.0}_{-0.1}$	21 ± 8
^{135}I	61 ± 8	-	-	$19\ ^{+7}_{-5}$
Cesium				
^{134}Cs	-	72 ± 6	-	40 ± 12
^{137}Cs	56 ± 3	59 ± 5	-	34 ± 7
Tellurium				
^{132}Te	20.8 ± 1.3	2.5 ± 0.7	-	1.1 ± 0.3
Mo/Tc				
^{99}Mo	6.3 ± 0.7	-	-	-
^{99m}Tc	0.08 ± 0.01	-	-	-
Low-Volatiles				
^{95}Zr	-	-	-	< 1
^{103}Ru	-	-	-	< 1
^{106}Ru	-	-	-	< 1
^{140}Ba	1.71 ± 0.01	1.4 ± 0.2	-	-
^{140}La	0.126 ± 0.001	-	-	-
^{144}Ce	-	-	-	< 1

* Note that throughout this report, σ symbolizes the sample deviation, not the probability distribution deviation that σ often symbolizes. Unless indicated otherwise, uncertainties are stated to 1 σ and a Gaussian distribution is assumed.

** ^{133}Xe activity was not detected in the blowdown tank liquid phase because of the low gamma-ray emission energy of the isotope.

*** The integral fission-product releases in the BTF-105A test are based on the blowdown tank gamma-spectrometry measurements before and after the blowdown line water flush, not taking into account measurements on the blowdown line, and the estimated uncertainties have been increased to take this into account.

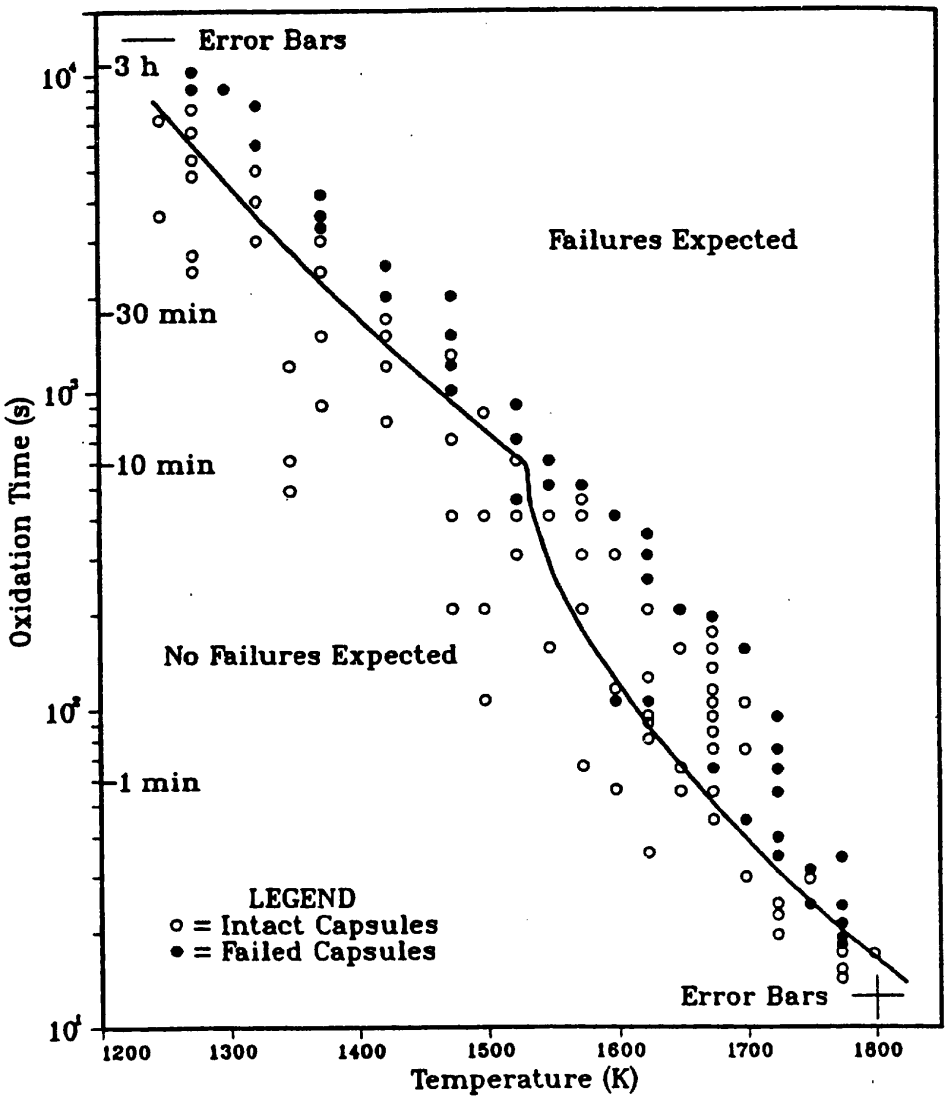

Figure 4-1 Fuel Cladding Failure Map for Sawatzky Failure Criterion (Solid Line)

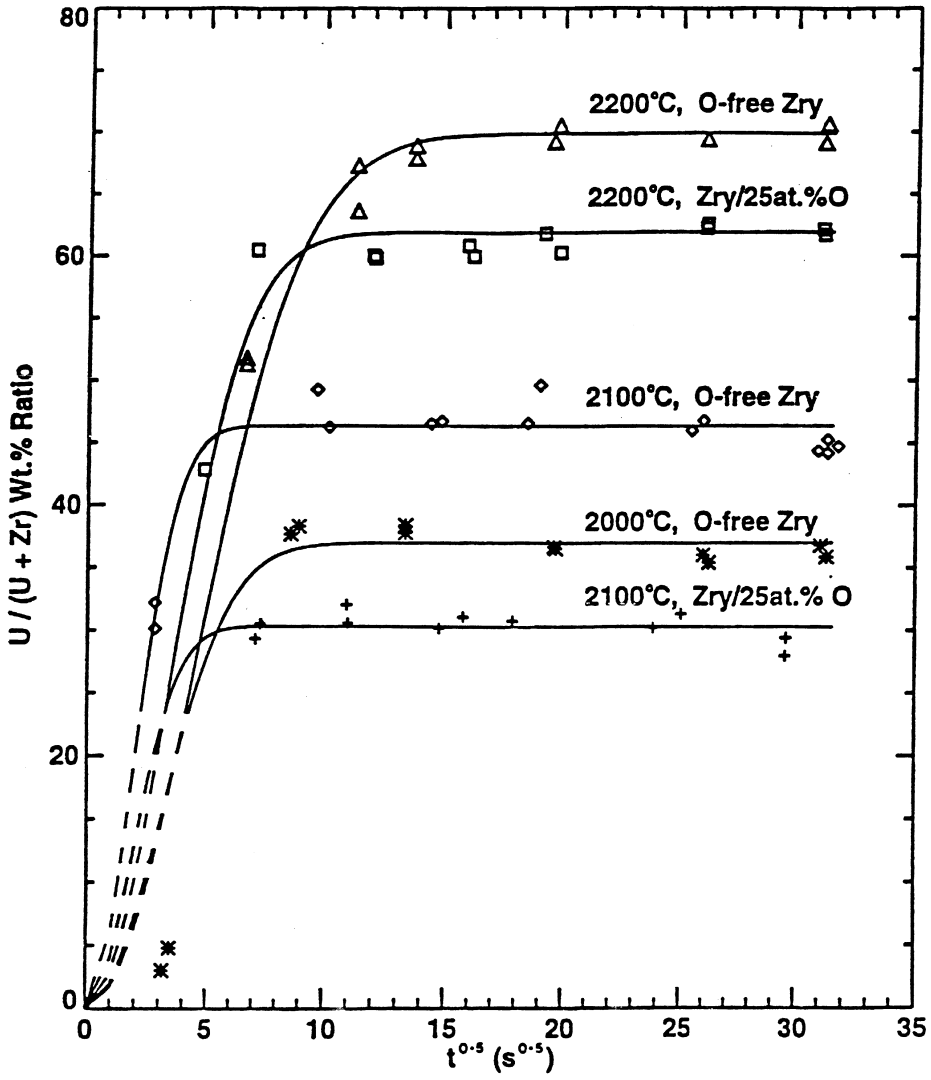

Figure 4-2 UO_2 Solubilities in Zircaloy at 2000, 2100 and 2200°C and in Zircaloy/25atom%O at 2100 and 2200°C

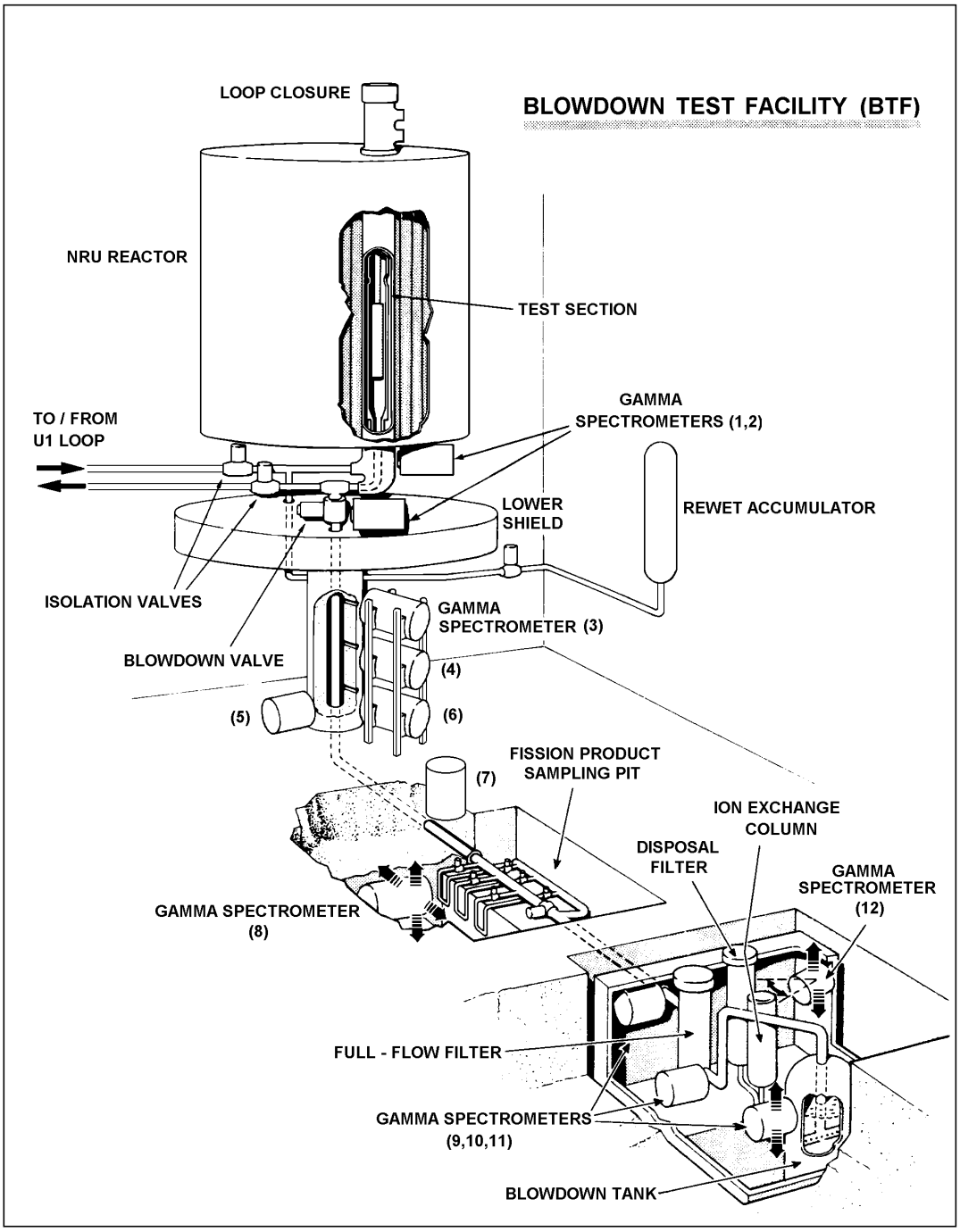

Figure 4-3 Schematic of the Blowdown Test Facility

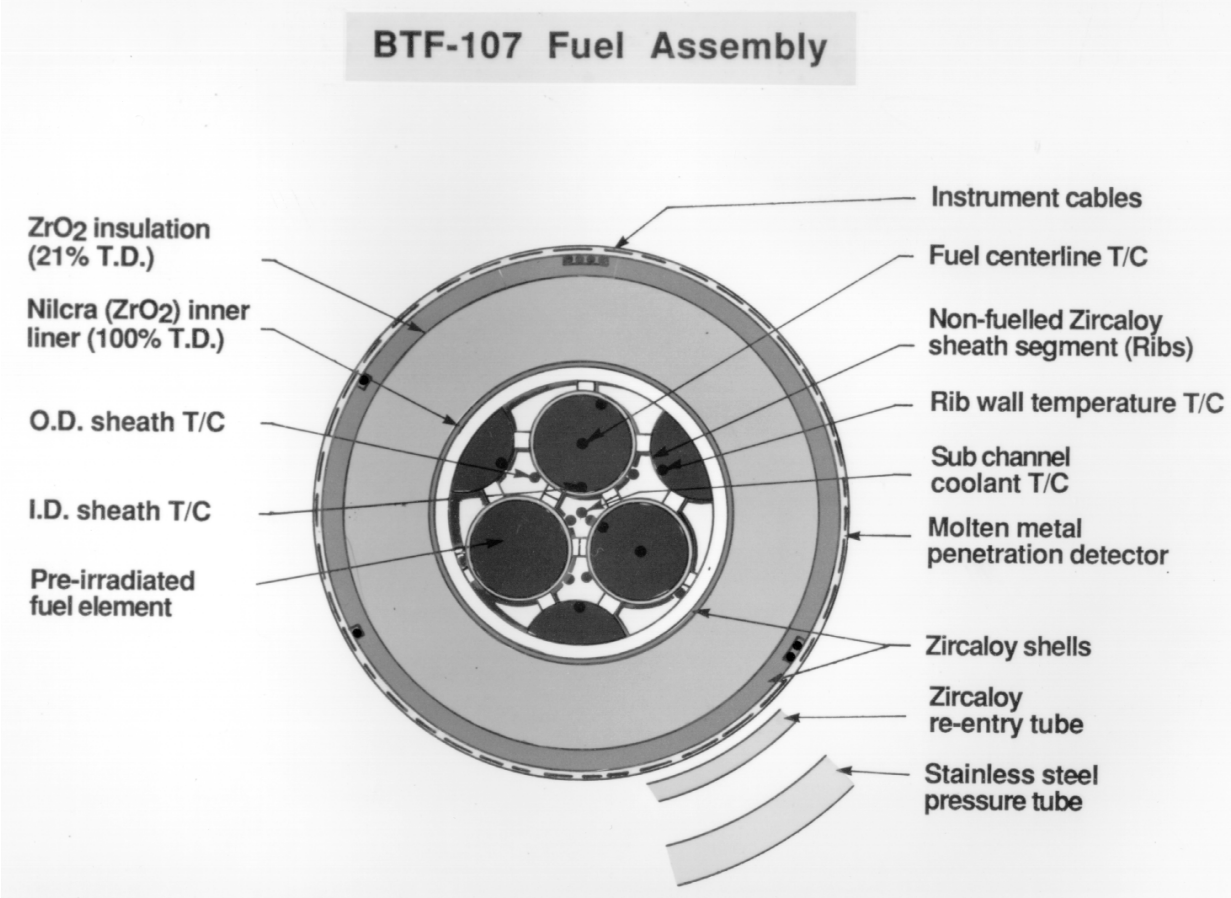

Figure 4-4 Transverse Cross Section of BTF-107 Fuel Assembly

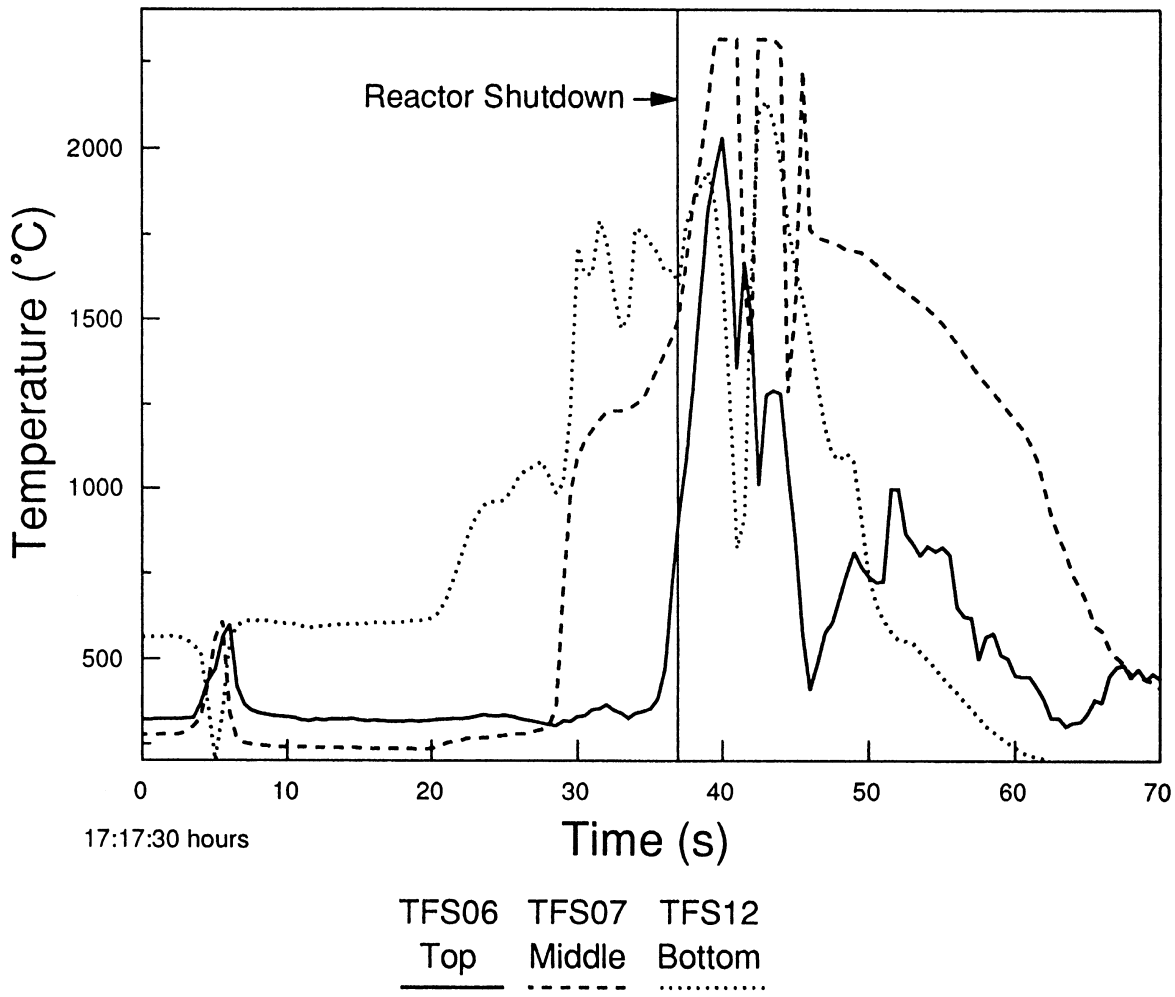

Figure 4-5 Cladding Temperatures at Three Axial Locations Along the Fuel Elements During the BTF-107 Transient

Figure 4-6 Composite Photograph of the Bottom Surface of a Section Cut near the Bottom End of the BTF-107 Fuel Assembly

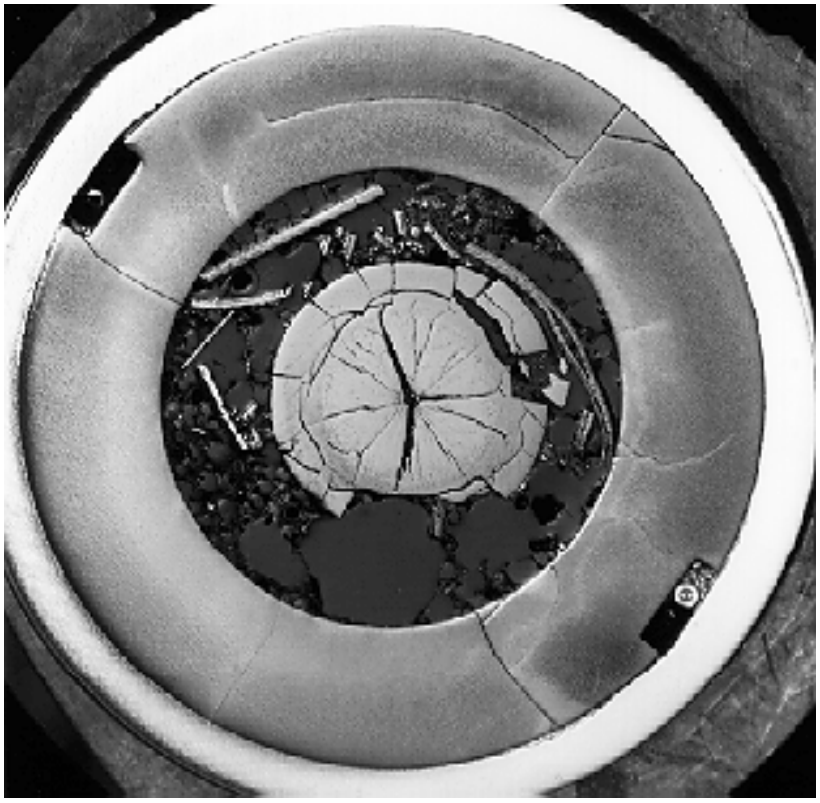

Figure 4-7 Polished Section of the BTF-104 Fuel Log, Elevation 36 mm

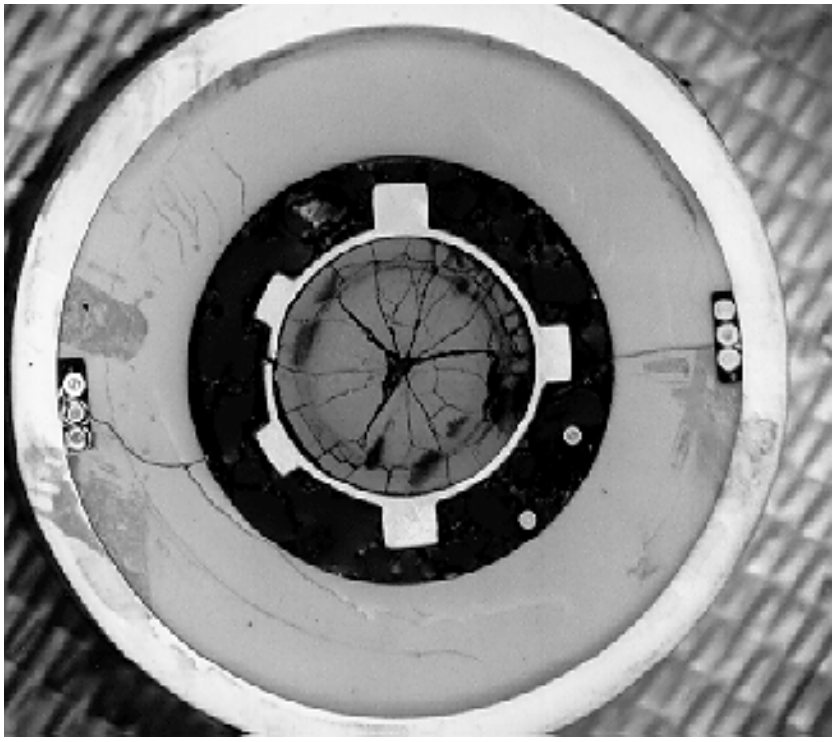

Figure 4-8 Polished Section of the BTF-104 Fuel Log, Elevation 252 mm

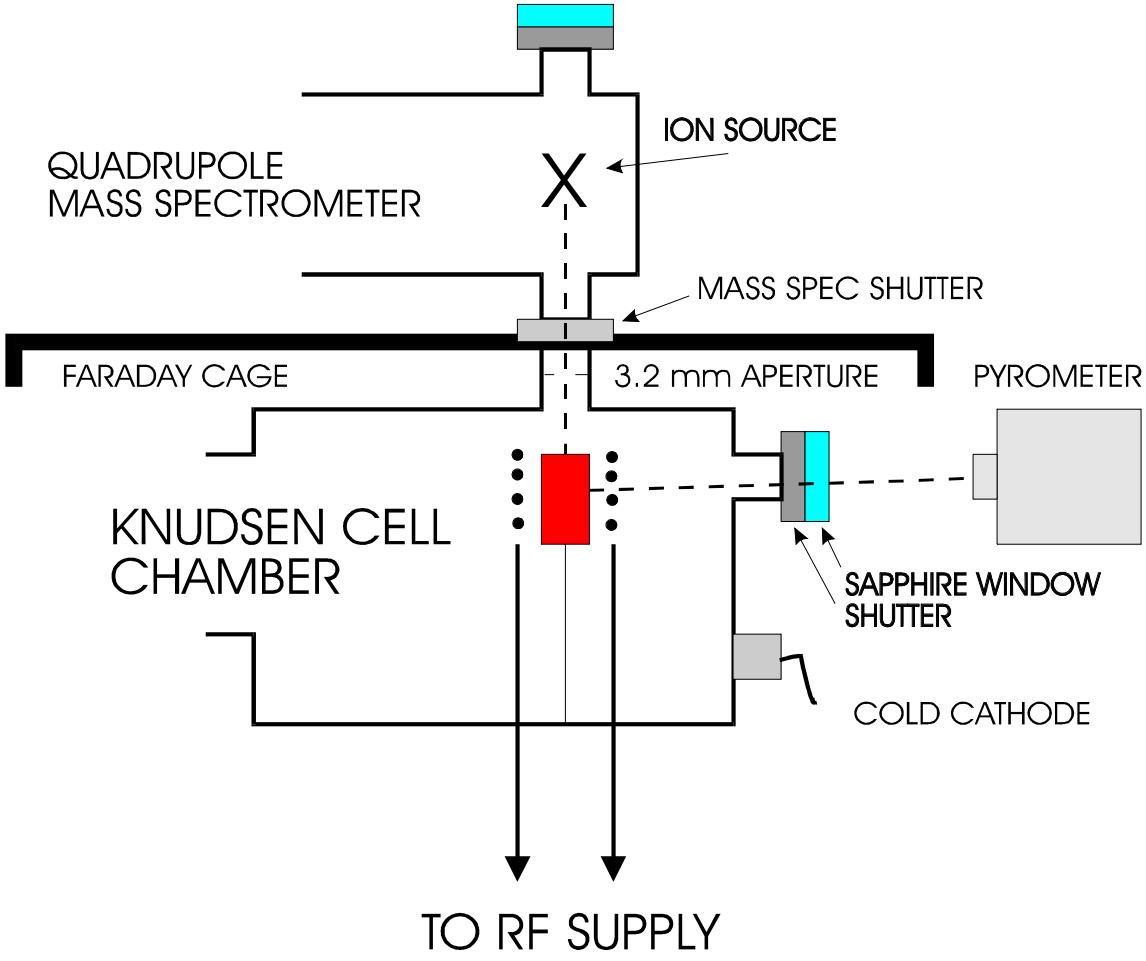

Figure 4-9 Schematic Diagram of the Knudsen Cell-Mass Spectroscopy Facility of AECL Knudsen Cell is Located in between the Coils Supplying the RF Power

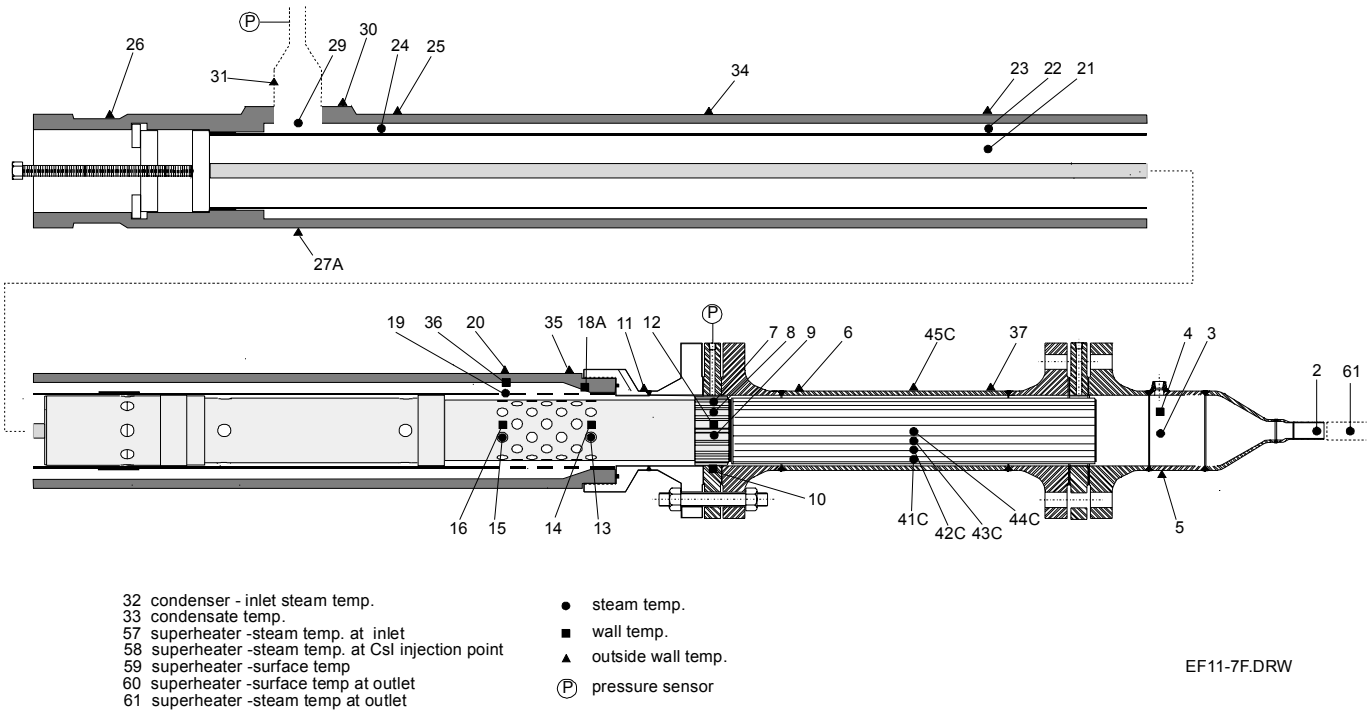

Figure 4-10 Schematic of End-Fitting Aerosol Deposition Rig

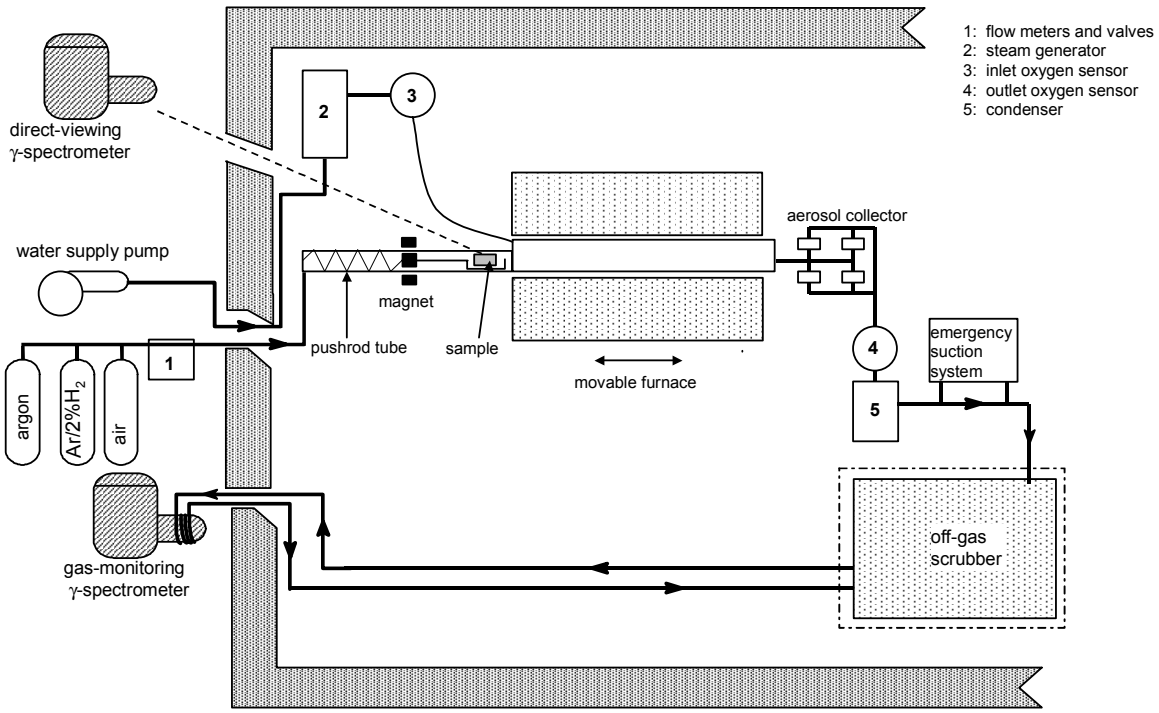

Figure 4-11 Schematic Of HCE4 Hot-Cell Apparatus

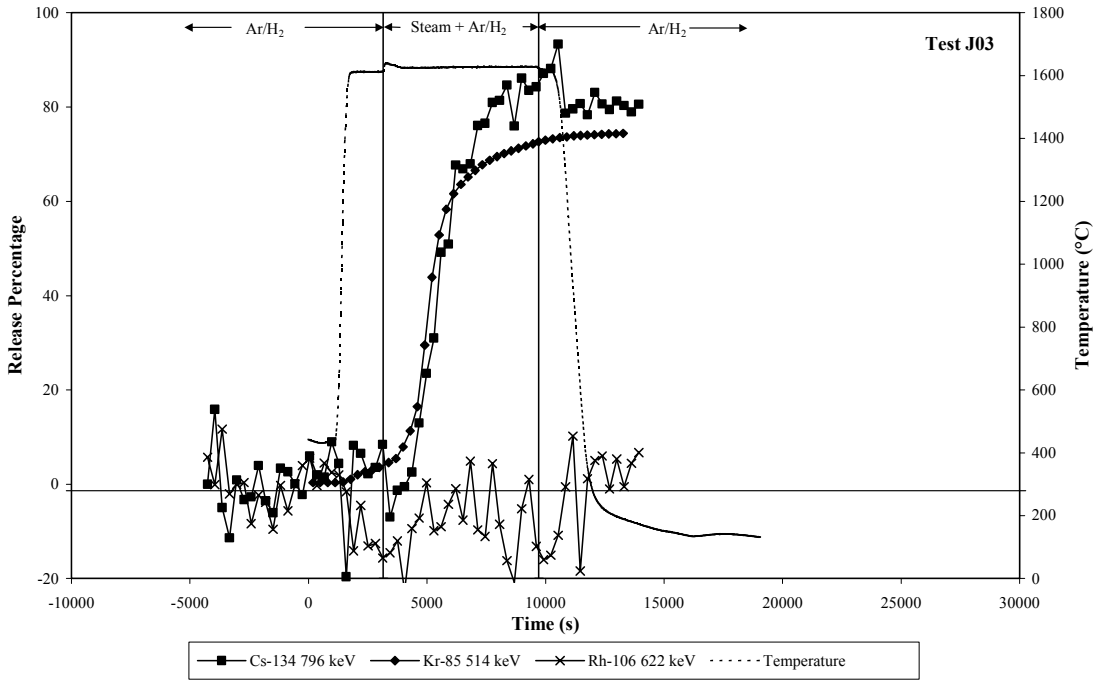

Figure 4-12 Cesium, Krypton and Ruthenium (AS Rh-106) Release (%) as a Function of Time for HCE4 Test J03 (20-mm-Long Clad Darlington Fuel, Steam + Ar/H_2, 1640°C

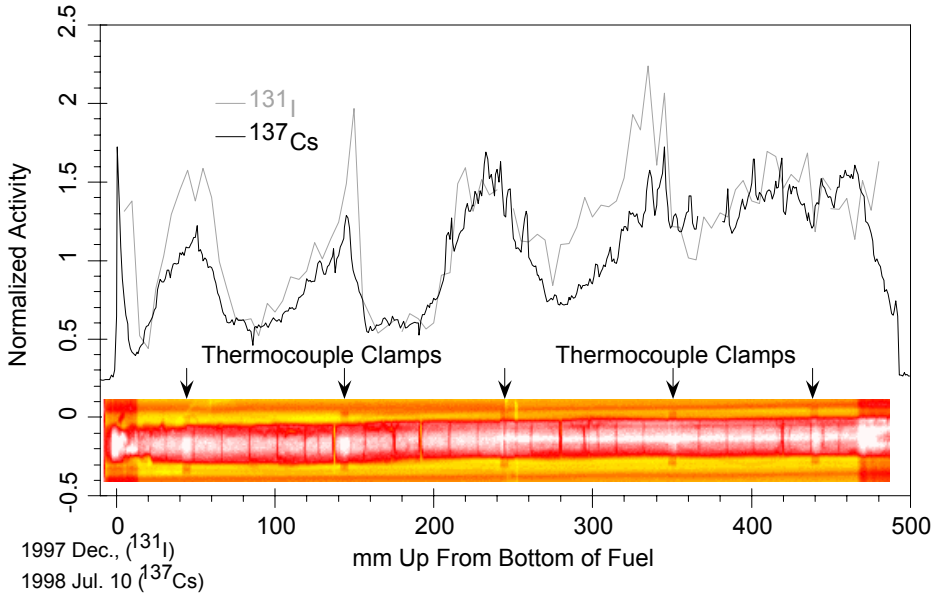

Figure 4-13 ^{131}I and ^{137}Cs Activity Along BTF-105B Fuel Element

5. FISSION PRODUCT SOURCE TERM IN CONTAINMENT (J.C. Wren)

5.1 Background

Radionuclides released from the Reactor Coolant System (RCS) into containment would be in the form of gases, particulates or dissolved species in liquid aerosols and bulk aqueous solutions. While undergoing the natural radioactive decay, the radionuclide fission products are transported, transformed and/or removed from the containment atmosphere. The key information needed for fission product source term analysis from containment to the outside atmosphere is the fractions of the nuclides in containment in airborne forms, gases and aerosols, as a function of time. That is, the change in the distribution of the fission products among various locations in containment (containment atmosphere, sump water and containment wall and equipment surfaces) needs to be predicted. The fission products in the containment atmosphere need to be further divided into gaseous species and aerosols, because of wide differences in their mobility and attenuation at release paths.

For simulating the transport and transformation of the nuclides in containment, the nuclides are grouped essentially into three categories: noble gases, iodine and the other fission products.

Noble Gases

The inert and relatively insoluble noble gases (xenon and krypton) are only subjected to convective flow and release to outside atmosphere through leak paths. No other transport processes or physical and chemical transformation (other than the natural radioactive decay) are applied to the simulation of the noble gas behavior in containment.

Iodine

Iodine is released from the RCS into the containment atmosphere mainly as highly soluble non-volatile species, and, hence, mainly as dissolved species in liquid aerosols or in bulk water phase. Only a small fraction would be released as gaseous species. However, exposed to highly oxidizing and radiation environment, non-volatile iodine species dissolved in liquid aerosols and bulk water could be slowly but continuously transformed to volatile species. Whether initially released from the RCS or later formed in containment, the volatile iodine species also have intermediate solubility in water and/or are easily adsorbed on various surfaces. Because of their ability to undergo chemical transformation and the different transport and removal mechanisms for different iodine species, iodine in various forms (gases, liquid aerosols, dissolved in aqueous solutions and adsorbed on surfaces) must be followed separately.

Other Fission Products

The other fission products released from the RCS would be non-volatile under post-accident containment conditions. Furthermore, they are not considered to transform to volatile species in containment. Thus, they are airborne only as dissolved species in liquid aerosols, and not as gases, and the transport and the removal of these fission products from the containment atmosphere follow the behavior of liquid aerosols. Liquid aerosols would be removed and transported by various mechanisms including jet impingement, pool scrubbing, agglomeration, gravitational settling, diffusiophoresis, thermophoresis and turbulent deposition.

The analysis of noble gases is straightforward. However, the behavior of liquid aerosols and iodine are rather complex and considerable R&D has been carried out in these two areas. The R&D performed at AECL in these two key areas are summarized.

5.2 AECL R&D on Iodine Behavior

Radioiodine is the most important nuclide for its potential for public dose in both licensing basis accidents and severe accidents. This is because of the combination of its large inventory in irradiated fuel, potential for formation of volatile chemical species under post-accident reactor conditions, and its hazardous radiological effects. Phenomena and processes governing iodine behavior in containment are also very complex. To understand this complex behavior and to develop analysis and predictive tools (i.e., models), extensive studies on iodine behavior in containment have been carried out at AECL for over 20 years. In that time, but particularly over the past 10 years, a detailed mechanistic understanding of iodine behavior in post-accident containment has evolved and mathematical models to capture this understanding have been developed.

5.2.1 Technical Problem Description

Iodine would be released from the RCS into containment as gases and dissolved species in liquid aerosols and in aqueous solutions. The fractions of iodine in the various forms would be provided by upstream analysis. Various experiments and thermodynamic and kinetic modeling studies have established that iodine would be released primarily as cesium iodide (CsI) and only a small fraction would be released as gaseous species such as HI and •I (iodine atom) [1]. Cesium iodide is an ionic salt that easily dissolves to form Cs^+ and I^- ions in liquid aerosols or bulk water. The gaseous species are also highly soluble in water and/or very unstable. To be conservative, the gaseous species initially released from the RCS into containment atmosphere are all assumed to be molecular iodine (I_2).

Once released into containment, iodine species would continually change their forms and speciation. In the presence of high radiation fields in a post-accident containment, non-volatile I^- in liquid aerosols or in aqueous solutions could be oxidized by radiolytic processes to form volatile molecular iodine (I_2). Molecular iodine in aerosols and aqueous solutions would partition into the gas phase where it could persist, be further oxidized to non-volatile iodine oxides (e.g., HOI, IO_3^-) or be reduced back to its original non-volatile I^- state by thermal or radiolytic processes. Iodine species in solution could also react with organic compounds present in containment to form organic iodides (RI), which, like I_2, could subsequently decompose to I^-, or partition into the gas phase. Finally, the deposition of both gaseous and aqueous iodine species on surfaces could alter the concentrations of iodine species or induce surface-catalyzed transformations. A simplified representation of the iodine chemical transformation (or speciation) and transport that may occur in containment following an accident is given in Figure 5-1.

Because of continuous presence of radiation field in containment following an accident, many of the processes described above circumvent the achievement of equilibria among aqueous iodine species that would be expected in non-radiolytic conditions. Therefore, the distribution and speciation of iodine expected at thermodynamic equilibrium would not be observed in an accident scenario. Instead, time-dependent processes, such as reactions of iodine with water radiolysis products, mass transfer, and surface adsorption, dominate iodine behavior. In fact, the

conversion of non-volatile iodine species to volatile iodine species in containment would contribute more significantly to iodine volatility than the gaseous fraction initially released from the RCS, except the initial stage of an accident. The rates of these processes determine the fraction of iodine in the forms of gas, aerosols, dissolved species in water and adsorbed species on surfaces in containment as a function of time following an accident. These rates are functions of other time dependent parameters such as iodine concentration, radiation dose rate, water pH, temperature, the presence and concentrations of organic and inorganic impurities, and the type of containment surfaces.

Consequently, predicting iodine volatility in containment requires a sound understanding of a large number of kinetic processes, schematically shown in Figure 5-1. The kinetics of these processes, which determines the gaseous iodine concentration in containment following an accident, is rather complex. There are many factors contributing to the complexity:

1. Iodine could exist in various oxidation states, ranging from −1 to +7 (such as I^-, RI, I_2, HOI, IO_2^-, IO_3^- and IO_4^-, where RI represents organic iodide). Only some of these iodine species (i.e. RI and I_2) are volatile. Thus, to determine iodine volatility (or the gaseous iodine concentration) in containment, the conversion between these iodine species must be considered. The number of reactions and the thermodynamic properties to be considered in modeling iodine behavior increases exponentially with the number of oxidation states.
2. Because of the continuous presence of radiation and because iodine would be present in containment water at a trace level, the iodine chemistry in containment under accident conditions would be water radiolysis driven. The conversion of iodine species will occur mainly via reactions with water radiolysis products (e.g., •OH, $•O_2^-$, H_2O_2). This complicates the kinetics of iodine reactions because water radiolysis products are very reactive and, as well, various impurities at trace levels could compete with iodine species for reaction with the water radiolysis products. The reactions of impurities with water radiolysis products can not only directly affect the concentrations of those water radiolysis products but they can also affect the chemical environment, such as pH, by producing different chemical species.
3. The chemical system present in containment after an accident would be under continuous irradiation. Because reactive chemicals are continuously produced by radiolysis and because the temperature in containment would be relatively low (<150°C), the system would never be in thermodynamic equilibrium, although it may reach steady state. Hence, chemical thermodynamic calculations are not sufficient to determine iodine speciation. The kinetics of each reaction path, not just the final stable chemical state, must be considered.
4. Because many of the reactions and transport processes are highly inter-dependent and have widely different dependences on conditional parameters such as temperature, dose rate, etc., one cannot easily separate the individual effects of the parameters from a limited number of engineering scale integrated effects tests.

5. In containment, both homogeneous and heterogeneous processes occur and are inter-dependent. For example, iodine partitioning between the gas and aqueous phases would be very dependent upon containment geometry but the homogeneous aqueous phase and gas phase reactions would not be affect by the containment geometry. As a result, it is difficult to establish a scaling factor, simply based on correlating the results from a limited number tests in facilities of different scales. Nevertheless, integrated effects tests in an engineering-scale test facility are necessary to establish the relative importance of various processes (both homogeneous and heterogeneous) and to prioritize the supporting bench-scale R&D activities that examine individual processes.

5.2.2 AECL Iodine Program Overview

To develop a comprehensive understanding of the chemical kinetics and transport of the complex system of iodine in containment, and so to develop a practical safety analysis tool, i.e., a predictive iodine behavior model, the AECL R&D program on iodine behavior in containment has taken an integrated approach. The program has consisted of:

1. Integrated-effects tests in an engineering-scale Radioiodine Test Facility (RTF),
2. Supporting bench-scale tests to separate and quantify individual processes and parametric effects,
3. Development and validation of containment iodine behavior models for safety analysis, LIRIC (Library of Iodine Reactions In Containment) and IMOD (Iodine MODule), and
4. International collaboration and commercial contracts to complement and broaden the knowledge basis.

5.2.2.1 RTF Program

The objective of the RTF test program was to provide a database for the validation of iodine behavior models through the study of the effects of individual model components and conditional parameters on iodine volatility in an integrated-effects test facility, and to evaluate the relative importance of various model processes. Tests in an integrated facility were also intended to ensure that unforeseen modeling phenomena were elucidated.

Description of RTF

Integrated effects tests were performed in the Radioiodine Test Facility (RTF) at AECL Whiteshell Laboratories over the period of 1988 to 1999. The RTF was an intermediate-scale facility that provided for many combinations of potential reaction media (gas phase, aqueous phase and a variety of surfaces) and conditions (pH, temperature, radiation, various initial concentrations and initial speciation of iodine) to simulate the chemical system expected in a reactor containment building following an accident. The schematic flow chart and a photograph of the RTF are shown in Figure 5-2.

The central feature of the RTF was a replaceable 340 L vessel that represented the interior of a containment building. The interior of the vessel could be coated to simulate a variety of containment surfaces. Electrical heaters around the outside of the vessel controlled the temperature of the vessel walls in contact with the gas phase up to 110°C and the water temperature up to 90°C. Cobalt-60 pencils could be inserted into the centre of the vessel to

provide an average absorbed radiation dose rate in the aqueous phase of about 2.0 $kGy \cdot h^{-1}$ in 1988[2]. Prior to a test, the vessel was partially filled with water and selected chemicals were added to the aqueous phase to simulate the sump water chemistry in containment following an accident. The ratio of gas to liquid volume for a typical test was about 10 (the gas volumes was typically about 315 dm^3).

A test generally started with an injection of ^{131}I-labelled CsI into the aqueous phase, providing an initial aqueous iodide concentration of about 1×10^{-5} $mol \cdot dm^{-3}$. Various auxiliary loops allowed for on-line measurement of the iodine concentration in the gas and aqueous phase, pH, redox potential and the concentration of dissolved oxygen. Gas and liquid samples were also taken periodically for off-line measurements of trace metals, hydrogen peroxide, hydrocarbon and organic iodide concentrations, using high-performance liquid chromatography (HPLC) and gas chromatography (GC). At the end of each test, the iodine surface loadings were determined by washing the vessel and measuring the ^{131}I activity in the washes and the residual ^{131}I activity on the surfaces.

The parameters studied in the RTF included: (1) type of vessel surface (stainless steel (electropolished, untreated), organic coatings (vinyl, epoxy, polyurethane) on carbon steel or concrete, and inorganic coatings (zinc primer)), (2) gamma radiation field (present or absent), (3) pH (controlled or uncontrolled) within a range of 4.5 to 10.5, (4) temperature constant throughout a test (25, 60, 90°C) or with steps from 25 to 80°C, (5) condensing or non-condensing steam atmosphere and (6) with or without organic or inorganic additives.

Technical Contributions of the RTF Test Program

Over 50 tests were performed in the RTF before it was decommissioned in 1999. The RTF program revealed the importance of a number of unexpected phenomena relating to iodine behavior that were not previously observed in large-scale studies or bench-scale studies. The integrated tests in the RTF have also allowed for the evaluation of the relative importance of physical and chemical processes in determining speciation and volatility of iodine, and have provided critical data for the development and validation of the models for predicting iodine behavior in an accident. Various chemical and physical measurements performed in each test (such as iodine speciation and measurements of water radiolysis products and impurities) have provided data with which to examine the validity and self-consistency of various subsets within the mechanistic models for predicting iodine behavior.

Most of the data reports on the RTF tests are propriety; however, some of key results have been presented in various publications [2-4]. Some of the RTF test results are also shown in Figures 5-3 - 5-6.

---

[2] The absorbed dose rate decreased with time over the operating life of the RTF due to decay of the cobalt source (half-life of 5.3 a). The average absorbed dose rate in the gas phase would have been about 10 times lower than the dose rate in the liquid. The ^{60}Co gamma radiation was not attenuated significantly by the depth of the water in the RTF.

The contributions of the RTF program to the understanding of iodine behavior have been significant. The key contributions include:

1. The RTF test program provided concrete data, showing that iodine behavior in the presence of a continuous radiation source dramatically differs from that of non-radiolytic conditions (Figure 5-3). Consequently, the gas phase iodine concentrations and iodine speciation observed in the RTF tests were very different from those predicted from the equilibrium thermodynamic calculations.The RTF studies firmly established the effect of pH on iodine volatility in a containment-like vessel (Figure 5-4). The gas phase concentration of iodine increases by a factor of 5 – 10 with a decrease in pH by one unit, having a higher dependence at a lower temperature. The early assessments emerged following the TMI accident postulated that a sufficiently high pH in containment water would keep iodine trapped in the containment sump water as I^-. However, the observed pH dependence of iodine volatility was different from those predicted from the equilibrium thermodynamic calculations.Iodine volatility does not vary appreciably with temperature (Figure 5-5). This observation was contrary to an earlier assumption that temperature would increase iodine volatility substantially. This assumption was mainly based on the fact that the partition coefficients of volatile iodine species (I_2 and organic iodides) would decrease exponentially with increasing temperature. The RTF tests show that iodine volatility is relatively insensitive to temperature. The subsequent bench-scale established that the hydrolysis rates of I_2 and organic iodides to non-volatile iodide in solution increases exponentially with temperature, effectively counterbalancing the partitioning behavior. Temperature also affects the net surface adsorption rates of iodine species.
4. The RTF program demonstrated that containment surfaces would have a major influence on iodine behavior, especially under radiation conditions. In a radiation field, surfaces (particularly organic-based paints) influence iodine volatility through more ways than simply iodine deposition and reactions on surfaces, i.e., through their indirect impacts on pH and iodine speciation (Figure 5-6). The subsequent bench-scale studies established that the surface impacts on pH are the result of organic impurities dissolved from the surface into the aqueous phase, and that a variety of organic iodides could be formed in the presence of organic-based painted surface; most of these organic iodides are, however, far less volatile than CH_3I.
5. Containment surfaces can absorb considerable amount of iodine, providing “iodine sinks”. The iodine-surface interaction is a dynamic process and is one of the key processes controlling the time-dependent concentration of gaseous iodine. Surface adsorption is greater in the presence of radiation, except for the test with the zinc primer surface. In the absence of radiation, adsorption occurred mainly in the aqueous phase. In the presence of radiation, the iodine adsorption occurred mainly in the gas phase and was more significant. The observed surface loading was related to the gas phase iodine concentration. The concentration was higher in the presence of radiation, and equally significant on bare stainless steel and painted surfaces. When the pH was kept high, the surface loading was significantly reduced.

The RTF studies have identified the key processes that must be considered in determining iodine volatility under post-accident containment conditions, and the parameters to which these processes are sensitive. The conditional parameters affect various chemical and transport

processes to different extents, but the RTF data only reflect the net effects of these parameters on iodine volatility. Therefore, to aid the interpretation of the RTF test results and to develop an iodine behavior model that would have solid technical basis and have a predictable capability, the key processes need to be understood as functions of containment conditions. To achieve this understanding, the key processes were studied under the bench-scale program.

5.2.2.2 Supporting Bench-Scale Program

Although the RTF tests were necessary and have provided many useful results, as with any engineering-scale integrated-tests on a complex system, the RTF test results were often difficult to analyze and interpret, and, hence, difficult to extrapolate to accident conditions. To aid in the interpretation of the RTF test results and to develop models that would have solid technical basis for their predictable capability, AECL has performed extensive bench-scale, separate effects studies in many key areas, including:

1. Aqueous Phase Chemistry
   - 1.1 Inorganic Iodine Reactions
   - 1.2 Water Radiolysis
   - 1.3 Reactions of Organic Impurities and Organic Iodides
2. Aqueous-Gas Partitioning of Volatile Species
3. Iodine – Surface Interaction

Aqueous Phase Inorganic Iodine Reactions

These reactions are the most basic process which converts non-volatile iodine species to volatile I_2, which then undergoes various reactions, including conversion back to non-volatile species, aqueous-gas phase interfacial mass transfer, organic iodide formation, etc. Under the post-accident containment conditions, as many as 80 reactions, including thermal iodine reactions and equilibria and reactions of iodine species and water radiolysis products, have been used to describe this process. For quantitative modeling of iodine volatility, the rate constants of these reactions need to be defined as a function of the parameters of containment conditions such as temperature, pH, radiation dose rate, initial iodide concentration, etc.

Many of the rate constants were available in literature. We have performed a critical review of all the potential inorganic iodine reactions and their rates and equilibrium constants, and concluded that, for most, the reaction mechanisms, individual rate constants and their dependence on pH and temperature were reasonably well established. For those identified as requiring re-evaluation from the review, we have performed detailed experimental and model analysis studies to re-establish their reaction mechanisms and kinetics. These reactions include HOI disproportionation (to I^- and IO_3^-) and iodine equilibria [5], reduction of I_2 by H_2O_2 [6] and temperature dependence of equilibrium constant of iodine hydrolysis.

Water Radiolysis

Water in containment following an accident is subjected to continuous irradiation. For iodine behavior in containment, β- and γ-radiation are of concern. The primary products of water radiolysis are:

$$H_2O \xrightarrow{\gamma} \bullet OH(2.7), e_{aq}^{-}(2.6), H^{+}(2.6), H\bullet(0.6), H_2(0.45), H_2O_2(0.7)$$

where the G-values (molecules/100 eV absorbed dose) for the production of the species from the γ-radiolysis of water at 25ºC are provided in brackets for reference.The primary water radiolysis products are very reactive and thus undergo various reactions with each other and any other reactive species dissolved in water. For modelling the behavior of the radiolysis products of pure water, the primary production process and about 40 reactions of the water radiolysis products with each other have been assembled in the mechanistic iodine behavior model, LIRIC. This reaction set has been used in kinetic models to reproduce the behavior of molecular products of water radiolysis such as H_2, O_2 and H_2O_2 as a function of dose rate, initial concentration of the molecular species and pH. (Note that free radicals, such as •OH, e_{aq}^{-}, H• are difficult to measure experimentally because they are highly reactive and, consequently, they exist at very low concentrations.)

The water radiolysis products also react with iodine, metal ions and organic impurities dissolved in water. Their reactions with iodine were described previously. Metal ions, such as Cu^{+}/Cu^{2+} and Fe^{2+}/Fe^{3+}, even at a trace level, can significantly affect water radiolysis product concentrations by catalytic consumption. These metal ions would be present in water in contact with metal surfaces and, hence, these reactions have been incorporated in LIRIC. The studies on the reactions with organic impurities are described below.

Reactions of Organic Impurities and Organic Iodides

In the presence of radiation, dissolved organic impurities react with the water radiolysis products to form organic radicals, which then react with dissolved oxygen to form organic acids and eventually CO_2 [7-9]. Thus, organic impurities dissolved in water can affect both the concentrations of available water radiolysis products and pH. Organic radicals also react with I_2 to form organic iodides, where some organic iodides are more volatile and more difficult to remove than I_2.

The key organic processes to consider for iodine modeling include

a) Sources of organic compounds dissolved in water
b) Radiolytic decomposition of organic impurities
c) Organic iodide formation, decomposition and aqueous-gas phase partitioning

These organic processes are, however, complex. An additional challenge is how to handle a wide range of organic impurities and organic iodides that could be present in containment following an accident.

Sources of Organic Compounds Dissolved in Water

The organic compounds that would have a significant effect on iodine behavior are dissolved organic compounds. We have established that the organic solvent material trapped in a paint polymer matrix could be released into the water and that painted surfaces could be the main

source of the dissolved organic impurities in the containment water following an accident. The solvents and thinners used in paint are generally small molecules (e.g., methylethylketone (MEK), methylisobutylketone (MIBK), toluene, xylene, ethylbenzene, methanol, ethanol and acetone) that have an intermediate volatility suitable for paint application. These compounds also have reasonably high solubilities in water. Relatively large concentrations, at the millimolar ($mmol \cdot dm^{-3}$) level, of MIBK (methyl isobutyl ketone), a major paint thinner constituent, released into water were observed. Also observed were micromolar ($\mu mol \cdot dm^{-3}$) quantities of MEK, toluene and xylene, other major components of paint solvents and thinners [10].

To establish the organic impurity concentrations in containment water, we have performed extensive studies on the release of organic solvents from painted surfaces into water [10,11]. The rates of release of various organic solvents were measured as a function of temperature, paint type, paint thickness and aging. These studies have shown that the release kinetics follow a first order dependence on the solvent concentration trapped in the paint matrix (an example shown in Figure 5-7). The first order rate constant is mainly a function of temperature and paint thickness and nearly independent of other parameters such as paint type, paint solvent, the pH of the water and radiation. The total amount released is the amount initially trapped in the paint matrix, which appears to depend on mainly the amount of solvent used in paint application, paint aging and paint thickness, but not on paint type, solvent type or temperature.

The simple dependence of the organic solvent release kinetics makes modeling of the organic solvent release into water manageable. A universal formula for the rate constant for the release of an organic solvent from an immersed painted surface into the aqueous phase has been established. This dissolution model has been incorporated into iodine behavior models, LIRIC and IMOD.

Radiolytic Decomposition of Organic Impurities

Once dissolved in water organic compounds undergo reactions with water radiolysis products, dissolved oxygen and molecular iodine. The reactions involved in the radiolytic decomposition of an organic compound to CO_2 are rather complex. As many as 130 reactions, in addition to about 40 water radiolysis reactions, have been used to describe the radiolytic decomposition of a relatively simple compound containing only four carbon atoms, MEK [11]. The number of reactions required to comprehensively address all possible reactions of intermediate species increases with the number of carbon atoms in the initial compound. It is not practical (or even possible) to model in detail the radiolytic decomposition reactions of all the potential organic compounds that may exist in containment water. The iodine behavior models, LIRIC and IMOD, needed a simpler, more generalized set of reactions in an organic-radiolysis sub-model. However, this simple model was required to be able to predict the following parameters as a function of time with acceptable uncertainties:

1. The pH of the containment sump water,
2. The effective concentrations of organic radicals,
3. The concentrations of water radiolysis products, such as •OH, e_{aq}^-, $\bullet O_2^-$, $HO_2\bullet$ and H_2O_2

A simple organic-radiolysis sub-model was developed through R&D conducted in the following steps:

1. A detailed experimental study on the radiolytic decomposition of methyl ethyl ketone (MEK) was performed. MEK was chosen as a representative organic compound.
2. A comprehensive kinetic model that reproduced results of MEK degradation was developed. The model consisted of about 130 organic reactions and was used in combination with the full water radiolysis model in LIRIC.
3. A simplified MEK model involving much fewer reactions was constructed by identification of the key components of the mechanistic model.
4. Experiments were performed using other organic compounds (MIBK and toluene) to quantify general trends.
5. A generic organic radiolysis model was developed by modifying the simple MEK model to take into account the trends and variations observed for different types of organic compounds.
6. The generic organic radiolysis model was further modified for inclusion in IMOD, which does not explicitly model water radiolysis product concentrations.
7. The generic organic radiolysis models for LIRIC and IMOD were evaluated by comparing the model predictions against relevant separate effects experimental data obtained from both laboratory and RTF tests.

Examples of the data and model calculation results from the study on the MEK decomposition are given in Figure 5-8.

Organic Iodide Formation, Decomposition and Aqueous-Gas Phase Partitioning

Organic radicals that would be produced during the radiolytic decomposition of dissolved organic impurities would react rapidly with I_2 to form organic iodides. Organic iodides can also decompose radiolytically to release iodide and organic radicals, hydrolyze to form non-volatile I^- and a corresponding alcohol, or partition into the gas phase. These individual reactions are relatively easy to model; there are no intermediate steps to be considered and their rates follow simple first or second order kinetics. However, the potential range of different organic compounds (and related organic iodides) poses a practical modeling difficulty. Even when one organic compound is considered, radiolytic decomposition will generate several intermediate smaller organic compounds from which various organic iodides could be formed. The rate constant of the radiolytic decomposition of organic iodide does not vary much from one organic iodide to another; being radical reactions, their rate constants are near diffusion controlled. However, the rate constant of the hydrolysis of organic iodide does vary considerably. In addition, the partition coefficient of organic iodide (the ratio of the aqueous phase concentration to the gas phase concentration) varies considerably from one organic iodide to another.

Inclusion of the reactions of every potential organic iodide in the LIRIC model is not practical. There is too much uncertainty in the different sources of organic material within containment and the variety of organic species that may be derived from these sources. Detailed physical modelling of all of the possible organic species would be also computationally intensive and fraught with uncertainty because precise rate information is lacking for most of the potential

species. One way to manage the variety of possible organic iodides is to consider them as members of a smaller number of groups.

In order to group organic iodides in such a way that the grouping does not jeopardize the iodine model performance significantly, the following model development steps were taken.

1. The hydrolysis rate constants and partition coefficients of a wide variety of organic iodides were reviewed (aqueous-gas phase partitioning is described in more detail later). Experiments were also performed to fill the important gaps in the literature data.
2. The review indicated that organic iodides could be grouped into two categories, HVRI (high volatility organic iodides) and LVRI (low volatility organic iodides). Average aqueous-gas phase partition coefficients and hydrolysis rates of HVRI and LVRI were assigned, based on the review.
3. The ratio of the production rate constants of HVRI and LVRI from I_2 and organic radicals in the aqueous phase was determined. This was accomplished by carrying out LIRIC model simulation studies of all the RTF tests performed with organic-painted vessels. A ratio that consistently reproduced the gas phase iodine speciation in these tests (i.e., gaseous I_2, HVRI and LVRI concentrations) was extracted. The value of this ratio was further determined by a bench-scale study.

These studies have been documented in detail [12].

Aqueous-Gas Partitioning of Volatile Species

The volatile iodine species, I_2 and organic iodides, formed in the aqueous phase would partition into the gas phase. Mass transfer of volatile iodine species across the aqueous-gas interfacial boundary is a key process to consider in determining the rate of airborne iodine formation. The aqueous-gas phase interfacial mass transfer rate in post-accident containment conditions is expected to be relatively fast, compared to the rate of change of volatile iodine species concentrations. (The rates of individual iodine reactions in the aqueous phase are very fast. However, the net changes in I_2 and organic iodides concentrations due to the chemical reactions are slow.) Under these conditions, mass transfer across the aqueous-gas phase interface is adequately described using a first-order rate based on a two-resistance model. For a given interfacial surface area and gas and aqueous volumes, the mass transfer rate of a species can be sufficiently described using two fundamental parameters: the overall mass transfer coefficient and the species dependent partition coefficient.

The partition coefficient for I_2 (79 at 25°C) and its temperature dependence is well established. However, there is a large range of partition coefficients for organic iodides [12], and this must be accounted for when modelling iodine behavior. The main contribution of AECL program in this area has been extension of the database of organic partition coefficients. Establishment of the database has been important because the partition coefficients of a wide range of organic iodides were required to support the grouping of the large number of possible organic iodide species into a small, more tractable number for modeling, based on commonalities in both their hydrolysis rates and partition coefficients.

Iodine – Surface Interaction

Iodine is a notoriously ‘sticky’ molecule, and iodide is also known to easily react with certain metals. The RTF results show that many surfaces in containment could absorb iodine, and have

a significant impact on iodine volatility. There are a variety of surfaces present in a containment building, including stainless steel, aluminium, organic-based painted surfaces, bare concrete, zinc primed surfaces and plastics. During an accident, these surfaces could be in contact with bulk water (referred to here as aqueous phase surfaces), dry surfaces in contact with the containment atmosphere (gas phase surfaces) and surfaces with a condensing water film (condensing surfaces). For many accident scenarios, condensing steam will be prevalent in the containment atmosphere, and adsorption of iodine on dry surfaces contacting the gas phase will be unimportant (because there will be no dry surfaces). However, many RTF and other intermediate-scale tests have been performed with relatively dry atmospheres to obtain 'baseline' iodine data and a model for adsorption of iodine on dry surfaces is required to analyze these tests.

In LIRIC and IMOD, the adsorption and desorption process on dry surfaces is formulated using a pseudo first-order physical adsorption-desorption model. The first order adsorption/desorption formula may be too simple to accurately describe iodine sorption on surfaces such as untreated stainless steel surfaces [13,14]. However, it is sufficiently versatile that it can be used to model adsorption on a variety of surfaces, assuming that the appropriate adsorption/desorption rate constants are known, and surface areas are well defined. Aqueous phase surfaces may also retain iodine, and therefore models for iodine adsorption and desorption from submerged surfaces are included in LIRIC. These processes are modeled in the same way as the analogous processes on gas phase surfaces with the exception that adsorption of iodide ion (I^-) and pH dependent adsorption can also be specified.

There are many different types of surfaces in containment, but there are not many adsorption rate constant data on these surfaces available. Therefore, current AECL R&D activities include building the database for the surface adsorption rate constants.

5.2.2.3 Model Development and Validation Program

The final goal of the AECL R&D program is to produce a tool that can be used to predict iodine volatility in containment following an accident within acceptable uncertainties. The RTF and the bench-scale experimental studies have supported the development of containment iodine behavior models, LIRIC (Library of Iodine Reactions In Containment) and IMOD (Iodine MODule for containment codes). LIRIC is a comprehensive mechanistic model, consisting of about 200 chemical reactions and transport processes [2]. The key model components of LIRIC are schematically shown in Figure 5-9. LIRIC represents the epitome of our current understanding of iodine chemical kinetics. Although it is still evolving, the updated version, LIRIC-3.2 has been demonstrated to reproduce the results of most of the intermediate scale tests performed in the RTF to within experimental uncertainties [2]. (Note that for these simulations some of the input parameters were estimated because they were not measured or determined in the RTF tests. Therefore, it is difficult to unequivocally establish the model performance at this time. Establishing the uncertainties in the input parameters for the RTF tests and under accident conditions is part of on-going R&D work).

Its complexity and size, however, makes it difficult to use LIRIC for routine safety analysis alone, or integrate it into a more comprehensive safety analysis code (e.g., SMART (Simple Model for Activity Removal and Transport)), which deals with the transport behavior of all fission products in containment. This difficulty prompted the development of another iodine

modelling code, IMOD that is smaller and less complex than LIRIC, but maintains the predictive capabilities of the comprehensive mechanistic LIRIC model. The IMOD code can be implemented as a module in the larger SMART code. IMOD was developed based on extensive LIRIC analysis to extract the most important reaction rate models and validated through simulations of various RTF tests.

Both LIRIC and IMOD have reproduced the results of RTF tests performed over a wide range of conditions to within experimental uncertainties (with the caveat that validation of the input parameters remains to be completed). The model predictions have been compared with the RTF test results on numerous parameters including the total gas phase iodine concentration, total aqueous phase iodine concentration, iodine speciation (i.e., I_2 and organic iodide fractions in the gas phase), and pH evolution (when pH was not controlled). In the prediction of iodine behavior for conditions outside the range available from the RTF experiments, IMOD results are comparable with LIRIC results. Some examples of the comparison of LIRIC and IMOD results with RTF data are given in Figures 5-10 - 5-13.

5.2.2.4 International Collaboration

In addition to the three main iodine programs, the iodine group at AECL has been involved in international collaboration on both a shared cost and contract basis. This work has complimented AECL's activities and contributed to the knowledge basis. The key activities in this area include:

1. ISP-41 (International Standard Problem) Iodine Behavior Code Comparison (conducted by the NEA/CSNI)
2. Contract work performed in support of the ACE (Advanced Containment Experiment) and ACEX (ACE Extension) projects,
3. PHEBUS RTF tests performed in support of the PHEBUS FP (Fission Product) project, and
4. COG-IRSN (Institute de Radioprotection et de Surete Nucleaire) information exchange.

5.2.3 IMOD in SMART

The computer program SMART is used to model aerosol behaviour in a CANDU containment. A simplified iodine behavior model, IMOD, has been incorporated into SMART. IMOD consists of the rate equations for the processes:

1. The interconversion between non-volatile iodine species (e.g., I^-, HOI, I_3^-, IO_3^-, I_xO_y, etc) and volatile molecular iodine (I_2),
2. The formation and destruction of volatile organic iodides (High volatility organic iodides, HVRI and Low volatility organic iodides, LVRI),
3. The partitioning of volatile species (e.g., I_2 and RI) between aqueous and gas phases,
4. The transport of iodine species to (adsorption) and from (desorption) surfaces both in the gas and aqueous phases, and
5. The transport of gaseous iodine species to condensing films and to the bulk aqueous phase by condensation flows.

These model components of IMOD are schematically shown in Figure 5-9, which capture the processes shown in Figure 5-1.

In addition to the transport and the physical and chemical transformation, IMOD also simulates the change in the chemical environment that could have a significant impact on iodine behavior, such as pH change (when pH is not controlled) and organic impurity concentration in aqueous solution.

The aqueous phase in Figure 5-9 refers to either liquid aerosols or bulk water phase (such as pool on the floor or sump water). It can be conservatively assumed that iodine in the collection of liquid aerosols is subject to the same chemical transformations in the aqueous phase and aqueous-gas phase interfacial mass transfer processes (Processes (1)-(3) listed above) as iodine in the bulk water phase. However, the chemical environment, such as pH and the organic impurity level, in liquid aerosols would be different from that of the bulk water phase. Iodine in aerosols is also subjected to the aerosol transport processes as described above.

The initial fractions of iodine in various forms (in gases, aerosols and aqueous solutions) and post-accident containment conditions (temperature, radiation dose rate, initial pH of the aqueous solution and surface type and surface areas) are assumed to be either provided by upstream analysis or defined by users. IMOD then calculates the changes in the iodine fractions in aerosols, in the gas and aqueous phases and on surfaces, due to the transport and physical and chemical transformation described above. IMOD can also provide detailed speciation of iodine in the gas phase into molecular iodine and organic iodides, if required. Although molecular iodine is known to easily adsorb on various surfaces, both molecular iodine and organic iodides are allowed to leak through the containment wall without attenuation.

5.3 AECL R&D on Aerosol Behavior

While undergoing the radioactive decay and build-up processes described in Section 2, the fission products embedded in airborne liquid aerosols transport as the aerosols do. Hence, the aerosol behavior needs to be modelled properly for fission product source term calculations. The main R&D activities on aerosol behavior in containment at AECL have consisted of mainly implementation of aerosol models in the SMART code and experimental studies on flashing jets and aerosol transport through containment leak paths.

5.3.1 Aerosol Models in SMART

Liquid aerosol is generated from the disintegration of liquid water as it is discharged into containment from a break in the primary heat transport system. The aerosol is transported within containment by carrier gas. Within a particular node or a room (up to 45 nodes can be used in SMART), the liquid aerosol droplets undergo coagulation and also deposit on walls and floors due to various natural phenomena (e.g., gravitational settling). To model the coagulation and removal processes mathematically, the continuous aerosol size spectrum is divided into a finite number of intervals, and within each interval, the aerosol size is assumed to be constant. The aerosol droplet sizes considered for analysis range from 0.1 μm to 10000 μm radius and a total of up to 30 particle size classes are modeled in SMART. The initial mass distribution of the fission products in the aerosol size classes are provided by upstream analysis, while the changes in the fission product masses in the size classes due to radioactive decay and build-up, coagulation and deposition in containment are calculated in SMART.

The physical law governing the transport of aerosols within containment is the conservation of aerosol mass. Processes that can cause a change in the airborne aerosol mass in a node are:

1. Source from a break or other discharge into the room
2. Removal from the break discharge
3. Coagulation or agglomoration
4. Removal due to aerosol deposition mechanisms
5. Convective flow from a room to next and flow through leak-paths to the external atmosphere

Source and Initial Size Distribution of Liquid Aerosols

Liquid discharging at high temperature/pressure from a pipe will break up or fragment into droplets of varying sizes. For a relatively high degree of superheat, the size of the liquid droplets formed by thermal fragmentation and aerodynamic fragmentation is approximately the same. For a lower degree of superheat, aerodynamic fragmentation results in a smaller droplet size, and is used to calculate the aerosol size distribution to be conservative. (Smaller droplets are generally removed more slowly than larger droplets and hence smaller droplet sizes provide a conservative aerosol removal rate.) Droplet size distribution is considered to be log–normal and is characterized by two parameters: the geometric mean diameter and the geometric standard deviation. In SMART the geometric mean diameter is considered to be equal to the critical diameter, where the critical diameter is defined as a diameter when the drag force on the droplet exceeds the surface tension forces. For jet disintegration by thermal flashing, the geometric standard deviation is less than 1.40. A value of 1.40 is used in SMART.

Aerosol Removal From Break Discharge

A significant fraction of the liquid aerosol formed in the break jet discharge from the primary heat transport system into containment may be removed by a mechanism referred to as jet impingement. WALE experiments performed at Stern Laboratories have demonstrated that a large fraction of the jet discharge mass entering a vessel is removed and only a small fraction becomes airborne. An empirical model derived from the WALE data is used in SMART for calculation of fractional removal of the jet aerosol mass.

If the discharge into containment occurs after passage through the moderator, a fraction of the aerosol and the associated fission products may also be removed in the moderator pool. As aerosol droplets suspended in a gas volume traverses the moderator pool, a fraction of the suspended aerosols deposit on the boundary between the gas volume and the moderator pool. The remaining fraction is released as airborne into the containment atmosphere. SMART uses a simple pool-scrubbing model and to be conservative assumes that only the coarse end of the original break discharge aerosol distribution is retained by the pool.

Liquid Aerosol Agglomeration

Agglomeration refers to the collision and adhesion of aerosol particles, which result in forming larger particles. Particle collisions can result from random thermal motions of the particles (i.e., Brownian agglomeration) or from kinematic processes such as gravitational, and turbulent mechanisms. Brownian agglomeration arises from particle diffusion due to Brownian motion, and is most effective for small, submicron particles. Gravitational agglomeration arises from particle collisions that result from the different settling rates of particles of differing mass, and is

most effective for larger particles. Turbulent agglomeration arises from relative motions between aerosol particles that are produced by turbulent gas flow, and is expected to be effective for intermediate-sized particles with diameters in the range of 1 to 100 μm.

Airborne Aerosol Removal

The airborne aerosol in containment may deposit on walls, floors and other surfaces due to a variety of removal mechanisms. The removal of aerosols from the containment atmosphere is modeled using: gravitational settling, diffusiophoresis (Stefan flow), thermophoresis, and turbulent deposition. Short descriptions of these removal mechanisms are provided in the Licensing Submission: Phenomenology for Limited and Severe Core Damage Accidents in an ACR [15].

Convective Flow Through Holes to the External Atmosphere

Aerosol droplets are typically larger than the microcracks in the containment perimeter wall and are therefore assumed to be unable to leak through the containment wall. However, they are assumed to leak through open pathways leading out of containment without attenuation (such as a pre-existing hole below the detection size threshold of the Gross Containment Leakage Monitor).

5.3.2 Aerosol Experimental Program

5.3.2.1 Droplet Size and Velocity Measurements of Flashing Water Jets

During a postulated accident condition involving a break in the primary heat transport system, the high-enthalpy water can discharge into the containment in the form of a flashing jet. The effluent jet consists of a two-phase mixture of steam and small water droplets generated by flash boiling and aerodynamic fragmentation. The presence of suspended or dissolved fission products in the high enthalpy fluid is a possible scenario and the water droplets formed can act as carriers of radioactivity. Experiments have been carried out to measure the size and velocity distribution of the droplets from flashing jests. The data obtained from this experimental study, and WALE experiments at Stern Laboratories on the removal and airborne fractions of the jet discharge mass entering a vessel, have been used to develop and validate mechanistic models for aerosol fission product removal and transport in the containment.

The experimental set-up for the droplet and velocity measurements of flashing jet is shown in Figure 5-14. The nozzle assembly consists of a straight section 150 mm-long and 4.83 mm in diameter with a male thread at its end, and a nozzle with a female thread to match the male thread. Two different nozzle types were used: one with flat geometry and the other a gradual linear contraction that was used in the WALE tests[3]. Flashing jets were studied under nozzle diameters ranging from 0.024" to 0.096" and pressures ranging from 1.0 to 10 MPa (saturation temperatures of 180.2 – 312.3°C). One of the flat nozzle assemblies used in the test and the flashing jet from this assembly are also shown in Figure 5-14.

[3] The WALE nozzle is a 20° cone with a contraction ratio of 7.92 over a length of 0.579 cm, where the contraction was followed by a straight throat of length 0.051 cm and a diameter of 0.061 cm.

Droplet size and velocity were simultaneously measured non-intrusively using the phase-Doppler anemometer (PDA)[4]. The measurements were conducted along the jet axis (z-direction) and at various radial locations along the width (x-direction) and the height (y-direction) of the jet. The variables of interest are: the mean velocity (U), the turbulence intensity (u'/U), the count geometric mean diameter (GMD = $\exp(D_g)$) and the geometric standard deviation ($\sigma_g = \exp(s_g)$). Here, D_g and s_g are defined as:

$$D_g = \frac{\sum_{i=1}^{N}(\ln(d_i))}{N} \quad \text{and} \quad s_g^2 = \frac{\sum_{i=1}^{N}(\ln(d_i) - D_g)^2}{(N-1)}$$

where N is the sample size and was typically 3000 in the measurements. Some of the data obtained from this study are given in Figures 5-15 and 5-16.

5.3.2.2 Aerosol Transport Through Containment Leakage

While undergoing radioactive decay and build-up processes, the fission products embedded in the airborne liquid aerosols may escape by convective transport through leak paths due to containment pressurization following the accident. Potential routes for aerosol leakage from containment include:

- airlock door seals
- containment-isolation damper valves,
- concrete penetration gaps, and
- concrete porosity, joints and cracks.

An experimental program is in place to determine liquid aerosol leakage through simulated containment leak paths in order to acquire qualified data for validation of SMART. Tests have been performed for aerosol leakage through containment isolation-damper valve connected to an aerosol-generating chamber (Figure 5-17). An industrial, cold-aerosol fogger was used in generating wet aerosols for the experiment. The fogger is capable of producing wet aerosols with a wide range of droplet diameters. Representative leak paths for the isolation damper valve were connected to one side of the aerosol chamber, and the paths contained filters for measuring penetration of aerosols (as uranine solution) as they pass through the leak paths (e.g., path U2 in Figure 5-18). A choked flow rate was established through both leak paths using a vacuum pump and two rotameters. A Phase Doppler Anemometer (PDA) was used for the aerosol size measurements. The size distribution of aerosols at the sampling port observed in one of these tests is shown in Figure 5-19. Uranine concentrations of the filters, connectors and leak paths were analyzed by a spectrophotometer. The test results show that about twice the amount of aerosols were deposited in the leak path compared to that penetrated or leaked through the leak path. The results are used to develop and validate aerosol transport model in SMART.

---

[4] The PDA system consisted of a variable-power Argon-Ion laser having a wavelength of 514.5 nm, a fiber-optic probe fitted with a lens of focal length 600 mm (transmitting optics), a convex lens with a focal length of 310 mm placed at an off-axis angle of 65° for receiving the scattered light in the first order refraction mode (receiving optics), and three photomultiplier (PM) tubes mounted on the receiving optics to obtain and validate the phase information contained in the Doppler signals.

5.4 Summary

AECL has a led broad research program on the behavior of fission products in a CANDU containment building during an accident. In particular, over the last decade, a detailed mechanistic understanding of iodine behavior has evolved and comprehensive mathematical models have been developed capturing this understanding. As there are no significant differences in the ACR design that would affect fission product behavior in a post-accident containment, this knowledge base is directly applicable to ACR.

5.5 References

1. J. McFarlane, J.C. Wren and R.J. Lemire, "Chemical Speciation of Iodine Source Term to Containment," Nucl. Tech., 138, 162 (2002).
2. J.C. Wren and, J.M Ball, "LIRIC 3.2 An Updated Model for Iodine Behavior in the Presence of Organic Impurities," Rad. Phys. Chem., 60, 577 (2001).
3. J.C. Wren, J.M. Ball and G.A. Glowa, "The Chemistry of Iodine in Containment," Nucl. Tech., 129, 297 (2000).
4. J.C. Wren, J.M. Ball and G. Glowa, "The Interaction of Iodine with Organic Material in Containment," Nucl. Tech., 125, 337 (1999).
5. J.C. Wren, J. Paquette, S. Sunder and B.L. Ford, "Iodine Chemistry in the +1 Oxidation State. II. A Raman and uv-visible Spectroscopic Study of the Disproportionation of Hypoiodite in Basic Solutions," Can. J. Chem., 61, 2284 (1986).
6. J.M. Ball and J.B. Hnatiw, "The Reduction of I_2 by H_2O_2 in Aqueous Solution," Can. J. Chem., 79. 1 (2001).
7. J.C. Wren and G.A. Glowa, "A Simplified Kinetic Model for the Degradation of 2-Butanone in Aerated Aqueous Solutions under Steady-State Gamma-Radiolysis," Rad. Phys. Chem., 58, 341 (2000).
8. G. Glowa, P. Driver and J.C. Wren, "Irradiation of MEK Part II: A Detailed Kinetic Model for the Degradation of 2-Butanone in Aerated Aqueous Solutions under Steady-State γ-Radiolysis Conditions," Rad. Phys. Chem., 58, 49, (2000).
9. P. Driver, G. Glowa and J.C. Wren, "Steady-State γ-Radiolysis of Aqueous 2-Butanone," Rad. Phys. Chem. 57, 37 (2000).
10. J.C. Wren, D.J. Jobe, G.G. Sanipelli and J.M. Ball, "Dissolution of Organic Solvents from Painted Surfaces into Water," Can. J. Chem. 78, 464 (2000).
11. J.M. Ball, J.C. Wren, and J.R. Mitchell, "The Dissolution of Solvents from Amerlock 400 Epoxy Paint," accepted for publication, Can. J. Chem. (2003).
12. G.A. Glowa and J.C. Wren, "Aqueous-Gas Phase Partitioning and Hydrolysis of Organic Iodides," Can. J. Chem. 81, 230-243 (2003).
13. J.C. Wren and G.A. Glowa, "Kinetic of Gaseous Iodine Uptake Onto Stainless Steel During Iodine-Assisted Corrosion," Nucl. Tech, 133, 33 (2001).
14. J.C. Wren, G.A. Glowa and J. Merritt, "Corrosion of Stainless Steel by Gaseous Iodine," J. Nucl. Material, 265, 161 (1999).

15. Licensing Submission: Phenomenology for Limited and Severe Core Damage Accidents in an ACR, AECL report, ACR 108-126810-LS-001 Revision 0 (2003).

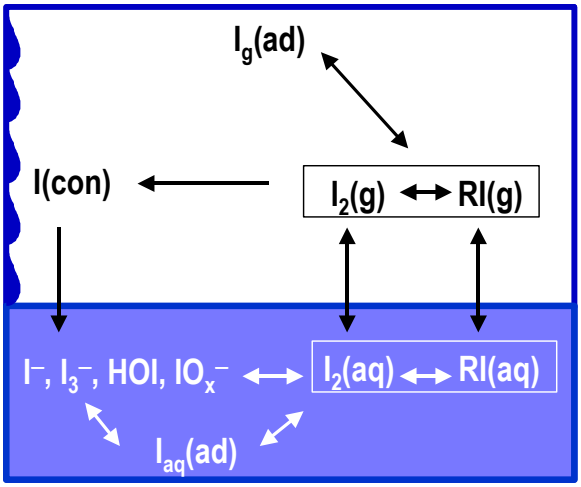

Figure 5-1 Iodine Reactions and Transport Processes in Containment Under Accident Conditions - RI Represents Organic Iodides, aq and g in Brackets Denote Aqueous and Gas Species, I_g(ad) and I_{aq}(ad) Adsorbed on Surfaces in Contact with the Gas and Aqueous Phase, and I(con) Represents Iodine Absorbed in Condensates - Note that the Collection of Liquid Aerosols Can Be Conservatively Treated as Another Aqueous Phase

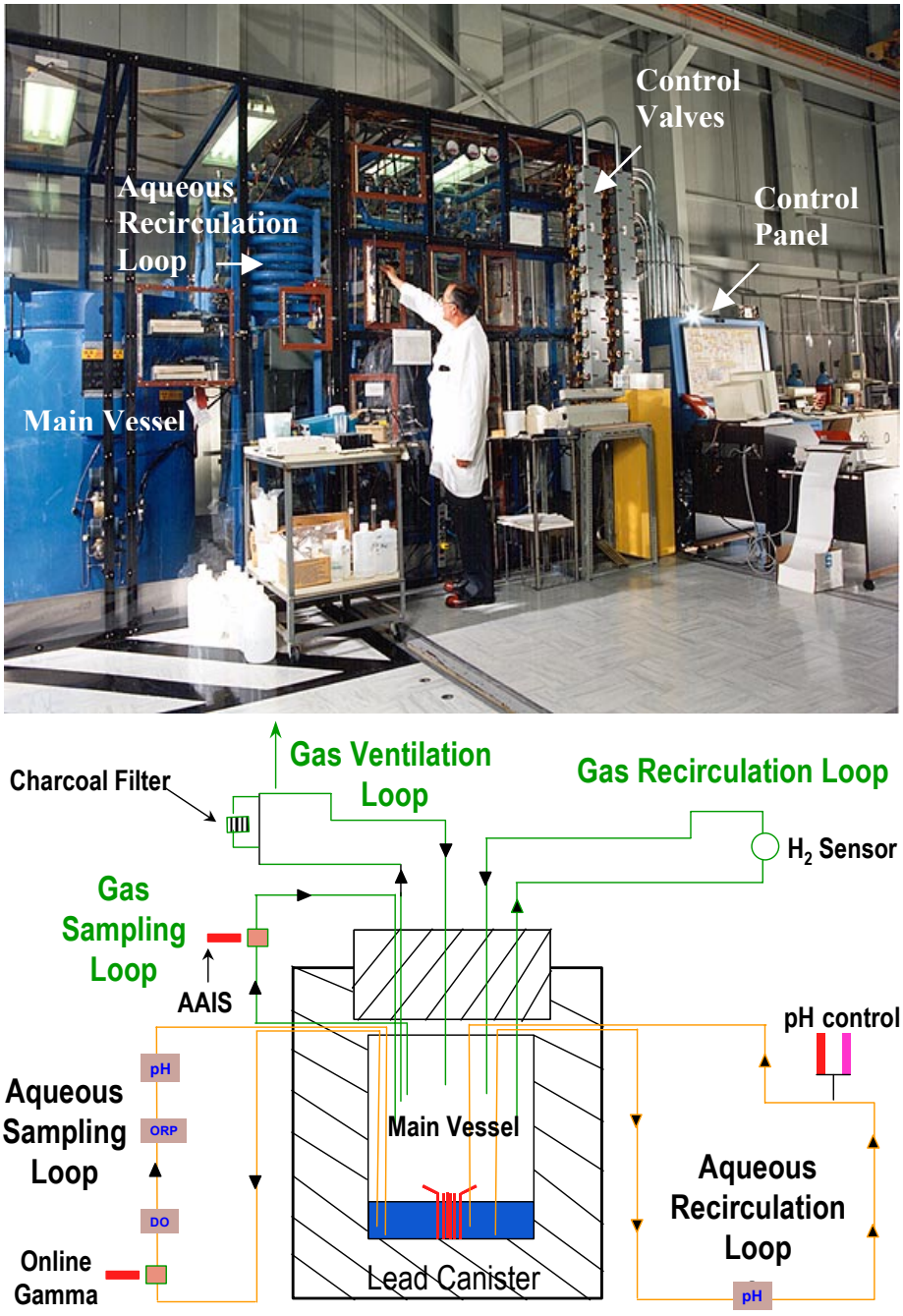

Figure 5-2 The Exterior and the Schematic Flow Chart of the Radioiodine Test Facility - AAIS, ORP and DO Refer to the Automated Airborne Iodine Sampler, Oxidation/Reduction Potential Probe and Dissolved Oxygen Probe

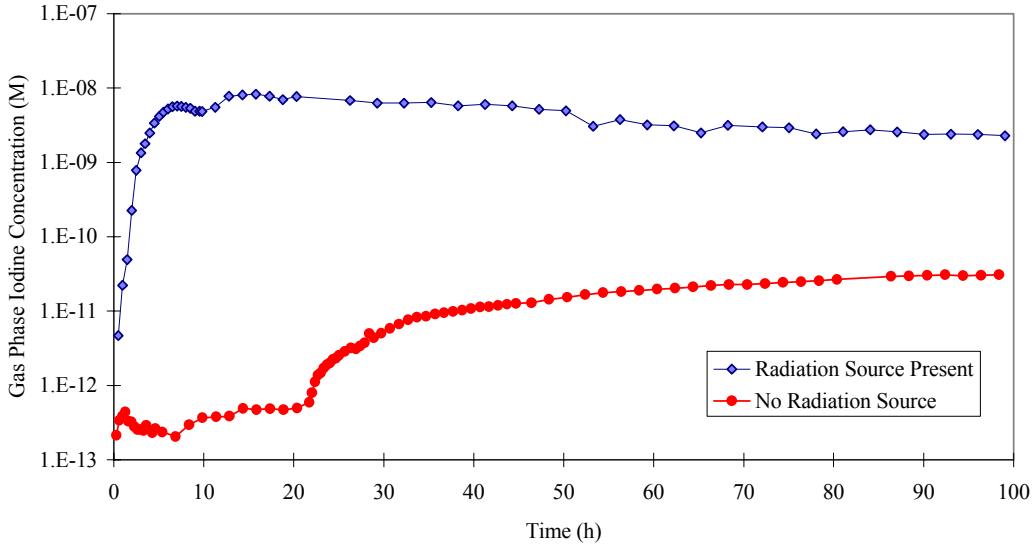

Figure 5-3 The RTF Test Results Illustrating the Effect of Radiation on Iodine Volatility - Both Tests were Performed in a Vinyl Painted Vessel and at 25°C - For the Radiation Test, the Absorbed Dose Rate was 1.4 kGy/h

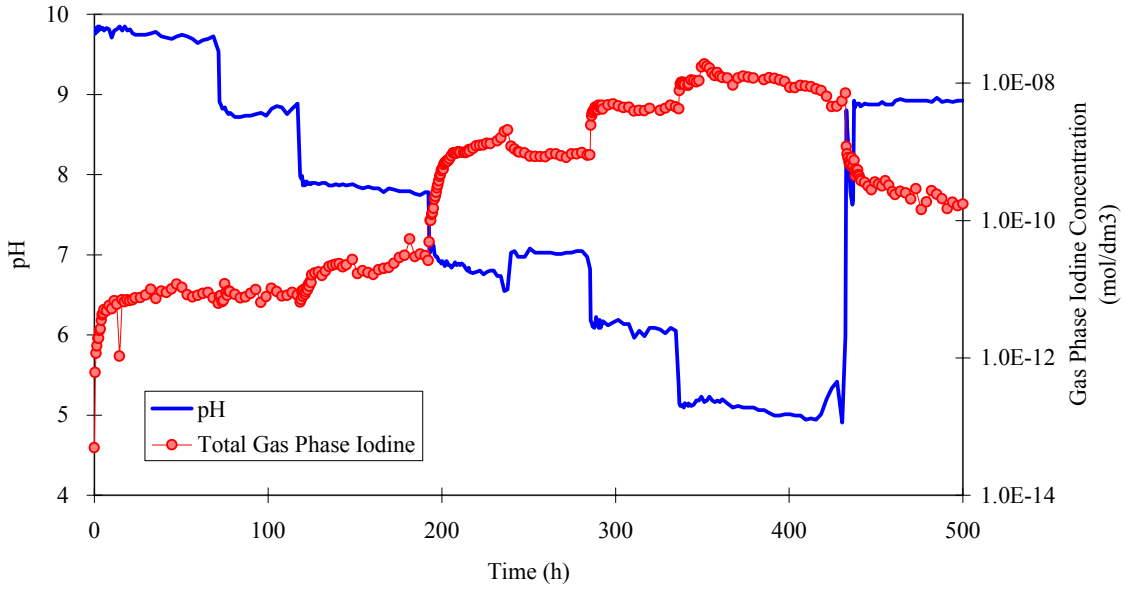

Figure 5-4 The RTF Test Results Illustrating the Effect of pH on Iodine Volatility - The Test was Performed in a Stainless Steel Vessel, 60°C, and Absorbed Dose Rate of 0.78 Gy/h

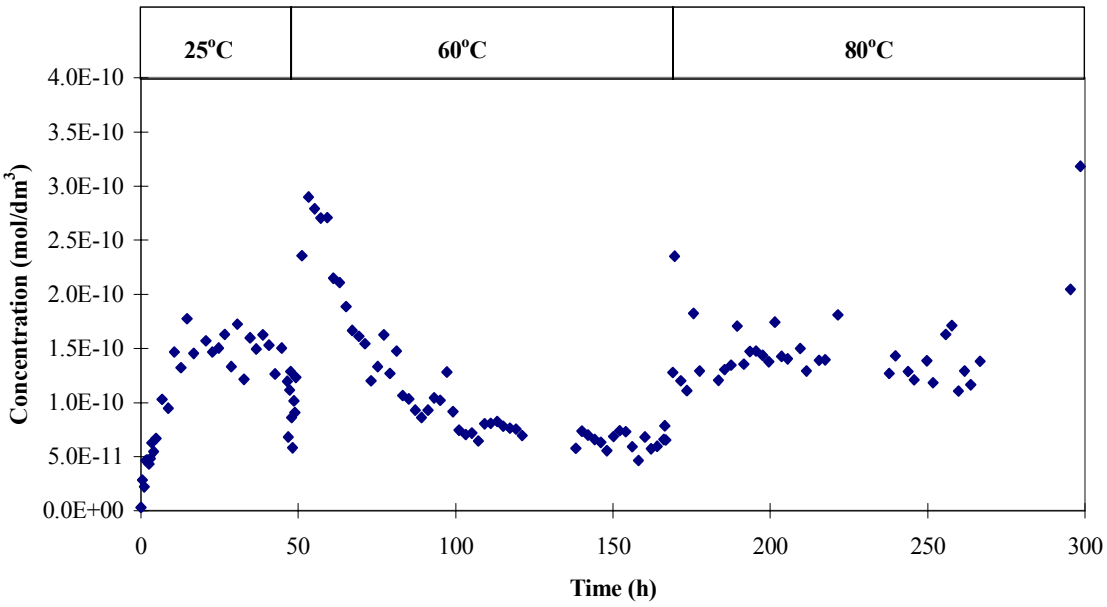

Figure 5-5 The RTF Test Results Illustrating the Effect of Temperature on Iodine Volatility - The Temperature Jump Test was Performed in a Stainless Steel Vessel and at Absorbed Dose Rate of 0.67 kGy/h

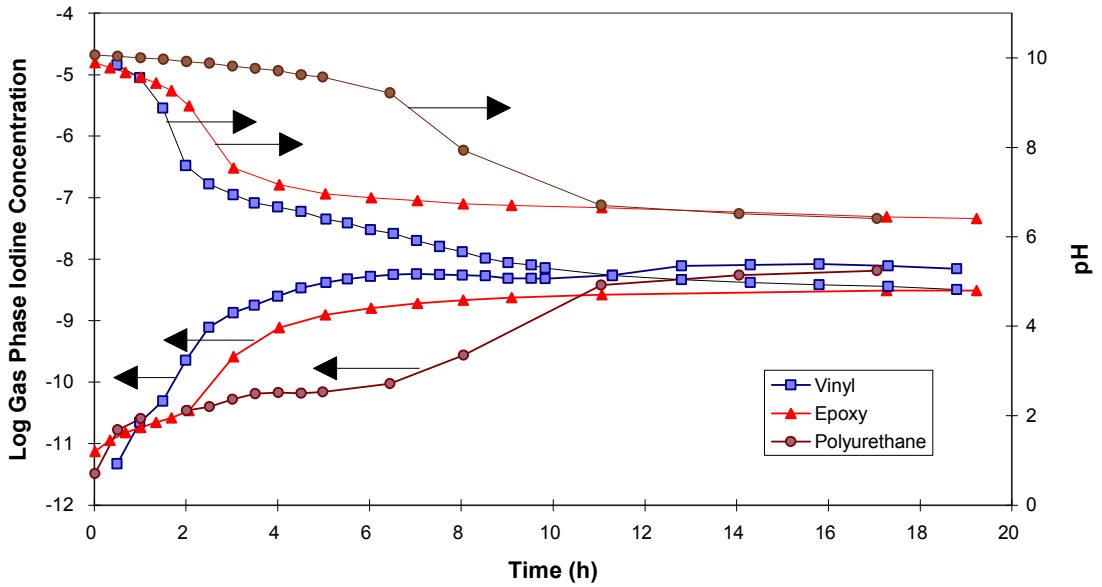

Figure 5-6 The RTF Test Results Illustrating the Effect of Painted Surface on pH and Iodine Volatility - These Tests were Performed at 25°C and Absorbed Dose Rate of ~ 1.5 Gy/h, in a Vessel Painted with Vinyl, Epoxy or Polyurethane

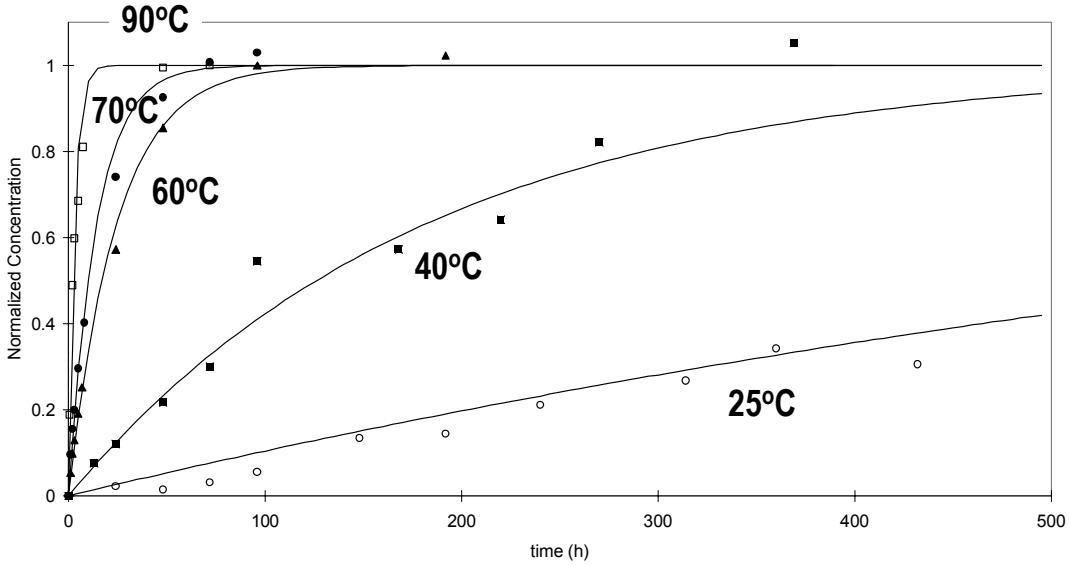

Figure 5-7 MIBK Release from Epoxy Surface into Water, Observed Versus Calculated Using the Organic Dissolution Sub-model in LIRIC and IMOD

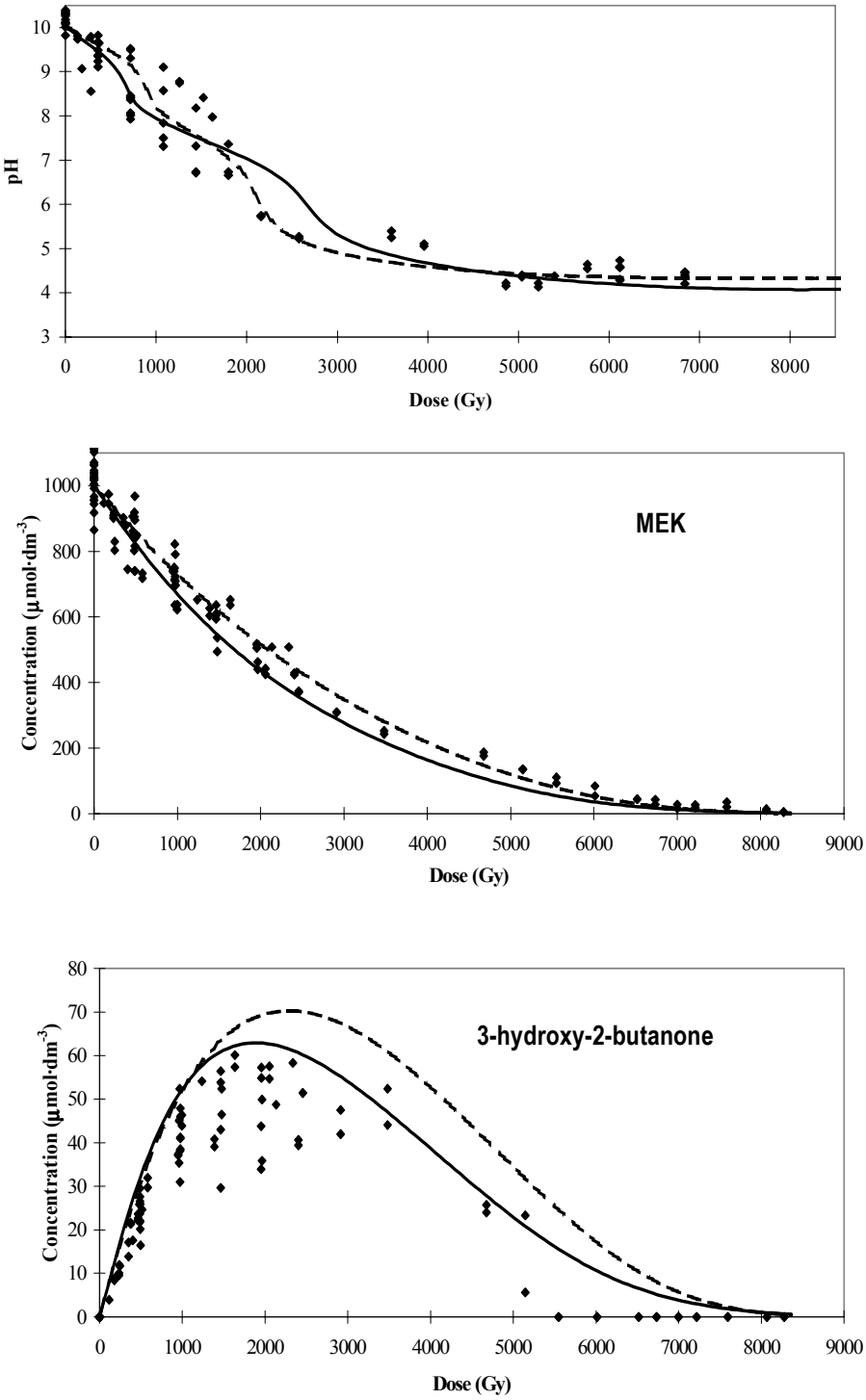

Figure 5-8 Dose Profiles of MEK, One of Its Intermediate Products, 3-Hydroxy-2-Butanone, and pH During the Irradiation of Aerated 10^{-3} mol·dm^{-3} MEK Solution: Experimental Data (♦), Full MEK Model Prediction (——), and Simplified MEK Model Prediction (-----)

(a) Model Components of LIRIC

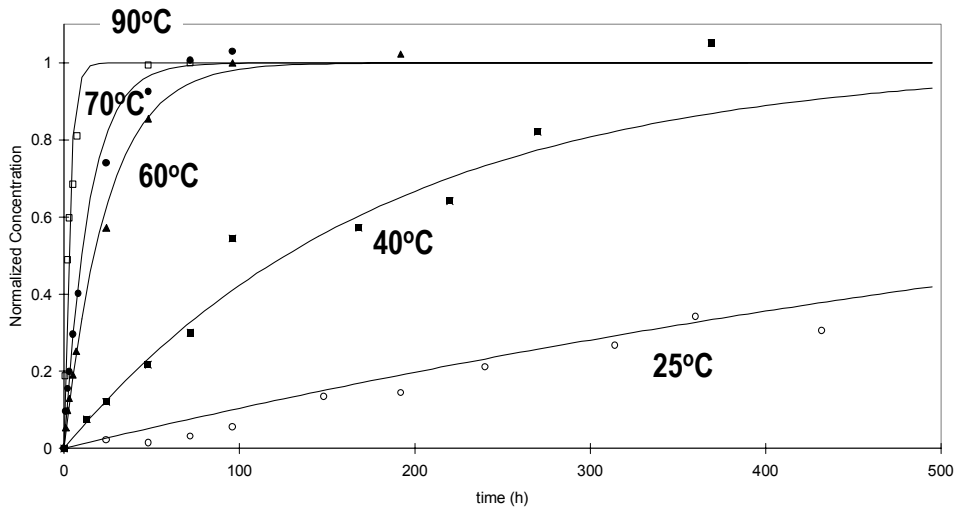

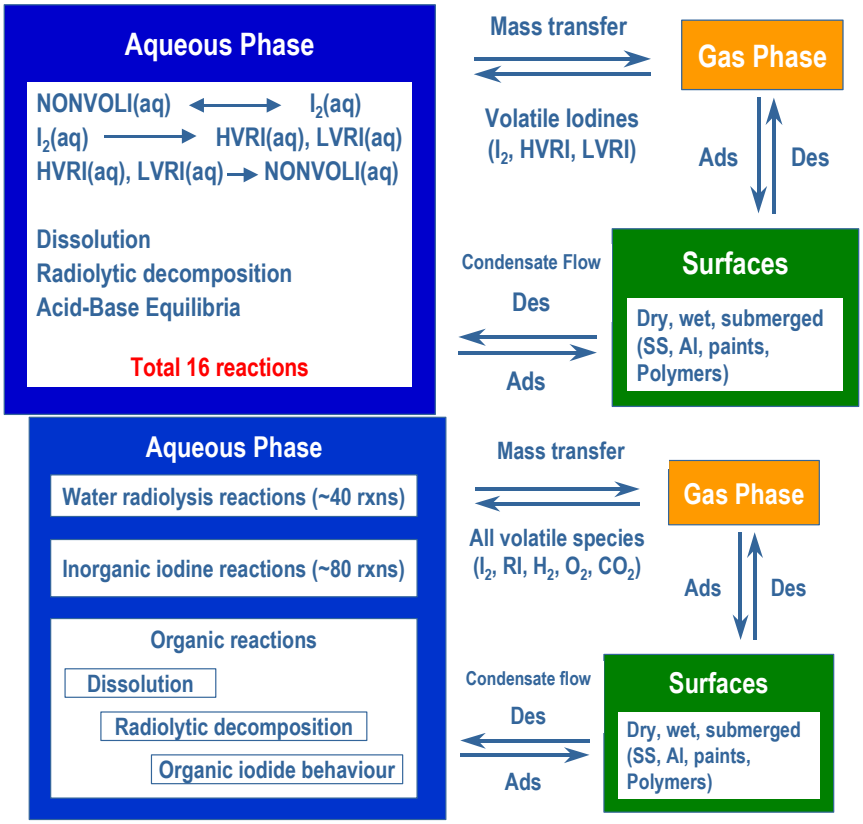

(b) Model Components of IMOD

Figure 5-9 Components of the Iodine Behavior Models, LIRIC and IMOD

(a)

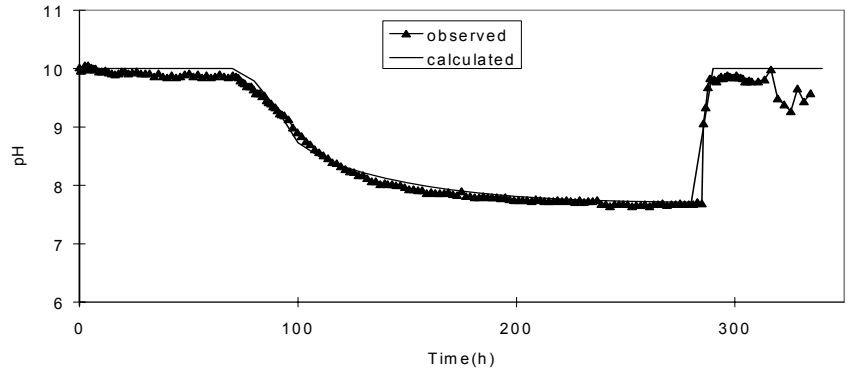

(b)

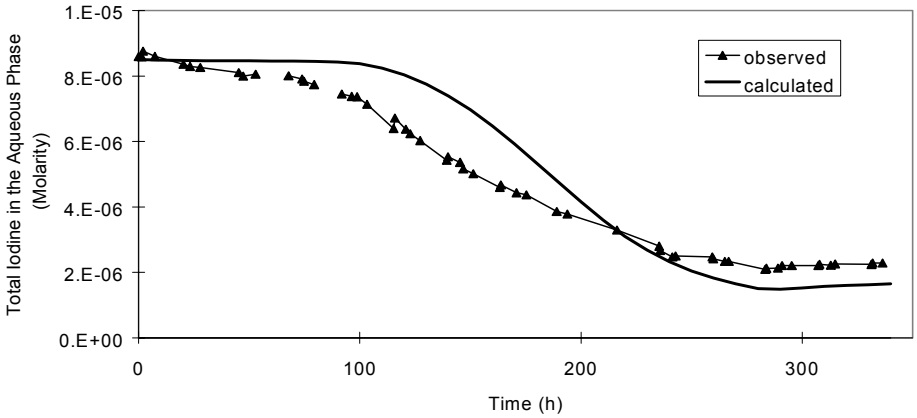

(c)

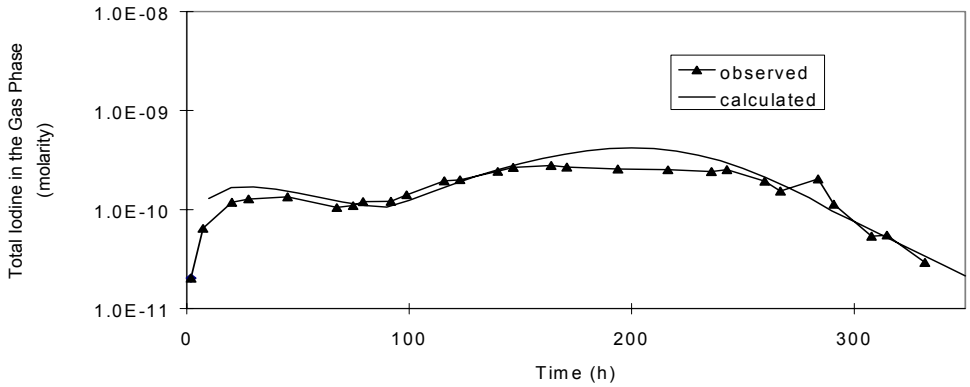

Figure 5-10 Comparison of LIRIC Calculations with RTF Data for (a) pH, (b) Total Iodine in the Aqueous Phase, and (c) Total Iodine in the Gas Phase for RTF Phase 1 Test 1 (10^{-5} mol·dm^{-3} CsI Irradiated at 0.6 kGy·h^{-1} at 60°C in an Amerlock 400 Epoxy Painted Vessel; the pH was Maintained at 10 for the first 75 h, After Which the pH was Allowed to Change and the pH was Intentionally Raised Again to 10 at 280 h

(a)

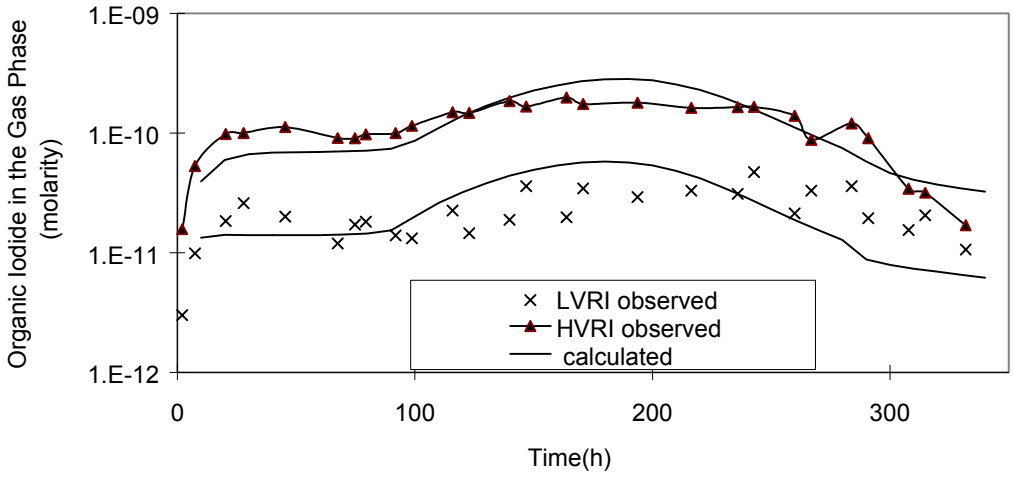

(b)

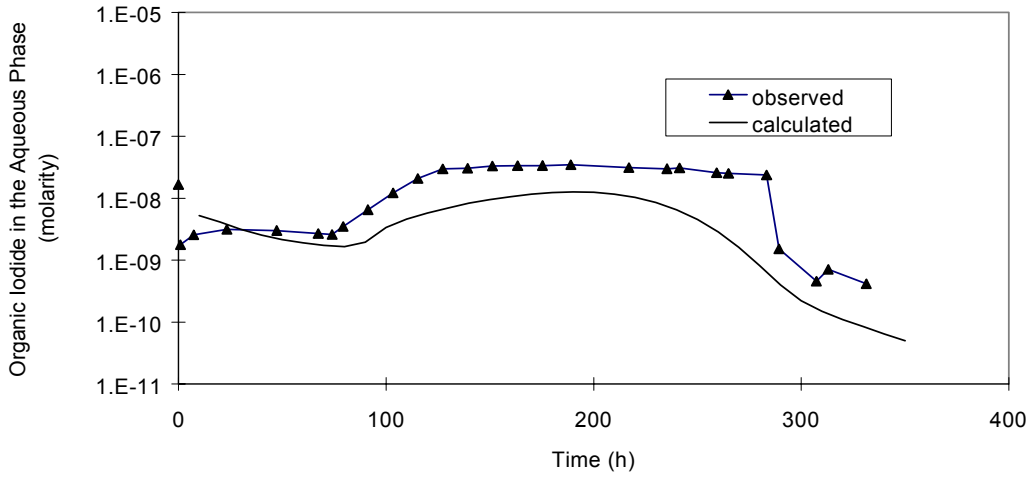

Figure 5-11 Comparison of LIRIC Calculations with RTF Data for (a) Low Volatility Organic Iodides (LVRI) and High Volatility Organic Iodides (HVRI) in the Gas Phase and (b) Total Organic Iodides in the Aqueous Phase for RTF Phase 1 Test 1 (10^{-5} mol·dm^{-3} CsI Irradiated at 0.6 kGy·h^{-1} at 60°C in an Amerlock 400 Epoxy Painted Vessel; the pH was Maintained at 10 for the First 75 h, After Which the pH was Allowed to Change and the pH was Intentionally Raised Again to 10 at 280 h

(a)

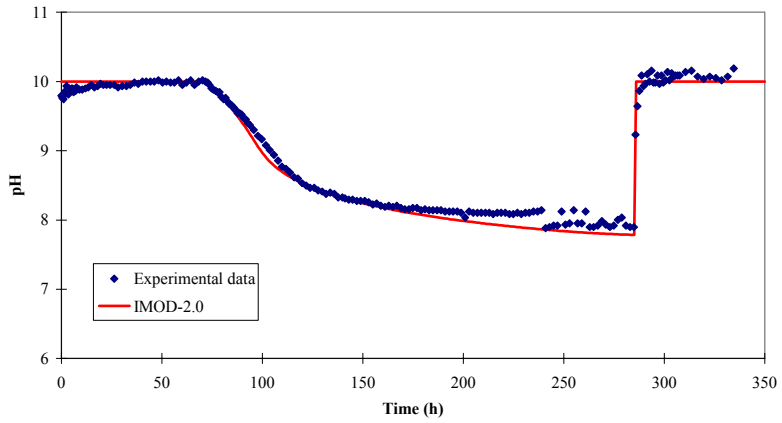

(b)

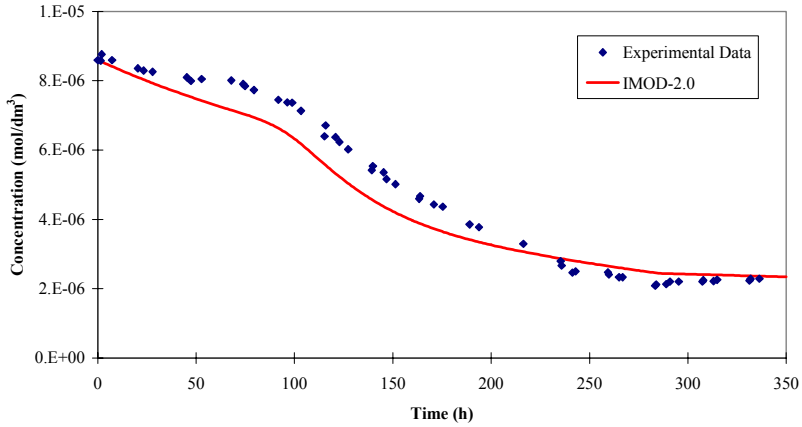

(c)

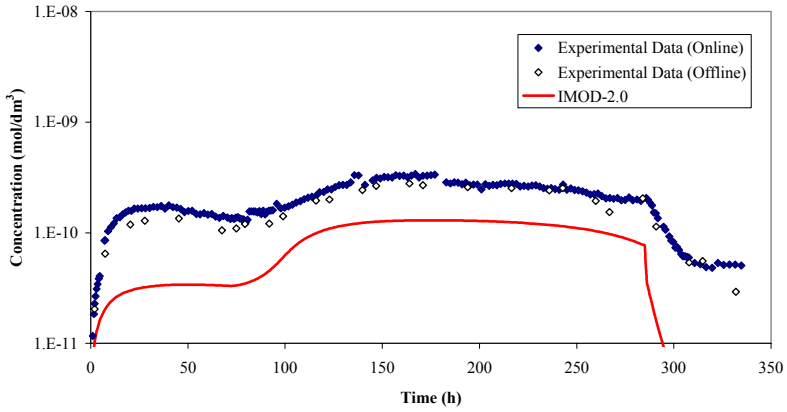

Figure 5-12 Comparison of IMOD Calculations with RTF Data for (a) pH, (b) Total Iodine in the Aqueous Phase, and (c) Total Iodine in the Gas Phase for RTF Phase 10 Test 1

(a)

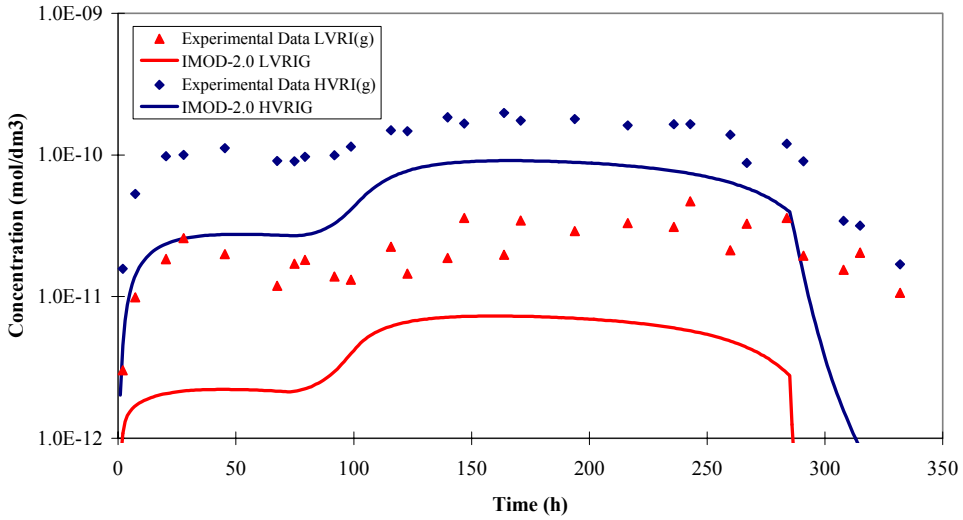

(b)

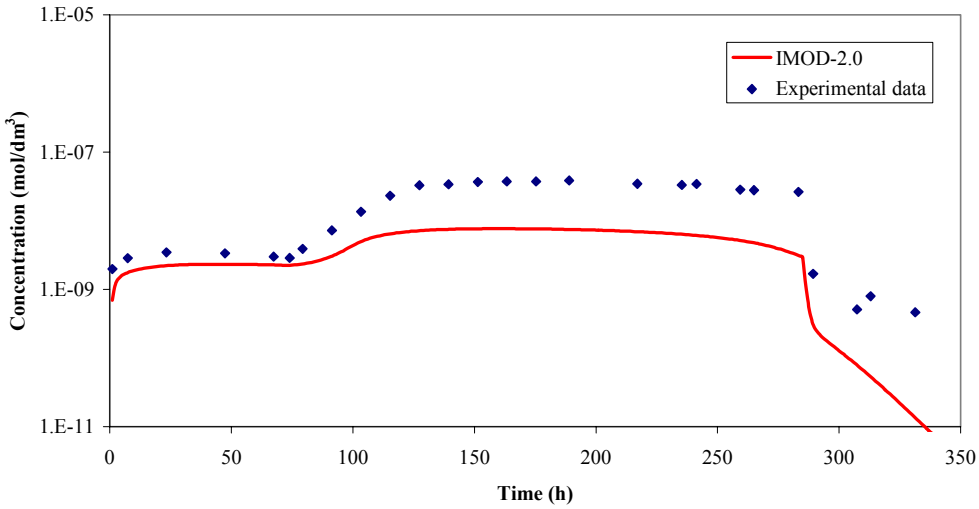

Figure 5-13 Comparison of IMOD Calculations with RTF Data for (a) Low Volatility Organic Iodides (LVRI) and High Volatility Organic Iodides (HVRI) in the Gas Phase and (b) Total Organic Iodides in the Aqueous Phase for RTF Phase 1, Test 1

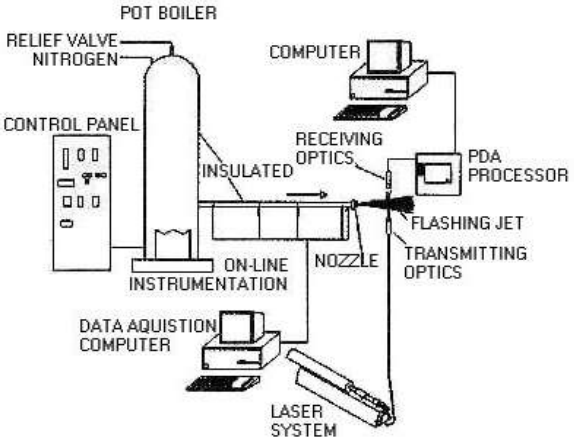

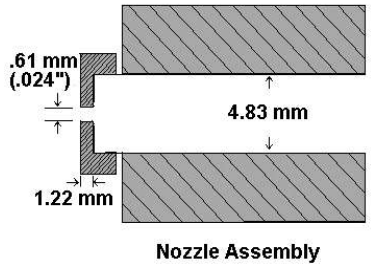

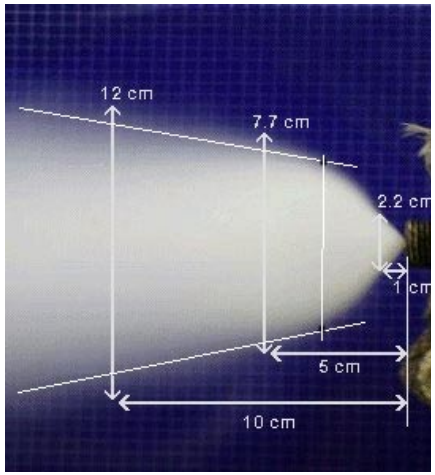

Figure 5-14 Experimental Set-up for Droplet Size and Velocity Measurements of Flashing Jets - It Consists of a Boiler in which Water is Heated to the Required Temperature By Means of a Heating Source Inside the Vessel - The Boiler is Pressurized By Adding Nitrogen Gas from the Top - After the Necessary Test Conditions Are Attained, the Pipe Connecting the Pressure Vessel to the Nozzle Arrangement is also Heated to the Required Value - The Boiler and the Piping Arrangements Are Well Insulated to Minimize Any Loss of Heat

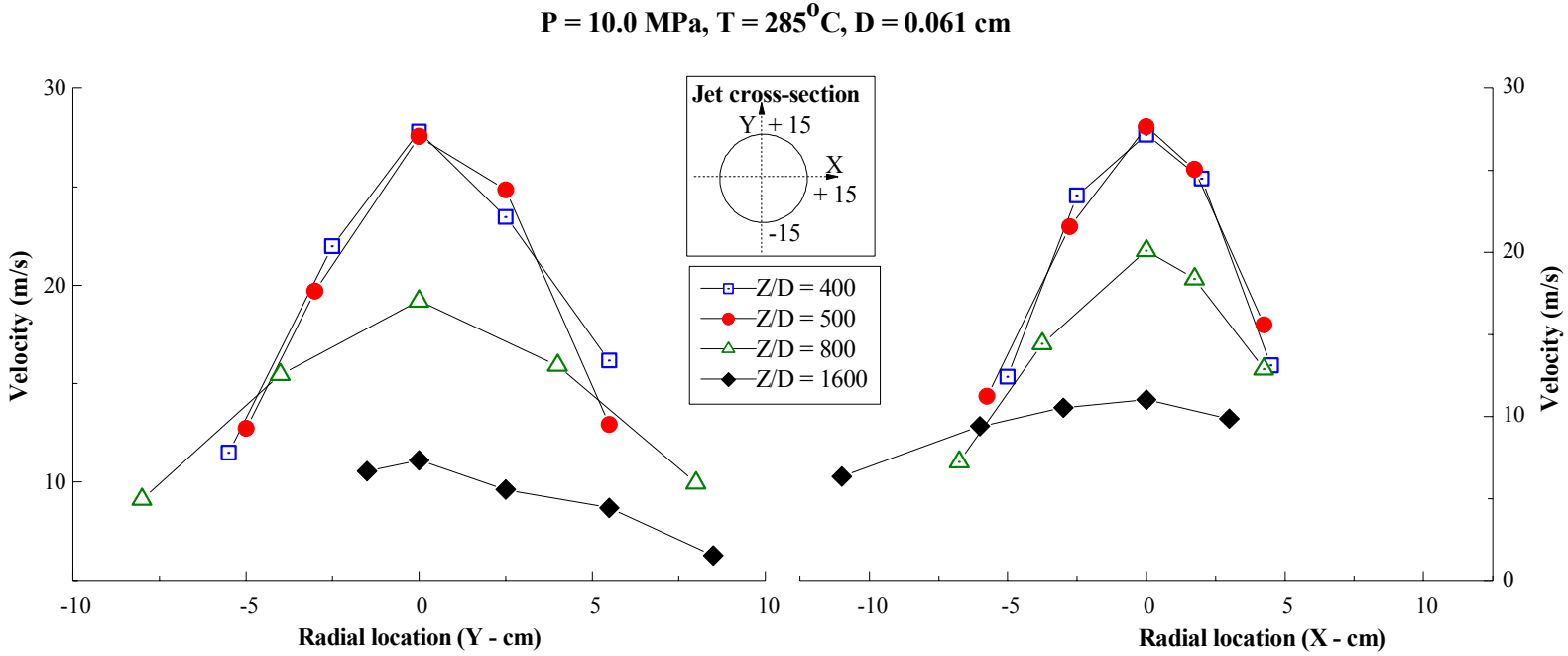

Figure 5-15 Radial Distribution (Y-axis and X-axis) of Mean Velocity at Various Axial Stations, Z/D, where D is the Diameter of the Nozzle

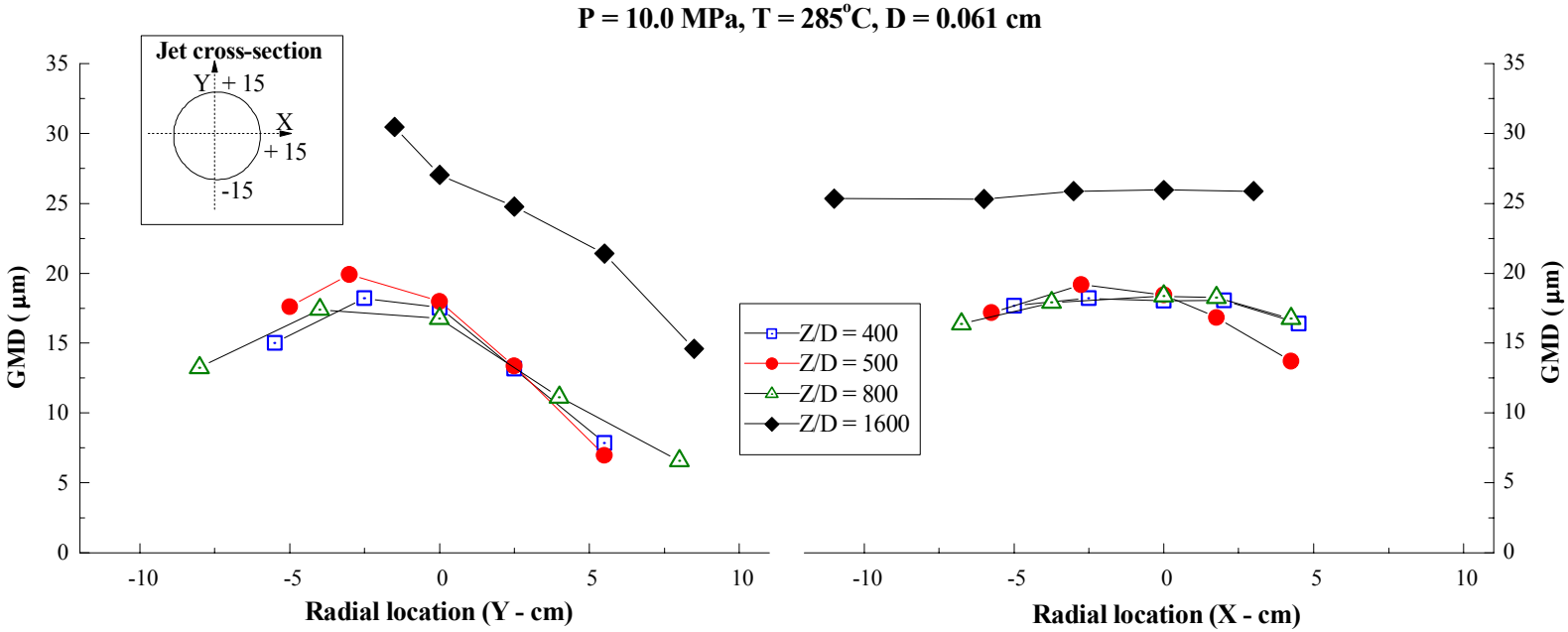

Figure 5-16 Radial Distribution (Y-axis and X-axis) of Geometric Mean Diameter of the Jet Aerosols at Various Axial Stations, Z/D, where D is the Diameter of the Nozzle

Figure 5-17 Aerosol Test Chamber at CRL

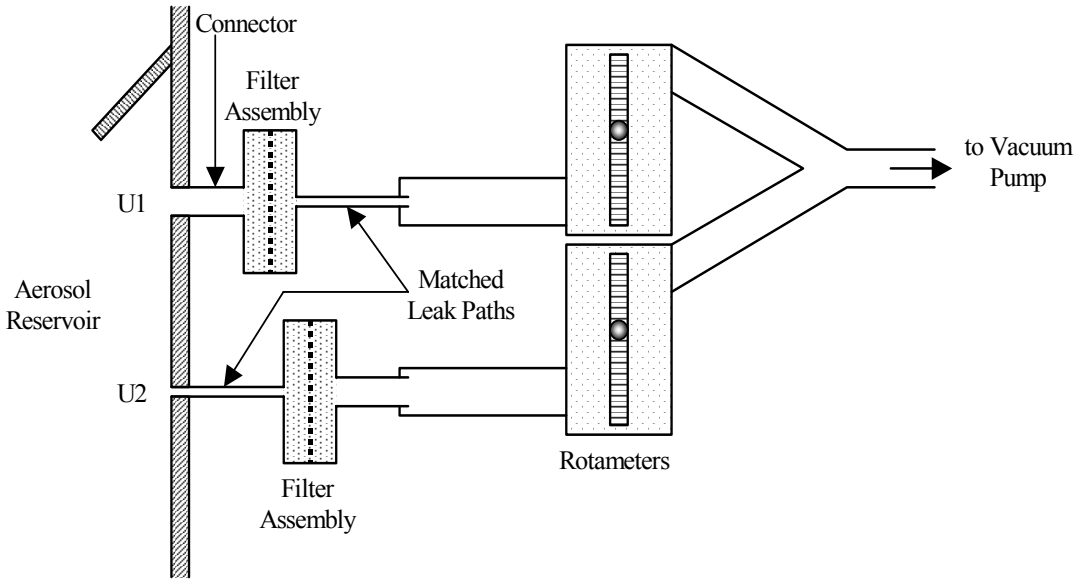

Figure 5-18 Schematic of Filtration Sampling Lines

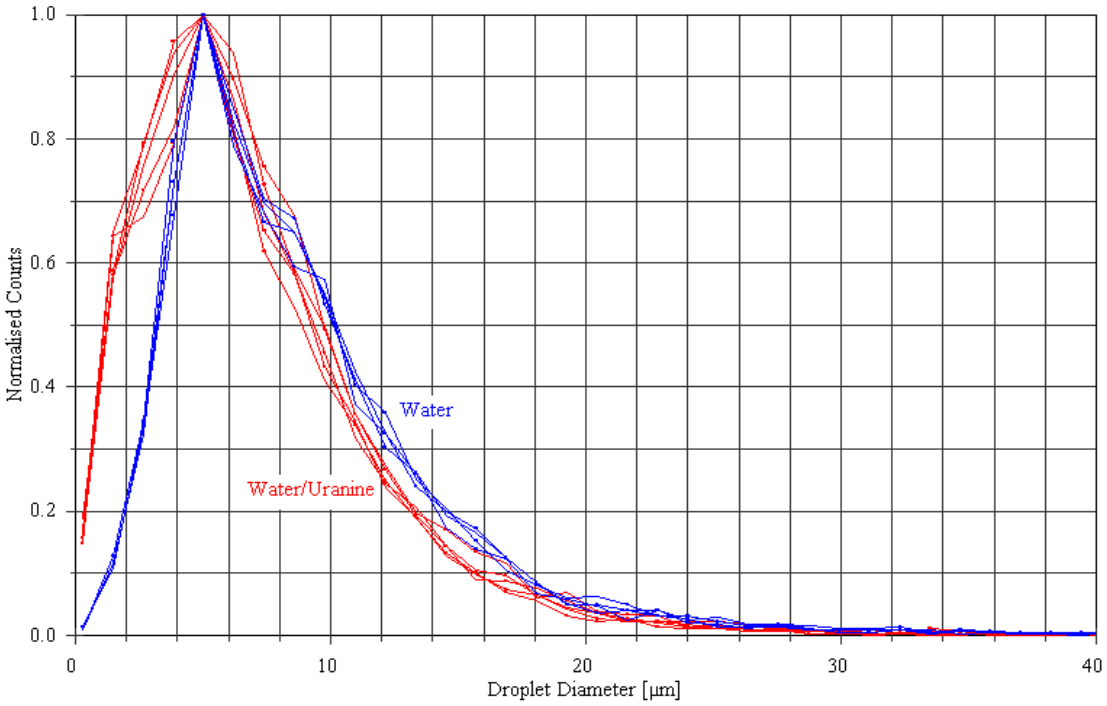

Figure 5-19 Droplet-size Distributions of Water and Water/Uranine Aerosols Measured at the Aerosol-characterization Port Using a PDA System

6. HYDROGEN BEHAVIOR
(R. Swartz and C. Chan)

During certain loss-of-coolant accidents in an ACR, hydrogen can be formed by zirconium-steam reactions, water radiolysis, and corrosion of metal. The subsequent release of hydrogen into the reactor containment could pose a threat to the integrity of the containment and essential equipment for accident management. It is therefore prudent to examine various accident scenarios, to predict the hydrogen source terms, to assess the potential hazard, and to develop mitigation measures.

The amount and rate of hydrogen generated in an accident differs for different accident scenarios. For design basis accidents the hydrogen source term is small. For limited core damage accidents, the hydrogen release is also limited for the ACR design is due to the heat sink provided by the moderator water, which effectively arrests severe-accident progression at the point of fuel cladding oxidation, and prevents the continued hydrogen releases associated with complete core melt. The thin collapsible CANDU fuel cladding limits the mass of hydrogen that can be released from fuel cladding oxidation.

Over the past 20 years, through a comprehensive R&D program, AECL has developed a good understanding of key phenomena on hydrogen behavior under various accident conditions. Analytical tools have also been developed to assess the potential risks of hydrogen in existing CANDU reactors. Existing methodologies and tools can be applied to ACR for accident analysis.

6.1 Hydrogen Source Term from Reactor Accidents

In a CANDU reactor, hydrogen can be produced in the event of a LOCA. The fuel heats up quickly during the blowdown phase of the event. As the temperature increases, the zirconium fuel cladding reacts at a higher rate with steam to form hydrogen. If emergency cooling is available, the fuel is cooled and the amount of hydrogen generated is very small – insufficient to pose any threat to the containment building. However, if emergency core cooling is unavailable (LOCA + LOECC), the temperatures continue to escalate and the zirconium-steam reaction can proceed. The hydrogen generation will be limited by cooling provided by the moderator.

In the long term, hydrogen can be formed by other means such as radiolysis of water, hydrogen degassing, and oxidation of metals. However, the rate of hydrogen production is very slow – usually takes days to produce a significant amount of hydrogen.

6.2 AECL Hydrogen Research Facilities

AECL has carried out a comprehensive R&D program over the past couple of decades to develop a good understanding of key hydrogen behaviour phenomena under various accident conditions. Four AECL experimental facilities are key to this R&D: Large-Scale Vented Combustion Test Facility (LSVCTF), Containment Test Facility (CTF), Diffusion Flame Facility (DFF), and Large-Scale Gas Mixing Facility (LSGMF).

6.2.1 Large-Scale Vented Combustion Test Facility

The Large-Scale Vented Combustion Test Facility (Figure 6-1) is a 10-m long, 4-m wide, 3-m high rectangular enclosure with an internal volume of 120 m^3. It is constructed of 1.25-cm-thick

steel plates welded to a rigid framework of steel I-beams. Two roller-mounted movable end walls are provided to open the vessel for internal modifications or to move in bulky experimental equipment as needed. The combustion chamber, including the end walls, is electrically trace-heated and heavily insulated to maintain temperatures in excess of 100°C for extended periods of time. The entire combustion chamber is enclosed in an insulated metal Quonset.

The Large-Scale Vented Combustion Test Facility was designed to systematically quantify effects of key thermodynamic and geometric parameters affecting pressure development during vented combustion under conditions relevant to ignition. The facility has good control of initial thermodynamic conditions, is sufficiently large to capture the effects of scale, and is geometrically similar to rooms (e.g., flat walls and square corners).

The combustion chamber can be subdivided into 2 or 3 compartments using structural steel partitions. A schematic of the facility configured with three internal compartments is shown in Figure 6-2. Variable sizes of vent openings are available between compartments and to the outside. The facility has three separate gas addition systems for steam, hydrogen, and inert gases. Hydraulic fans inside the test chamber are used to mix the gases and can be used to provide turbulent conditions during combustion. Instrumentation includes pressure transducers, thermocouples, and gas sampling by a mass spectrometer, at several locations inside the test chamber.

Key features of the Large-Scale Vented Combustion Test Facility are:

- Variable vent opening (size and location),
- Rectangular interconnected chambers,
- Removable end walls for easy access,
- 200 kPa design pressure,
- State-of-the-art data management system,
- Chambers can be trace heated in excess of 100°C,
- Mass spectrometer for gas concentration measurements,
- High-speed pressure transducers to capture the transient overpressures due to combustion, and
- Remote operation for operator safety.

The facility has been used to perform a wide variety of experiments, including:

- Vented combustion experiments in interconnected volumes to study the effects of hydrogen concentration (same or different concentrations in the compartments), vent size, and ignitor location,
- Vented combustion experiments in approximately 30, 60, or 120 m^3 volumes to evaluate the effects of scale,
- Vented combustion experiments under continuous hydrogen injection with an operating ignitor,
- Turbulent vented combustion experiments to study the effects of initial turbulence,
- Flame propagation studies between interconnected compartments, and

- Passive Autocatalytic Recombiner (PAR) development and qualification for hydrogen mitigation applications in large enclosures.

Data from the hydrogen combustion tests are used to validate combustion codes used in safety and licensing. In addition to combustion testing, as discussed above, the Large-Scale Vented Combustion Test Facility has been used in testing Passive Autocatalytic Recombiners. In particular, it was used for many of the qualification tests for AECL's recombiner design, as well as tests used to validate recombiner models in combustion codes.

6.2.2 Containment Test Facility

Several test rigs make up the Containment Test Facility. These include a 6-m^3 sphere and a 10 m^3 cylinder, that may be interconnected by 30-cm and 50-cm diameter ducts (Figure 6-3), and a 28-cm diameter, 9-m long combustion duct (Figure 6-4). Each vessel is rated for pressures up to 10 MPa, and trace-heated for operation at temperatures up to 150°C. The facility is designed to investigate the fundamentals of combustion phenomena. These include flammability limits, ignition, turbulent combustion, flame acceleration, detonation, and detonation transition.

The Containment Test Facility has been used to perform a wide variety of experiments, including:

- Ignition by hot surfaces,
- Flame jet ignition,
- Vented and unvented combustion,
- Burns in interconnected vessels,
- Obstacle-induced flame acceleration, and
- Burns in non-uniform mixtures.

Data from the hydrogen combustion tests are used to validate combustion codes used in safety and licensing. Also, data from flame acceleration tests was used to develop a code that determines whether or not a flame is capable of accelerating to supersonic velocities and, under appropriate conditions, triggering a Deflagration-to-Detonation Transition (DDT).

6.2.3 Diffusion Flame Facility

The Diffusion Flame Facility (Figure 6-5) consists of a burner with associated gas supply lines and instrumentation housed within a modified grain silo (5-m diameter and 8-m height), which was elevated 1 m off the ground for ventilation purposes and insulated to retain heat for experiments that involve an air/steam environment. Tests with H_2/steam jet flames (up to 15 cm in diameter) in air/steam atmosphere (up to 30% steam by volume) can be performed in this facility.

Diffusion-flame tests were carried out to examine some of the fundamental properties of hydrogen jet flames such as time-averaged flame temperature, flame length, and flame stability limits. To assist reactor safety analysts, relevant parameters such as the maximum thermal load and time-averaged heat transfer coefficient to nearby objects by an impinging flame were also determined. Results from these tests enable safety analysts to assess the potential threat of hydrogen standing flames and to predict the potential energy load to nearby equipment.

6.2.4 Large-Scale Gas Mixing Facility

The Large-Scale Gas Mixing Facility (Figure 6-6) is a 10.3 m by 11.0 m by 8.2 m concrete enclosure with an internal volume of approximately 1000 m^3. Helium and steam can be injected into the enclosure at various locations to simulate a break in the reactor cooling system inside a containment building following an accident (helium is used instead of hydrogen as their densities are similar and helium is not combustible). Internal partitions can also be added to the facility to simulate sub-compartments inside a reactor building. Removable ceiling tiles allow large pieces of equipment to be placed inside the facility for environmental qualification.

Tests have been carried out in the Large-Scale Gas Mixing Facility to determine the effects of phenomena such as condensation, buoyancy-induced mixing, and jet-momentum-induced mixing, on the distribution of hydrogen in a post accident containment atmosphere. Data from the gas mixing tests are used to validate analytical tools used for predicting the hydrogen distribution.

The Large-Scale Gas Mixing Facility was located at Whiteshell Laboratories, but has now been decommissioned. A new facility with ~50% greater volume is currently being established at Chalk River Laboratories.

6.3 Experimental Observations

Observations from experiments carried out over many years at AECL include:

- Flammability limits and other combustion properties vary with initial (i.e., pre-burn) conditions (temperature, pressure, gas composition, turbulence intensity). Starting with containment conditions associated to a limited severe accident scenario, fast flames (i.e., near-sonic velocities) are unlikely to be achieved without initial hydrogen concentrations of at least 15%. Without flame acceleration to supersonic velocities, transition to detonation (DDT) is impossible.
- A hydrogen burn in interconnected compartments can lead to higher overpressure peaks as compared to unconnected deflagrations).
- The possibility of transition from deflagration to detonation depends on a number of conditions (size of combustible cloud, hydrogen and steam concentrations, initial temperature, turbulence intensity, etc.) The possibility of DDT can be assessed by the DDTINDEX code developed in AECL using an internationally accepted methodology [3,4].
- The stability range for hydrogen-steam diffusion flames is extremely wide. Results suggest that if any ignition source is present, formation of a hydrogen diffusion flame (commonly referred to as a standing flame) after a reactor accident that involves a release of hydrogen from a break in the cooling system is a likely scenario.
- The time-averaged flame temperature of hydrogen diffusion flames was measured to be about 1440°C, much lower than the theoretical flame temperature of a hydrogen-air mixture (2080°C). It was also observed that the maximum temperature attainable by a flame-impinged body, about 1000°C, is even lower because of heat loss by conduction and radiation.
- For steam concentrations up to 10% (saturation condition at 50°C), diffusion flame properties (such as flame stability, flame length, max flame temperature) are not changed significantly.

- For injection of a light gas such as helium or hydrogen into a large enclosure with velocities less than 25 m/s, momentum effects are generally insignificant. The jet does not penetrate very far into an enclosure before buoyancy dominates the movement of the gas.
- Helium gas mixing experiments have shown that buoyancy-induced convection is very effective in limiting the accumulation of hydrogen in a reactor vault.

6.4 Summary

AECL has a mature and widely recognized hydrogen behavior program. Over the last couple of decades, AECL has investigated various hydrogen mixing, mitigation, and combustion phenomena relevant to CANDU reactor safety. Through these programs, the dynamics and mechanisms associated with hydrogen behavior in CANDU containment have been examined. The ACR design is effectively equivalent to the CANDU design for hydrogen combustion phenomena. Models to capture the key phenomena have been developed and validated. AECL has also developed an accepted mitigation device (PAR) for CANDU and other reactor designs. The existing knowledge base is fully applicable to analysis of reactor accidents in ACR.

6.5 References

1. G.W. Koroll, A.P. Muzumdar, M.A. Cormier and N.G. Hunt, "Hydrogen Management in CANDU Reactors," OECD/CSNI Specialist Meeting on Selected Containment Severe Accident Strategies, Stockholm, 1994.
2. C.K. Chan, W.A. Dewit and G.W. Koroll, "Criteria for Transition from Deflagration to Detonation in H_2-air-steam Mixtures," Heat and Mass Transfer In Severe Nuclear Reactor Accidents, ed. by J.T. Rogers, p.372, 1996.
3. C.K. Chan, et al., "State-of-the-Art Report on Flame Acceleration and Deflagration to Detonation Transitionm in Nuclear Reactor Safety," NEA/CSNI/R(2000)7, 2001.

Figure 6-1 Photograph of the Large-Scale Vented Combustion Test Facility

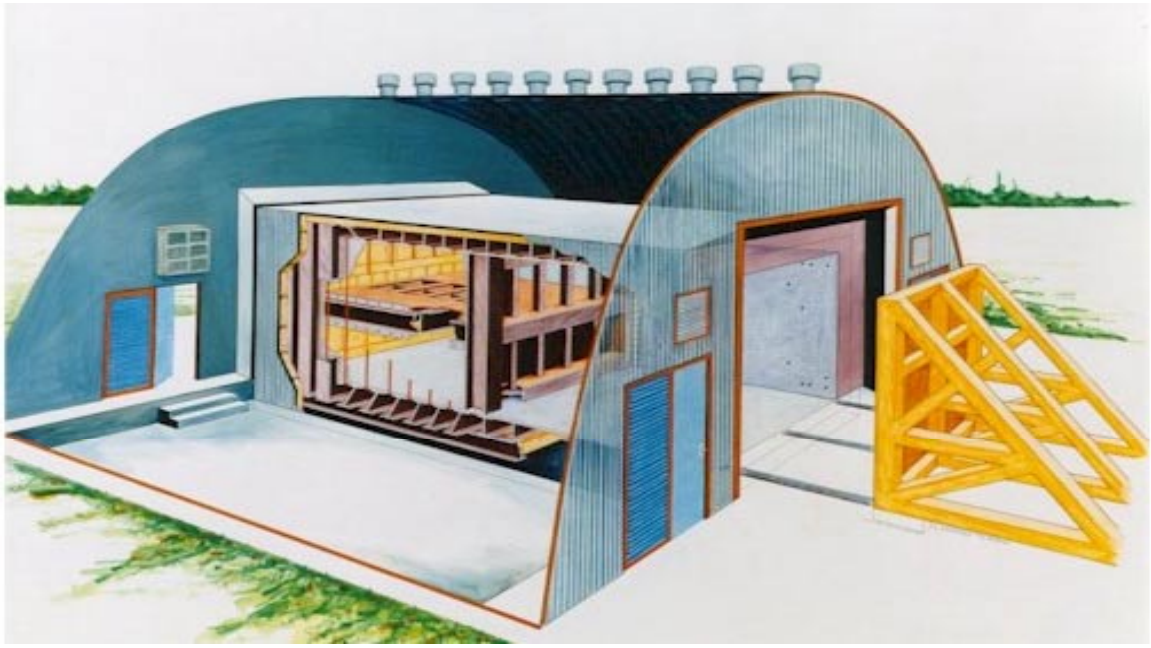

Figure 6-2 Schematic of the Large-Scale Vented Combustion Test Facility

Figure 6-3 Photograph of the Containment Test Facility Sphere and Cylinder

Figure 6-4 Photograph of the Containment Test Facility Combustion Duct

Figure 6-5 Photograph of the Diffusion Flame Facility

Figure 6-6 Schematic of the Large-Scale Gas Mixing Facility

7. CORE DISASSEMBLY

(P.M. Mathew)

Core degradation during a severe core damage accident in an ACR/CANDU reactor is a relatively slow event. The core disassembles in a gradual process mitigated by the requirement to boil off the moderator water that surrounds the fuel channels.

7.1 Background

During an accident with degraded cooling at decay power (e.g. LOCA + LOECC) and loss of moderator cooling, the fuel channels heat up, sag, break-up, separate and eventually fall into the remaining moderator, where the debris will be cooled. During the core disassembly process, a sagging channel contacts a lower channel. When the lower channel is also uncovered, it will sag under its own weight as well as that of the supported channel. This process would continue, as more channels are uncovered. As sagging increases, it is expected that the sagged channels break near the bundle junctions. A suspended debris bed is thus formed, which moves downward with the falling moderator level. The submerged channels will be able to support a finite number of channels before they are also expected to fail. The loading on the submerged channels increases with the accumulation of debris from top channels, thereby leading to progressive failure of the lower channels and ultimately resulting in the collapse of the entire core into the moderator pool in the bottom of the calandria. The core disassembly experiments described in this section address the behavior of CANDU channels during the moderator boil-off, and debris bed formation process [1,2].

7.2 Core Disassembly Experiments

This section addresses the CANDU-specific small-scale experiments and supporting analysis conducted to improve our understanding of the disassembly behavior of a CANDU core under a severe core damage accident scenario [3]. Single channel and multiple channel disassembly tests are being conducted to study channel deformation, failure and disassembly mechanisms for a current generation CANDU core. These tests are described here to understand the core disassembly phenomena in a CANDU reactor. The ACR-700 core disassembly phenomena will be similar to the current generation CANDU reactor core disassembly phenomena.

7.2.1 Experimental Apparatus

To study the disassembly behavior of a CANDU core, a facility called the Core Disassembly Test Facility, was designed and built using scaled channels, Figure 7-1. The facility can test up to four channels in a vertical column. The stress level of a CANDU fuel channel was retained in the small-scale test channel and a constant scaling ratio of the significant dimensions of the full-size channel and reactor core are maintained in the reduced-scale geometry. Twelve reduced scaled tungsten heaters were selected to simulate the 12 fuel bundles in a CANDU channel. Table 7-1 summarizes the results of the scaling calculations.

One end of the channel is completely fixed against any movement, and the “floating” end, is allowed to move horizontally, but not rotate, mimicking the fuel channel position support mechanisms in a CANDU reactor. As channel sag increases with temperature, the floating end moves inward. The horizontal movement of the channel is measured with a linear variable

displacement transducer. Vertical movement is monitored with a laser. The typical maximum channel temperature during a test is about 1400°C. Several Pt-PtRh Type R thermocouples, spot-welded to the cladding along the top and bottom sides of the channel at different locations, measure the channel temperatures.

7.2.2 Experimental Results

Six single channel tests have been conducted in an inert atmosphere, where the channel was allowed to sag freely. A summary of the test results is shown in Table 2. The reference temperature was chosen as 800°C because no significant sag was observed below that temperature. The heat-up rate was calculated from the total time the channel spent above 800°C until the test was terminated (Table 2). Major conclusions from these tests include:

- As expected, time-dependent material creep is the main mechanism for channel deformation.
- The end loads from channel sag are insufficient to cause the fuel channels to "pull-out" of the reactor end shield.
- The channel wall thins at bundle junctions along the bottom side of the fuel channel.

Multiple channel tests have been conducted in an inert atmosphere using two and three channel rows with an appropriately scaled pitch (see Table 1). Measured channel temperatures showed that heat was transferred from the hotter top channels to the lower cooler channels as they sag into contact. The top and bottom channels of the two-channel row test were sectioned along the vertical axis and the wall thickness of the top and bottom wall was measured. Significant wall thinning of the bottom wall of the top channel was observed after the second and the tenth bundle locations from the fixed end. The channel of the second row showed some localized wall thinning at the bundle junctions as well. The top channel continues to creep and as a result breaks up near the ends. As observed from this test, debris formed by this mechanism can be almost 10 bundles long. Figure 7-2 is a photograph of one end of the three-channel test assembly after it was removed from the test chamber. The photo shows break up of the top channel near the ends forming long and coarse debris.

7.2.3 Channel Sag Model

An ABAQUS finite element model was developed for the experimental findings of the single channel tests, Figure 7-3, using creep equations for Zr-2.5Nb [4,5]. As in the test channel, one end (fixed end) is restrained against displacements and rotations in all directions. The other end (the floating end) is similarly restrained in all directions except for the axial.

Since the modelling of mechanical interaction between the heaters and the softening tube wall is complicated, a simplified approach was adopted whereby the creep rate equation was multiplied by a constant factor to capture the effect of stress concentration in the gap region. This stress intensity factor was obtained by matching the measured transient sag of CD-9 with the calculated results, Figure 7-4. The same factor was applied to calculate also all the independently measured test data of the single channel test CD-7, Figures 7-5 and 7-6. Good agreement between the experimental data and the model predictions was obtained for both tests, which demonstrated that such a simple approach adequately models the complicated mechanical interaction.

7.3 Summary

Scaled experiments have been performed to investigate core disassembly behaviour in CANDU reactors. These experiments have confirmed the slow nature of core disassembly, driven by high temperature creep of the fuel channels. They have also demonstrated that the debris from core disassembly will tend to be long fragments of fuel channels that break at bundle junctions near the channel ends. While specifically aimed at current generation CANDU reactors, the results are generally applicable to the ACR design.

7.4 References

1. V.G. Snell, M. Bonechi, and W.C.H. Kupferschmidt, ”Advances in Nuclear Safety,” Proceedings of Pacific Basin Nuclear Conference, Seoul, Korea, October 29-November 2, 2000.
2. D.A. Meneley, C. Blahnik, J.T. Rogers, V.G. Snell, and S. Nijhawan, “Coolability of Severely Degraded CANDU Cores,” International Seminar on Mass and Heat Transfer in Severe Reactor Accidents, Cesme, Turkey, May 22-26, 1995.
3. P.M. Mathew, W.C.H. Kupferschmidt, V.G. Snell, and B. Bonechi, “CANDU-Specific Severe Core Damage Accident Experiments in Support of Level 2 PSA,” Proceedings of 16th International Conference on Structural Mechanics in Reactor Technology, SMiRT 16, Washington DC, August 12-17, 2001.
4. R.S.W. Shewfelt, and L.W. Lyall, “A High-Temperature Longitudinal Strain Rate Equation for Zr-2.5 wt% Nb Pressure Tubes,” Journal of Nuclear Materials, Vol. 132, (1985).
5. R.S.W. Shewfelt, L.W. Lyall, and D. Godin, “A High-Temperature Creep Model for Zr-2.5 wt% Nb Pressure Tubes,” Journal of Nuclear Materials, Vol. 125, (1984).

Table 7-1 Dimensions of a Current Generation CANDU Channel, Small-Scale Channel and Scaling and Aspect Ratios

Parameter	CANDU Channel	Small-scale Test Channel	Scaling Ratio
Channel Length (m)	5.994	1.2	5.0
Channel Vert. Separation (mm)	160	32	5.0
Channel ID (mm)	122.1	24.1	5.1
Bundle O.D. (mm)	102.8	20.8	4.9
Bundle Length (mm)	495.3	99	5.0
Bundle-Channel Gap (mm)	19.3	3.3	5.8
Wall Thickness (mm)	5.0	0.4	12.5
Max. Stress at Mid-span (MPa)	14.5	14.5	1.0
Channel Aspect ratio (L/D)	49	50	1.0
Bundle Aspect Ratio (L/D)	4.9	4.8	1.0

Table 7-2 Summary of Single Channel Test Results in Argon Atmosphere

Test No.	Number of Powered Heaters Per channel	Max. Temp. at Mid-point (°C)	Transient Max. Sag at mid-point (mm)	Heat-up Rate from 800°C (°C /s)
CD-3	4	1415	24	0.26
CD-4	10	1320	117	0.10
CD-5	10	1415	100	0.11
CD-6	10	1310	88	1.20
CD-7	10	1307	120	0.09
CD-9	10	1390	132	0.048

Figure 7-1 A View Of The Test Chamber Of The Core Disassembly Test Facility

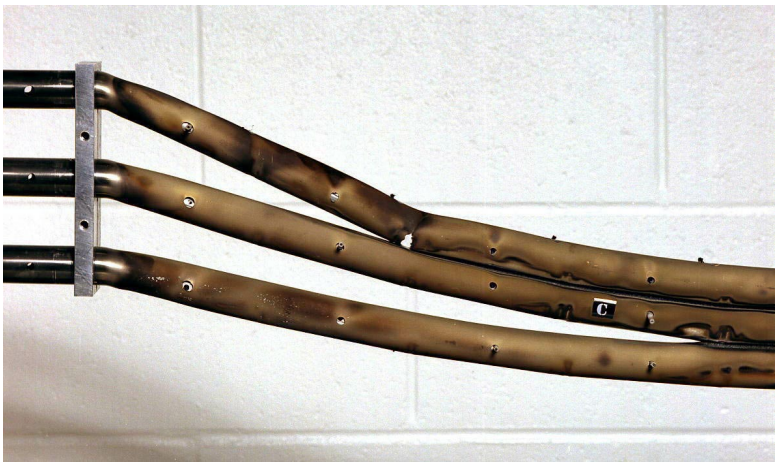

Figure 7-2 Photograph of One End of the Three-channel Test Assembly Showing Channel Failure

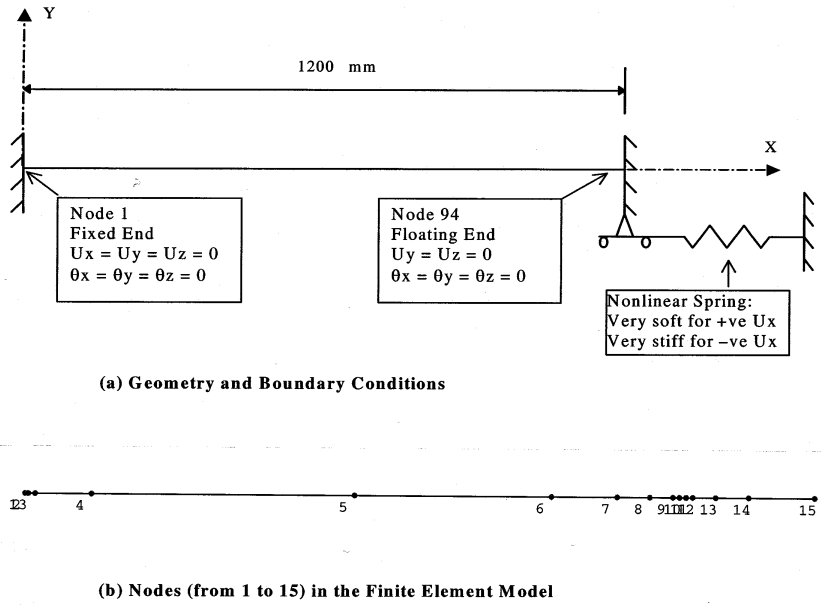

Figure 7-3 ABAQUS Finite Element Model for Single Channel Test Simulations

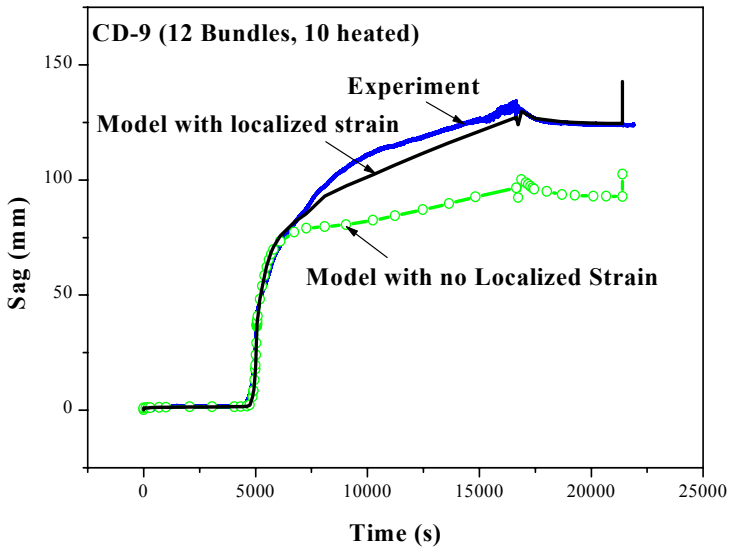

Figure 7-4 Comparison of Model Calculations with and without Localized Strain Model with Test Results

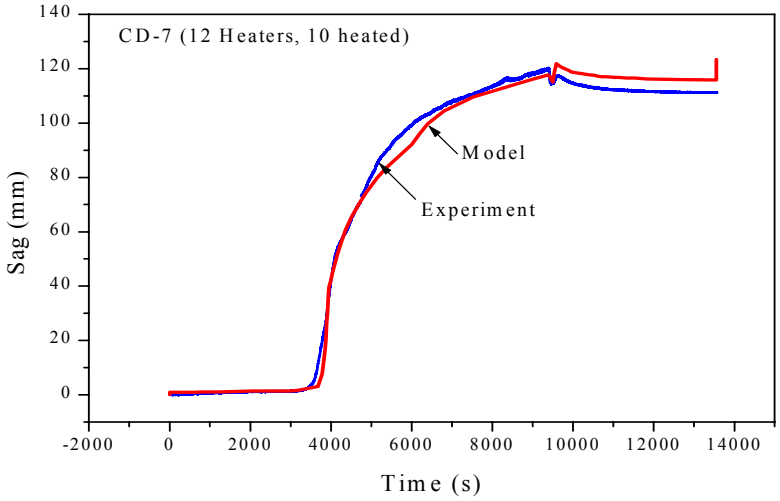

Figure 7-5 Comparison of Model Predictions with Measured Sag for a Single Channel Test (CD-7)

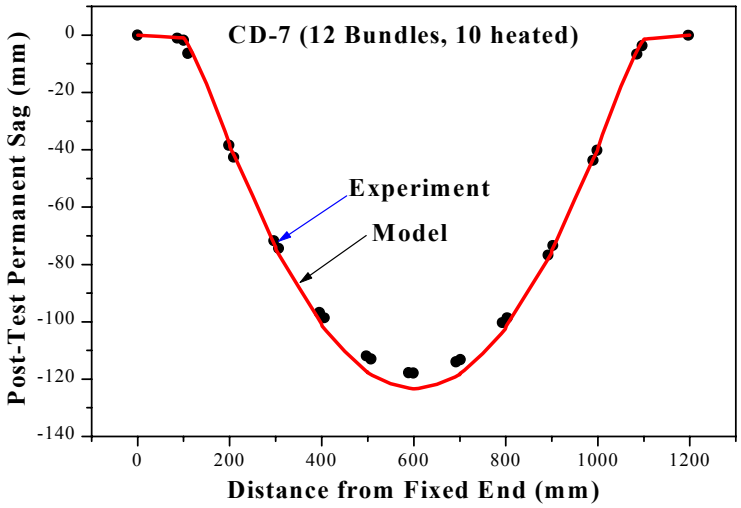

Figure 7-6 Comparison of Model Predictions with Measured Post-test Axial Profile for Test (CD-7)